
Contents

1	Introduction	1
1.1	Background and Motivation	4
1.1.1	Cognitive Small Cell: A Prominent Use-case	5
1.1.2	Performance Analysis	9
1.1.3	Imperfect Channel Knowledge for CR systems	10
1.2	Main Contributions	12
1.3	Organization	16
2	Interweave System	18
2.1	Related Work	19
2.2	Contributions	21
2.2.1	Analytical framework	21
2.2.2	Imperfect channel knowledge	21
2.2.3	Estimation-sensing-throughput tradeoff	22
2.3	System Model	22
2.3.1	Deployment Scenario	22
2.3.2	Signal model	23
2.4	Problem Description and Proposed Approach	24
2.4.1	Problem Description	24
2.4.2	Proposed Approach	26
2.4.3	Validation	30
2.4.4	Assumptions and Approximations	31
2.5	Theoretical Analysis	32
2.5.1	Deterministic Channel	32
2.5.2	Random Channel	39

2.6	Numerical Results	43
2.6.1	Deterministic Channel	43
2.6.2	Random Channel	49
2.7	Summary	55
2.8	Proofs	56
2.8.1	Proof of Lemma 5	56
2.8.2	Proof of Lemma 6	57
2.8.3	Proof of Theorems 5 and 2	57
3	Underlay System	59
4	Hybrid Systems	60
4.1	Related Work	61
4.2	Contributions	62
4.2.1	Analytical framework	62
4.2.2	Estimation-sensing-throughput tradeoff	62
4.3	System Model	63
4.3.1	Deployment Scenario and Medium Access	63
4.3.2	Signal Model	63
4.3.3	Problem Description	65
4.4	Proposed Approach	67
4.4.1	Frame Structure	67
4.4.2	Channel Estimation	69
4.4.3	Characterization of performance parameters	71
4.4.4	Sensing-Throughput Tradeoff	74
4.5	Numerical Analysis	75
4.6	Summary	81
5	Hardware Validation and Demonstration	83
5.1	System Model	84
5.1.1	Simplifications	84
5.1.2	Underlay Scenario and Medium Access	85
5.1.3	Signal Model	86
5.2	Theoretical Analysis	88
5.2.1	Characterization of the System Parameters	89
5.2.2	Estimation-Throughput Tradeoff	91
5.3	Validation	92
5.3.1	Experimental Setup	92
5.3.2	Knowledge of Noise Power	95
5.3.3	Validation of System Parameters	96

5.3.4	Validation of the Estimation-Throughput Tradeoff	98
5.4	Implementation of a Demonstrator	100
5.4.1	Estimation Time	101
5.4.2	Simplifications	102
5.4.3	User Interaction and Observations	105
5.5	Summary	107
6	Conclusion	108
Acronyms and Abbreviation		109
Notations and Symbols		111
Bibliography		115
Related Publications		122

CHAPTER 1

Introduction

Since the invention of smart devices, the mobile traffic has been increasing tremendously over the last decade. According to the recent surveys on mobile traffic by prominent market leaders (Cisco [1] and Ericsson [2]), the existing mobile traffic is expected to increase $11\times$ by 2021. The wireless community including the standardization bodies (3GPP [3]) believe that the state-of-the-art standards (fourth-Generation (4G) – LTE, WiMAX) are not capable of sustaining these ever-increasing demands in the upcoming decade. With this situation in hand, the standardization bodies are currently in the phase of conceptualizing the requirements of the fifth-generation (5G) of mobile wireless systems. Some of these major requirements are: (i) areal capacity in bits/sec/m² must increase by a factor of 1000 compared to 4G, (ii) low latency of approximately 1 ms, and, (iii) energy- and cost-efficient deployment [4, 5]. The feasibility of these requirements can be ensured by applying promising approaches such as small cell deployment and extension to the already allocated spectrum. Before moving any further, let us first capitalize on the underlying facts that make these approaches or their combination suitable candidates for the 5G networks.

Small Cell

In the recent past, Small Cells (SCs) have emerged as a potential solution for coverage and capacity enhancements inside a wireless network. A SC represents a low power station that ranges from 10 m to 100 m, comparable to the

size of a **femtocell**. The reduced transmit distance accomplished with the deployment of SCs enhances the link quality and aids spatial reuse [6]. As a result, ultra-densification by deploying SCs can leverage the areal capacity of a 5G network [5]. The capacity, however, increases linearly with the number of SCs, hence, it is **infeasible** to procure the factor of 1000 in the areal capacity with ultra-densification alone. Not only this, the operation and the integration of these substantial number of SCs to the backhaul network are cost- and energy-intensive for the mobile operator, which somehow limits the degree to which the densification can be achieved by a wireless network.

Spectrum extension

Complementing the link quality by means of SCs, the spectrum represents a major contribution to the desired areal capacity. Given the present situation of the spectrum allocated to different mobile applications, it is difficult to procure an extension to the already allocated spectrum. Before investigating the potential candidates for the spectrum extension, it is necessary to consider the following classification of the spectrum: (i) ≥ 6 GHz; (ii) ≤ 6 GHz. The prime objective of this sort of classification is to shift the focus on the propagation characteristics and the issues thereof.

The spectrum beyond 6 GHz largely entails the millimeter Wave (mmW), which is well-known for point-to-point communications. Recently, it is envisaged as a powerful source of spectrum for 5G wireless systems. However, the millimeter wave technology is still in its initial stage and along with complex regulatory requirements in this regime, it has to address several challenges like propagation loss, low efficiency of radio frequency components such as power amplifiers, small size of the antenna and link acquisition [7]. Therefore, in order to capture a deeper insight of its feasibility in 5G, it is essential to overcome the aforementioned challenges in the near future

Besides the spectrum beyond 6 GHz, an efficient utilization of the spectrum below 6 GHz presents an alternative solution. The use of the spectrum in this regime (below 6 GHz) is fragmented and statically allocated [8, 9], leading to inefficiencies and the shortage in the availability of the spectrum for new services. To justify the statement that the spectrum is under-utilized, a glimpse of the measurement campaign conducted during the peak hours for determining the spectral occupancy for the GSM 1800 MHz downlink channels is presented in Figure 1.1. Hence, the demand for the additional spectrum can be fulfilled

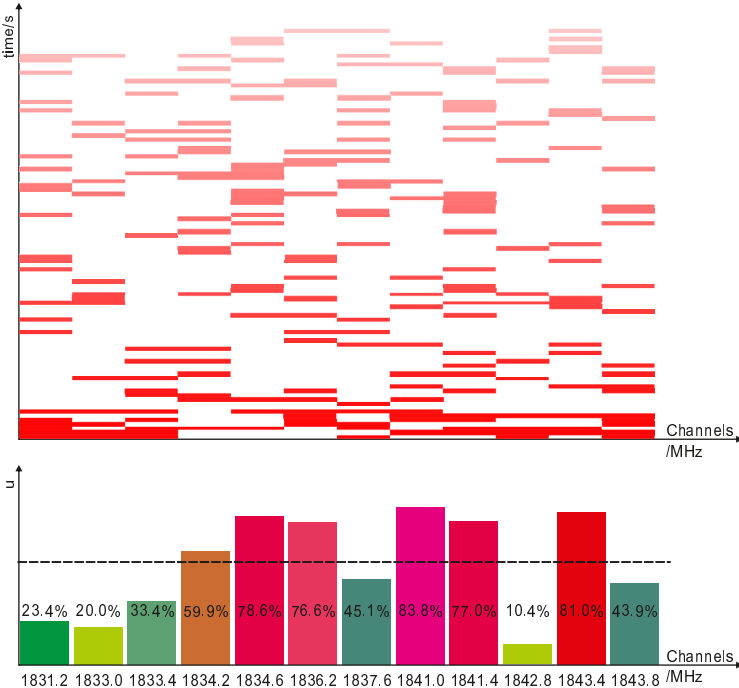


Figure 1.1: A snapshot of a hardware demonstrator that measures the spectral occupancy in GSM 1800 MHz downlink channels, whereby the slices (red and white) represent the channel occupancy (1 or 0) corresponding to a single measurement at a given time instant. The bar plots illustrate the channel occupancy (u) for each channel with a history of 500 measurements [K1].

only if we manage to utilize this radio spectrum efficiently. In this perspective, Cognitive Radio (CR) is foreseen as one of the potential contenders that addresses the spectrum scarcity problem. Since its origin by Mitola *et al.* in 1999, this notion has evolved at a significant pace, and consequently has acquired certain maturity. Despite the existence of the theoretical analysis, from a deployment perspective, this technology is still in its preliminary phase [10]. Due to this large gap between the theoretical models and practical implementations, recently, the wireless community has started to show an inclination towards models and/or techniques that enable the placement of this concept

over a hardware platform so that the disposition of CR systems in the upcoming 5G wireless networks can be facilitated. Understanding the significance of these facts, this thesis **capitalizes** on the deployment of the CR system.

1.1 Background and Motivation

Cognitive Radio Systems

In order to proceed further, it is essential to understand the classification of different CR systems described in the literature. An access to the licensed spectrum is an outcome of the paradigm employed by the Secondary User (SU). In this context, all CR systems that provide **dynamic access** to the spectrum mainly fall under the following categories [11] (please consider Figure 1.2 for a graphical illustration of these paradigms):

- According to Interweave Systems (ISs), the SUs render an interference-free access to the licensed spectrum by exploiting spectral holes in different domains such as time, frequency, space and polarization.
- Underlay Systems (US) enable an interference-tolerant access under which the SUs are allowed to use the licensed spectrum (e.g. Ultra Wide Band) as long as they respect the interference constraints of the Primary Receivers (PRs).
- Hybrid Systems (HSs) combine the benefits of the IS (agility to detect spectrum holes in different domains) and the US (interference-tolerant capability) to enhance the spectral usage efficiency.
- Overlay systems consider the participation of higher layers for enabling the spectral coexistence between two or more wireless networks.

Since the IS, US and HS are closely associated with the physical layer, these systems are mostly considered not only for the theoretical analysis but for practical implementations as-well [K1,K3,K7,K12,K13], [12–14]. Taking this into account, the thesis focuses on the performance analysis of these CR systems from a deployment perspective. In order to illustrate the successful incorporation of a CR technique in a 5G network, a specific use-case (deployment scenario) is presented subsequently.

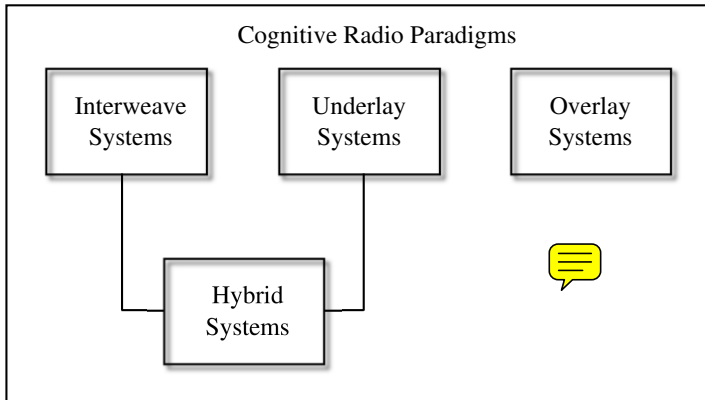


Figure 1.2: Classification of different CR paradigms enabling secondary access to the licensed spectrum.

1.1.1 Cognitive Small Cell: A Prominent Use-case

Following the previous discussion, it is evident that **spectrum extension and SCs are key-enablers** for the 5G system. **Utilizing this knowledge**, a preliminary concept of Cognitive Small Cell (CSC), a promising application that combines the benefits from the SC deployment and the efficient usage of the spectrum below 6 GHz by implementing CR techniques to accomplish the requirements of 5G networks is presented. The notion of CSC has been previously investigated by Elsawy *et al.* [15, 16] and Wildemeersch *et al.* [17], where the authors primarily emphasized on the modelling techniques¹ that depict the positioning of several CSCs inside the network. Due to this, the performance analysis of the CSC has been limited mainly to network abstraction. In contrast, this thesis emphasizes on key-aspects encountered while deploying a CSC, which otherwise could forbid its realization on a real hardware. A comprehensive incorporation of CSC in a preliminary 5G architecture is illustrated in Figure 1.3. In order to enhance the **plausibility** of the proposed network architecture, it is interesting to highlight some of the essential ingredients pertaining to the deployment of the CSC.

¹The modelling is based on stochastic geometry, which allows a spatial averaging over multiple network geometries [18, 19].

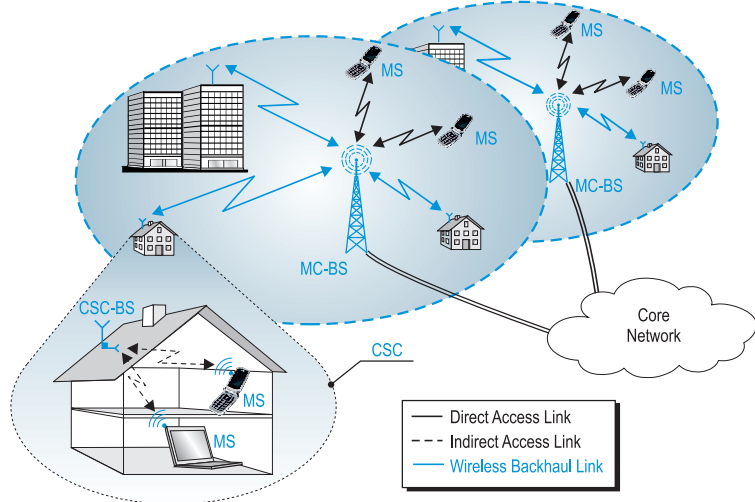


Figure 1.3: An illustration of the CSC deployment in a 5G network.

Network Elements

In order to propose a successful integration of CSC in a 5G network, the following key elements are essential: a CSC-Base Station (CSC-BS), a Macro Cell-Base Station (MC-BS) and Mobile Stations (MSs), cf. Figure 1.3. MSs are the devices either served by the MC-BS over a *direct access* link or the CSC-BS over an *indirect access* link. The direct access and the indirect access are the nomenclature used to distinguish a start-of-the-art (spectrum) access between the MC-BS and the MS from an access between the CSC-BS and the MS representing a CR communication, respectively. Furthermore, the MC-BS is connected to several CSC-BSSs over a *wireless backhaul* link. Although the MC-BS and the MS already exist in the conventional cellular architecture, to incorporate the opportunistic access inside the CSC, it is necessary to consider a functionality upgrade.

Spectrum Access

In the proposed network architecture, the access to the spectrum is realized over the wireless backhaul, the direct access and the indirect access links, cf.

Figure 1.3.

1. A wireless backhaul is a point-to-point wireless link between the CSC-BS and the MC-BS that relays the traffic generated from the CSC to the core network. Accounting the feasibility of ultra-dense CSC, the wireless backhaul link, in contrast to the optical fiber link, presents a cost-effective and energy-efficient alternative to the mobile operator. With the limited infrastructure required for deployment, it accelerates the installation process and promotes scalability of the network. For the wireless backhaul link, an exclusive spectrum for a longer duration is desired. Hence, it is sensible to nominate a mmW band; alternatively, an exclusive band below 6 GHz can be acquired using the principles of Licensed Shared Access [20].
2. A direct access link represents a direct access of the MS at the MC-BS over the allocated spectrum. Consequently, the spectrum access for this link is analogous to the one existing in the state-of-art wireless standards.
3. The CSC elements (the CSC-BS and the MS) are responsible for executing the secondary access to the licensed spectrum. The additional spectrum acquired is used for the communication between the CSC-BS and the MS over the indirect access link.

Network Compatibility

Besides secondary access, CSC has to co-exist harmoniously with the other elements existing in the network. In this context, the network elements are embedded with additional functionality such as:

- The MS procures the control information (signalling and synchronization) over the indirect access link after connecting to the near-by CSC-BS.
- In order to accomplish a logical placement of CSCs inside the network, the CSC employs S1 and X2 interfaces over the wireless backhaul link.
- For situations where several CSC-BSs co-exist under a MC-BS, operations like seamless cross-tier and co-tier mobility constitute a challenging task for the network.

Hardware Feasibility

Along with other ingredients, it is essential to outline certain aspects that pertain to the hardware realizability of the CSC. For the CSC-BS, an antenna mount system consisting of an indoor and an outdoor antenna is proposed. Whereby, the indoor antenna exploits the walls of the building to physically separate the indoor transmissions over the indirect access link, in this way, it curtails the interference to the primary system and to the neighbouring CSCs. Whereas, the outdoor antenna secures a narrow beam transmission to enhance the link quality for the wireless backhaul link. Besides this, it is a well-known fact that Software Defined Radio (SDR) has played an important role in the genesis of the CR [21]. Which means that the SDR can serve as a suitable platform for practicing CR techniques, thereby accomplishing rapid prototyping for the CR systems. Taking this into account, the SDR platform is utilized for realizing (or demonstrating) the CR functionality pursued by the CSC-BS on a real hardware.

Indoor Deployment

From a market survey, it has been depicted that 70% of the mobile traffic is originated from indoor locations [6]. Another survey of the leading WiMax operators revealed that the 80% of their subscribers will be connected indoors [22]. In addition, a new range of wireless services, categorized as Internet of Things, will operate indoors. Following these facts, it is clear that the performance gains in terms of spectrum reuse will be far more consequential if we manage to consolidate these sources of traffic by means of SCs deployment. Hence, it is sensible to consider the residential and enterprise as the main deployment scenarios for the CSC, cf. Figure 1.3. Except for a different coverage regime, the operating principles of these scenarios are analogous. Besides, in context with the CR, where the interference mitigation between the primary and secondary systems is a significant aspect, exercising the CR communication within the walls (which attributes to an indoor deployment) provides a spatial separation between the two systems. This, however, does not signifies that CR communications are only feasible for indoor scenarios. As the matter of fact, the indoor deployment is a technique for exploiting the behavioral dimension of the traffic source for the CR communication so that co-existence with the licensed users is encouraged. Based on this knowledge, an indoor scenario is considered for the deployment of the CSC, cf. Figure 1.3.

1.1.2 Performance Analysis

Since the evolution of wireless systems, understanding the performance of novel algorithms/techniques related to the wireless systems has always been a challenging task. With regard to this, for a CR system, because of the involvement of two different systems namely primary and secondary systems, this task becomes even more difficult. On one end, it has been engaging a large number of researchers that are eager to find solutions for the new set of problems, leading them to develop theoretical models (system models). As a result, these models allows us to determine the performance limits of the CR system. However, to sustain analytical tractability, they tend to consider assumptions that in most situations are unrealistic for deployment. On the other end, due to the co-existence of the two systems sharing the same spectrum, the performance has been critically looked by the regulatory bodies and the mobile operators². In this regard, despite the numerous theoretical models that exist in the literature, when it comes to judging the performance of a CR, they give more preference to the hardware implementations that offer complete solutions by the regulatory bodies.

These different mindsets and the lack of clear guidelines ultimately lead to a mismatch between the two communities, and consequently slows down the evolution of the CR in realistic scenarios. Under this situation, it is advisable to merge these mindsets and establish a deployment-centric viewpoint towards the CR systems, according to which, the upcoming models and/or techniques are not only associate themselves to the performance characterization (by means of theoretical expressions) but are eligible for practical implementations as well. This viewpoint, also the main motivation behind this work, is emphasized throughout the thesis.

In order to accomplish the co-existence between the primary and the secondary systems, it is important to quantify the performance of the two systems. In this context, the CR systems can successfully co-exist with the primary system, only if they respect the interference at the primary system caused due to an access to their spectrum. This can be achieved by means of constraints by the primary system or the regulatory bodies so the interference to the primary system can be effectively regulated. With regard to these constraints, the CR system intends to deliver a certain Quality of Service/Quality of Experience (QoS/QoE) in the form of throughput to their Secondary Receiver (MS). As a

²These operators are the ones who are willing to share their license (as primary system) or the ones who are willing to access the licensed spectrum (as secondary system).

result, the performance of a CR system can be jointly characterized in terms of the interference received by the primary system and the throughput achieved by the secondary system.



1.1.3 Imperfect Channel Knowledge for CR systems

In a nutshell, a CR is an agile system possesses the ability to adapt to the changes in the environment. From a physical layer perspective, this also corresponds to its response to any kind variations in the system that can degrade its performance. Inherent to the wireless systems, these variations can arise due to the presence of the thermal noise at the receiver and the fading in the channel. It is well-known from the text books related to the wireless communications [23–25], that the channel fading, in particular, is critical for wireless systems. Besides, its knowledge (in the form of Channel State Information at the Transmitter (CSIT)) available through a feedback from the receivers has rendered a substantial improvement in the performance, for instance, multiplexing gains for a MIMO systems [26].

In context with a CR system, the channel knowledge, unlike conventional or state-of-the-art wireless systems, is not confined to a single transmitter-receiver link, rather it includes all the related channels that exist within as-well-as across the primary and the secondary systems, cf. Figure 5.1. Now, since the performance of CR system jointly depends on these two systems, the channel knowledge is a paramount for the performance characterization. In absence of this knowledge, especially of those channels that are related to the interference at the primary systems render the performance characterization of a CR system incomplete and inappropriate for practical implementations. Despite the existence of multitude of analytical models in the literature that consider with the performance analysis of a CR, its performance with regard to the channel estimation, due to the complexity of the problem, has never been completely understood. In order to curtail this gap, this thesis capitalizes on the estimation of the involved channels in a CR system. The accessibility of the channel knowledge at the CSC-BS enables the implementation of cognitive radio techniques (as interweave, underlay and hybrid systems) at the CSC-BS, and allows it to establish the CR communication link with the MS over the acquired spectrum without exceeding the desired level of interference at the PR.

The inclusion of channel estimation demands an allocation of a certain time interval by the CSC-BS. In consideration to this allocation, a certain degradation in the performance in terms of the throughput is obvious. Besides, the

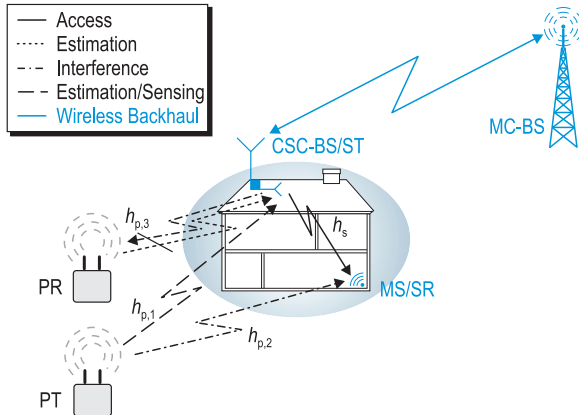


Figure 1.4: A cognitive small cell scenario demonstrating: (i) the CR systems employed at the CSC-BS, (ii) the associated network elements, which constitute Cognitive Small Cell-Base Station/Secondary Transmitter (CSC-BS/ST), Mobile Station/Secondary Receiver (MS/SR), Macro Cell-Base Station (MC-BS) and Primary Transmitter (PT), (iii) the interacting channels: sensing ($h_{p,1}$), interference ($h_{p,2}, h_{p,3}$) and access (h_s) channels.

variations introduced due to the estimation process, also treated as imperfect channel knowledge, may cause an *uncertain interference*³ to the primary systems. If not considered, this uncertain interference may severely degrade the performance of the CR systems. In order to approach a successful integration of channel estimation into the CR system, it is essential to consider these effects in the system model, which are non-existent in the models that consider the perfect knowledge of the involved channels. Taking these effects into account, the established analytical framework allow us to understand the performance of the CR system under situations that are much closer to realistic scenarios. Following these arguments, an analytical framework corresponding to the different CR systems is proposed. Subsequently, these frameworks are utilized to characterize the performance of the respective CR systems.

Shifting the focus back to the deployment, it is worthy to understand that the secondary access to the licensed spectrum is viable only if the CR system is

³The uncertain here symbolizes the interference that exists only because of the imperfect channel knowledge, which is not dealt in the literature.

equipped with the knowledge about to the primary system, thus, it is dependent on the wireless standard followed by the primary system. This signifies that a preliminary processing in the form of synchronization and demodulation of the baseband signal received from the primary system is necessary. The existence of multiple wireless standards and their complexity preclude us from deploying a dedicated circuitry corresponding to each primary system [27]. Under these circumstances, it is advisable to consider only those solutions that offer low complexity and show versatility towards different primary user signals. Generally speaking, such solutions will not only ease the deployment process but also has a large acceptance among the community. For instance, energy based detection has been a popular choice compared to its counterparts such as matched-filtering and cyclo-stationary based detection for detecting a PU signal, required for performing spectrum sensing for the interweave systems (discussed later in chapter 2). A direct comparison of these techniques by counting their implementations for hardware demonstration has been done in [10].



On similar grounds, in order to approach the channel estimation for the CR system, particularly for the channels that involve the primary systems, a receive power-based channel estimation technique is proposed as a part of the analytical framework in the thesis. This technique is introduced for substituting the conventional techniques such as pilot-based channel estimation, which exists in the literature, because, like energy detection, employing received power-based estimation assures the low complexity and the versatility towards unknown primary user signal requirements of the CR system and consequently facilitates its deployment. Besides, the channel within the secondary framework, treated as a conventional transmitter-receiver link, does not fall in the aforementioned category. Therefore, its knowledge is procured by employing a pilot-based channel estimation technique.

1.2 Main Contributions

At this stage, **it been** well-recognized that the knowledge of related channels is crucial for the application of CR techniques in practical scenarios. In order to facilitate the hardware deployment of a CSC, a CR application, this thesis capitalizes on the successful integration of this knowledge for different CR systems, namely interweave systems, underlay system and hybrid systems. In this context, the main contributions and the observations of this thesis (cf. Figure 1.5) are summarized as follows:

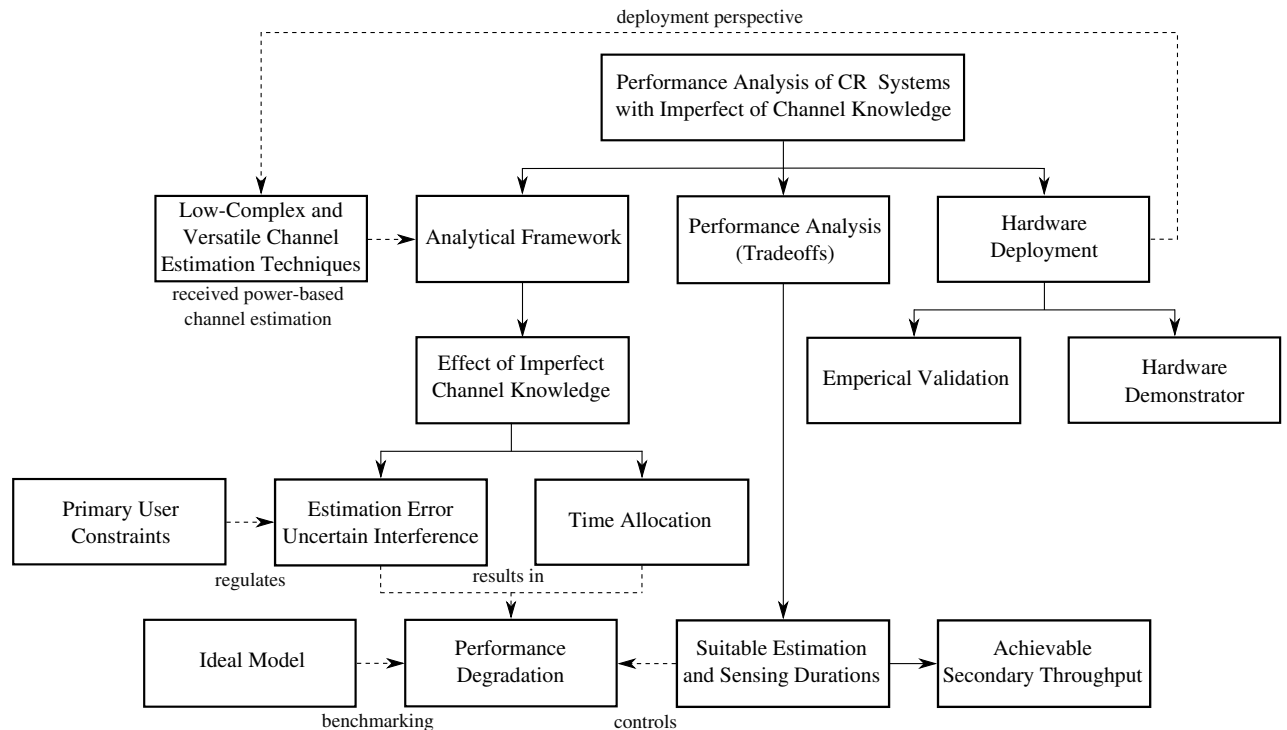


Figure 1.5: An illustration of the interconnect between the major contributions and the key observations.

- *Analytical Framework:* As a major contribution, this thesis proposes an analytical framework, corresponding to the different CR systems (which are followed in chapter 2, chapter 3 and chapter 4, respectively), that incorporates the estimation of the involved channels between the primary and the secondary systems. In order to satisfy the low complexity and versatility towards unknown Primary User (PU) signal requirements, which are necessary for the deployment of the CR systems, a received power-based channel estimation is included in the proposed framework. In addition, a careful allocation of the time interval, for the purpose of performing channel estimation, in the medium access of the secondary system is proposed. Apart from this, this thesis considers a probabilistic approach to tackling the variations in the CR system that arise due to the imperfect channel knowledge (estimation error). In contrast to the existing models that precludes⁴ channel estimation (or consider perfect channel knowledge), thereby overestimating the performance of the CR systems, this thesis captures a clear insight on the influence of the time allocation and the imperfect channel knowledge on performance of the CR system. Obviously, such an influence has an detrimental effect on the performance of the CR system, thus, leads to a *performance degradation*. This degradation is qualified through a comparison between the existing models and the estimation model, included as a part of the proposed framework. Particularly, the variations cause uncertain interference to the primary system, which in some situations could be deleterious to the primary system, are captured by means of novel constraints introduced as the part this framework. In order to closely examine the relationship between the system parameters, theoretical expressions pertaining to the performance analysis of the CR system are derived. Furthermore, to understand the performance of the proposed framework in fading scenarios, especially the interweave and the underlay systems, the analysis is extended to obtain the theoretical expressions that incur the effect of fading in the involved channels. Finally, to exclude any discrepancy in the analysis, the obtained expressions are validated by means of Monte-Carlo simulations.
- *Tradeoffs:* As a major outcome of the analysis, it has been identified that the estimation time is closely associated with the performance of the CR systems. On one side, it is related to the variations incurred in



⁴In context to the US, certain works have dealt with the issue of channel estimation in a CR system, however, unlike this thesis, the investigation has not been exhaustive. This issue is extensively outlined in chapter 3 under the section related work.

the system, whereby the level of uncertain interference induced in the system can be effectively controlled. While on the other side, it has a great influence on the throughput achieved at the SR. In this thesis, this kind of dual dependency of the performance parameters, classified as the uncertain interference and the secondary throughput (which are individually associated to the performance of primary and secondary system, respectively) on the estimation time has been investigated in the form of tradeoffs, namely *estimation-sensing-throughput* tradeoff for the IS and the HS, and *estimation-throughput* tradeoff for the US. These tradeoffs present a useful tool for visualizing the response of a CR system (in terms of performance) to different choices of the estimation time so that the performance degradation introduced due to the channel estimation can be effectively controlled. In other words, a system designer can utilize these tradeoffs to preclude situations under which the performance degradation becomes intolerable. Conversely, from a theoretical perspective, these tradeoffs can be used to determine a suitable estimation time that yields the maximum achievable throughput while fulfilling the related constraints.

- *Hardware deployment:* In contrast to the theoretical analysis, this thesis lays emphasis on the portability of the analytical framework on a hardware platform. To a great extent, this not only validates the accuracy of the assumptions made while deriving the theoretical expressions but also justifies the applicability of the proposed framework in realistic scenarios. With the implementation of the received power-based estimation technique, this thesis adds further justification to the claims such as the low-complexity and the versatility to unknown PU signals, presented while developing the analytical framework. Considering these facts, a software-defined radio platform is deployed for obtaining the measurements required for the validation process. In order to complement the validation, the theoretical expressions, which include the probability density functions that characterize the variations in the estimated parameters and the performance tradeoff are compared with their empirical counterparts. Besides validation, this thesis presents a demonstrator that certifies the necessity of channels' knowledge for the performance characterization as-well-as for the deployment of a CR system. In this regard, following the guidelines of an US, a demonstrator is deployed. As a part of the deployment process, in order to illustrate a successful deployment of the CR systems, this thesis identifies the key challenges and proposes the corresponding simplifications/solutions, which otherwise are left aside

in the proposed analysis.

1.3 Organization

Reconsider
er
while
revising
the individ-
ual chapters.
Also,
update
the
hyper-
links
to the
Sections
below.

The rest of the chapters in this thesis are organized as follows:

Chapter 2 develops an analytical framework that incorporates the estimation of involved channels in accordance with the interweave scenario. In this context, the indoor deployment scenario is transformed into an interweave scenario, whereby a spectrum sensing mechanism is employed at the CSC-BS (which represents the ST) that enables a secondary access to the licensed spectrum. Section 2.4 derives the theoretical expressions that captures the effect of imperfect channel knowledge on the performance. Further, Section 2.5 establishes an estimation-sensing-throughput tradeoff that depicts the suitable estimation and the suitable sensing time at which the maximum throughput is achieved by an IS.

Following a similar methodology as chapter 2, chapter 3 develops an analytical framework that incorporates the estimation of involved channels in accordance to the underlay scenario. To implement the underlay technique within the CSC, the deployment scenario is modified such that a power control mechanism is employed at the CSC-BS. As a part of the proposed framework, Section 3.2 derives the theoretical expressions for the power control and the secondary throughput, which captures the effect of imperfect channel knowledge and characterizes the performance of the US. The performance of a US is jointly characterized in terms of estimation-throughput tradeoff that determines the achievable throughput by an US.

Despite the interweave and the underlay systems, discussed in previous chapters (chapter 2 and chapter 3), propose different mechanisms (i.e., sensing and power control, respectively) of controlling the interference, individually these systems do not offer the best techniques of efficiently utilizing the licensed spectrum. In this regard, to promote the efficient usage of the licensed spectrum by the secondary users, the underlay and the interweave techniques are combined to realize a hybrid scenario. Motivated by this fact, chapter 4 develops an analytical framework that incorporates the estimation of involved channels with respect to the hybrid scenario. In this context, the indoor scenario is modified such that the CSC-BS employs spectrum sensing as-well-as power

control mechanism to perform secondary access to the licensed spectrum. The theoretical expressions derived in this chapter incorporates the effect of imperfect channel knowledge, and consequently depicts the performance of a HS. Analog to chapter 2, an estimation-sensing-throughput tradeoff that yields the achievable throughput for the HS is characterized in this chapter.

In order to reveal the ground truth regarding the analysis proposed in previous chapters, chapter 5 takes into account the deployment aspects of the proposed framework. In this regard, a hardware that implements the channel estimation, realizes the interference constraints, validates the performance analysis and illustrates the principle working of the US, is deployed.

Finally, chapter 6 summarizes the thesis and presents some extensions for the future.

CHAPTER 2

Interweave System

Secondary access to the licensed spectrum is viable only if the interference is avoided at the primary system. Among the different paradigms conceptualized in the literature, ISs have been extensively investigated. In order to enable interference-free access to the licensed spectrum, ISs employ spectrum sensing at the ST. Spectrum sensing (or only sensing) is necessary for detecting the presence or the absence of a PU signal. In this way, sensing assists the ISs in protecting the PRs against harmful interference. A sensing mechanism at the ST can be accomplished by listening to the signal transmitted by the PT. The existing models termed as baseline models investigated in the literature [28–30] characterize the performance of IS in terms of a sensing-throughput. However, this characterization assumes the perfect knowledge of the involved channels at the ST, which is unavailable in practice. Motivated by this fact, this chapter proposes a novel approach to incorporate channel estimation corresponding to the IS in the system model, and consequently investigates the impact of imperfect channel knowledge on the performance of the IS. More particularly, the variations induced in the detection probability affect the detector’s performance at the secondary transmitter. Since the detector installed at the ST is largely responsible for regulating the interference, uncertainty in its performance may result in severe interference at the PRs. In order to capture these uncertainty, an average constraint and an outage constraint on the detection probability are proposed. The analysis, which is based on [K5, K8, K9], reveals that with an appropriate choice of the estimation time determined by the proposed approach, the degradation in performance of the IS can be effectively controlled,

and subsequently the achievable secondary throughput can be significantly enhanced.

2.1 Related Work

For detecting a PU signal, several techniques such as energy detection, matched filtering, cyclostationary and feature-based detection exist [31, 32]. Because of its versatility towards unknown PU signals and its low computational complexity, energy detection has been extensively investigated in the literature [33–37]. In this technique, the decision is accomplished by comparing the power received at the ST to a decision threshold. In reality, the ST encounters variations in the received power due to the existence of thermal noise at the receiver and fading in the channel. Subsequently, these variations lead to sensing errors described as misdetection and false alarm, which limit the performance of the IS. In order to determine the performance of a detector, it is essential to obtain the expressions of detection probability and false alarm probability.

In particular, detection probability is critical for ISs because it protects the PR from the interference induced by the ST. As a result, the ISs have to ensure that they operate above a target detection probability [38]. Therefore, the characterization of the detection probability becomes absolutely necessary for the performance analysis of the IS. In this context, Urkowitz [33] introduced a probabilistic framework for characterizing the sensing errors, however, the characterization accounts only for the noise in the system. To encounter the variation caused by channel fading, a frame structure has been introduced in [28] assuming that the channel remains constant over the frame duration, however, upon exceeding the frame duration, the system may observe a different realization of the channel. Based on this frame structure, the performance of the IS has been investigated in terms of a deterministic channel [28–30] and a random channel¹ [34–36]. Complementing the analysis in [28–30], the involved channels are considered to be deterministic and random.

Besides the detection probability, false alarm probability has a large influence on the throughput achieved by the secondary system. Recently, the performance characterization of CR systems in terms of a sensing-throughput trade-off has received significant attention [28, 30, 39, 40]. According to Liang *et*

¹In the literature, deterministic and random channels are interpreted as path-loss and fading channels, respectively.

al. [28], the ST assures a reliable detection of a PU signal by retaining the detection probability above a desired level with an objective of maximizing the throughput at the SR. In this way, the sensing-throughput tradeoff depicts a suitable sensing time that achieves a maximum secondary throughput. However, to characterize the detection probability and the secondary throughput, the system requires the knowledge of interacting channels, namely, a *sensing* channel, an *access* channel and an *interference* channel, refer to Figure 5.1². The baseline models investigated in the literature assume the knowledge of these channels to be available at the ST. However, in practice, this knowledge is not available, thus, needs to be estimated by the secondary system. As a result, from a deployment perspective, the existing solutions for the IS are considered inaccurate for the performance analysis.

In practice, the knowledge about the involved channels can be estimated either (i) directly by using the conventional channel estimation techniques such as training sequence based [41] and pilot-based [42, 43] channel estimation or (ii) indirectly by estimating the received signal to noise ratio [44, 45]. It is worthy to note that the sensing and the interference channels represent the channels between two different (primary and secondary) systems. In this context, it becomes challenging to select the estimation methods in such a way that low complexity and versatility (towards different PU signals) requirements are satisfied. These issues, discussed later in Section 2.4.2, render the existing estimation techniques [41–45] unsuitable for hardware implementations. To this end, a received power-based estimation at the ST and at the SR for the sensing and the interference channels is employed, respectively. Considering the fact that the access channel corresponds to the link between the ST and the SR, conventional channel estimation techniques such as pilot-based channel estimation at the SR is employed.

Inherent to the estimation process, the variations due the channel estimation translate to the variations in the performance parameters, namely detection probability and secondary throughput. In particular, the variations induced in the detection probability causes uncertain interference at the PR, which may severely degrade the performance of a CR system. In this context, the performance characterization of an IS with imperfect channel knowledge remains an open problem. In this regard, this chapter focuses on the performance characterization of the IS in terms of sensing-throughput tradeoff taking these aforementioned aspects into account.

²As the interference to the PR is controlled by a regulatory constraint over the detection probability, in this view, the interaction with the PR is excluded in the considered scenario [28].

2.2 Contributions

The major contributions of this chapter can be summarized as follows:

2.2.1 Analytical framework

In contrast to the existing models that assume the perfect knowledge of the channels, the main goal of this chapter is to derive an analytical framework that constitutes the estimation of: (i) sensing channel at the ST, (ii) access channel and (iii) interference channel at the SR. Under this framework, a novel integration of the channel estimation in the secondary system's frame structure is proposed, according to which, the samples considered for channel estimation (of the sensing channel) are accounted also for the sensing such that the time resources within the frame are utilized efficiently. Furthermore, the estimation techniques are selected in such a way that the hardware complexity and the versatility towards unknown PU signals requirements (as considered while employing an energy based detection) are not compromised. In this context, a received power-based estimation for the sensing and the interference channels is proposed. Based on this framework, this chapter characterizes the performance of the IS by considering: (i) the variations due to imperfect channel knowledge and (ii) the performance degradation due to the inclusion of channel estimation. The proposed analytical framework is further complemented by considering a random behaviour of the interacting channels (or channel fading). Based on the derived expressions, the performance of the IS that employs channel estimation, where the interacting channels are subject to Nakagami- m fading, is evaluated.

2.2.2 Imperfect channel knowledge

In order to capture the variations induced due to imperfect channel knowledge, the cumulative distribution functions (cdfs) of performance parameters such as detection probability and achievable secondary throughput are characterized. More importantly, the cdf of the detection probability is utilized to incorporate two PU constraints, namely, an average constraint and an outage constraint on the detection probability. In this way, the proposed approach is able to control the amount of uncertainty in the interference caused at the PR due to the imperfect channel knowledge.

2.2.3 Estimation-sensing-throughput tradeoff

Subject to the average and the outage constraints, the expressions of the sensing-throughput tradeoff that capture the aforementioned variations and evaluate the performance loss (in terms of the achievable secondary throughput) are established. In particular, two different optimization approaches for countering the variations in sensing-throughput tradeoff and determining a suitable sensing time, which attains a maximum secondary throughput are proposed. Finally, a fundamental tradeoff between estimation time, sensing time and achievable secondary throughput is depicted. This tradeoff is exploited to determine a suitable estimation time and a suitable sensing time that depicts the maximum achievable performance of the IS. Besides, the variations due to the channel estimation and the channel fading are jointly captured by means of an outage constraint on the detection probability. Subsequently, an expression of the sensing-throughput tradeoff subject to the aforementioned constraint is obtained. In addition, an estimation-sensing-throughput tradeoff is established for the random scenario. In this regard, the estimation-sensing-throughput tradeoff is adapted to the scenarios with channel fading to determine the suitable estimation and the suitable sensing time such the maximum secondary throughput is achieved.

2.3 System Model

2.3.1 Deployment Scenario

To consider the applicability of IS, the CSC, a CR application illustrated in the previous chapter, is transformed into an interweave scenario. Considering the fact that the IS is employed at the CSC-BS, the CSC-BS and the MS represent a ST and a SR, respectively. A hardware prototype of the CSC-BS operating as IS was presented in [K1]. For simplification, a PU constraint based on false alarm probability was considered in [K1]. With the purpose of improving system's reliability, we extend the analysis to employ a PU constraint on the detection probability. Complementing the analysis depicted in [28], a slotted medium access for the IS is considered, where the time axis is segmented into frames of length T , according to which, the ST employs periodic sensing. Hence, each frame consists of a sensing slot τ_{sen} and the remaining duration

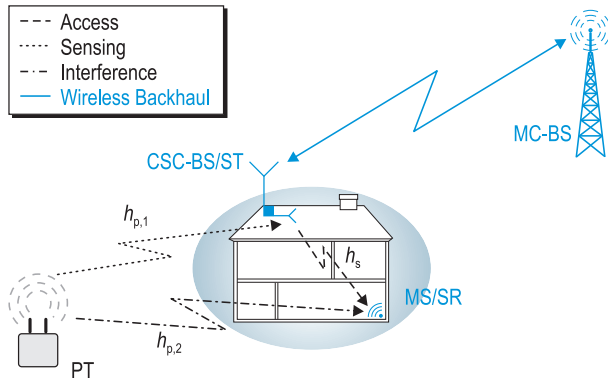


Figure 2.1: A cognitive small cell scenario demonstrating: (i) the interweave paradigm, (ii) the associated network elements, which constitute cognitive small cell-base station/secondary transmitter (CSC-BS/ST), mobile station/secondary receiver (MS/SR), macro cell-base station (MC-BS) and primary transmitter (PT), (iii) the interacting channels: sensing ($h_{p,1}$), access (h_s) and interference ($h_{p,2}$).

$T - \tau_{\text{sen}}$ is utilized for data transmission. For small T relative to the PUs' expected ON/OFF period, the requirement of the ST to be in alignment to PUs' medium access can be relaxed [46–48].

2.3.2 Signal model

Subject to the underlying hypothesis that illustrates the presence (\mathcal{H}_1) or the absence (\mathcal{H}_0) of a PU signal, the discrete and complex signal received at the ST is given by

$$y_{\text{ST}}[n] = \begin{cases} h_{p,1} \cdot x_{\text{PT}}[n] + w[n] & : \mathcal{H}_1 \\ w[n] & : \mathcal{H}_0 \end{cases}, \quad (2.1)$$

where $x_{\text{PT}}[n]$ corresponds to a discrete and complex sample transmitted by the PT, $|h_{p,1}|^2$ represents the power gain of the sensing channel for a given frame and $w[n]$ is circularly symmetric additive white Gaussian noise at the ST. According to [28], the signal $x_{\text{PT}}[n]$ transmitted by the PUs can be modelled as: (i) a phase shift keying modulated signal, or (ii) a Gaussian signal. The signals that are prone to high inter-symbol interference or entail precoding can be

modelled as Gaussian signals. In this chapter and the chapter 4 dedicated to the HS, the analysis is focussed on the latter case. In contrast, chapter 3 associated with the US considers the former case for the analysis. As a result, the mean and the variance for the signal and the noise are determined as $\mathbb{E}[x_{\text{PT}}[n]] = 0$, $\mathbb{E}[w[n]] = 0$, $\mathbb{E}[|x_{\text{PT}}[n]|^2] = \sigma_s^2$ and $\mathbb{E}[|w[n]|^2] = \sigma_w^2$. The channel $h_{p,1}$ is considered to be independent of $x_{\text{PT}}[n]$ and $w[n]$, thus, y_{ST} is also an independent and identically distributed (i.i.d.) random process.

Similar to (2.1), during data transmission, the discrete and complex received signal at the SR conditioned on the detection probability (P_d) and the false alarm probability (P_{fa}) is given by

$$y_{\text{SR}}[n] = \begin{cases} h_s \cdot x_{\text{ST}}[n] + h_{p,2} \cdot x_{\text{PT}}[n] + w[n] & : 1 - P_d \\ h_s \cdot x_{\text{ST}}[n] + w[n] & : 1 - P_{fa} \end{cases}, \quad (2.2)$$

where $x_{\text{ST}}[n]$ corresponds to discrete and complex sample transmitted by the ST. Further, $|h_s|^2$ and $|h_{p,2}|^2$ represent the power gains for the access and the interference channels, refer to Figure 5.1.

2.4 Problem Description and Proposed Approach

2.4.1 Problem Description

In accordance with the conventional frame structure, the ST performs sensing for a duration of τ_{sen} . The test statistics $T(\mathbf{y})$ at the ST is evaluated as

$$T(\mathbf{y}) = \frac{1}{\tau_{\text{sen}} f_s} \sum_{n=1}^{\tau_{\text{sen}} f_s} |y_{\text{ST}}[n]|^2 \begin{matrix} \mathcal{H}_1 \\ \geqslant \\ \mathcal{H}_0 \end{matrix} \mu, \quad (2.3)$$

where μ is the decision threshold and \mathbf{y} is a vector with $\tau_{\text{sen}} f_s$ samples. $T(\mathbf{y})$ represents a random variable, whereby the characterization of the distribution function depends on the underlying hypothesis. With regard to the Gaussian signal, $T(\mathbf{y})$ follows a central chi-squared (χ^2) distribution for both hypotheses \mathcal{H}_0 and \mathcal{H}_1 [49]. As a result, the detection probability (P_d) and the false alarm probability (P_{fa}) corresponding to (2.3) are determined as [50]

$$P_d(\mu, \tau_{\text{sen}}, P_{\text{Rx,ST}}) = \Gamma \left(\frac{\tau_{\text{sen}} f_s}{2}, \frac{\tau_{\text{sen}} f_s \mu}{2 P_{\text{Rx,ST}}} \right), \quad (2.4)$$

2.4 Problem Description and Proposed Approach

$$P_{fa}(\mu, \tau_{sen}) = \Gamma\left(\frac{\tau_{sen}f_s}{2}, \frac{\tau_{sen}f_s\mu}{2\sigma_w^2}\right), \quad (2.5)$$

where $P_{Rx,ST}$ is the power received over the sensing channel and $\Gamma(\cdot, \cdot)$ represents a regularized upper-incomplete Gamma function [51].

Following the characterization of P_{fa} and P_d , Liang *et al.* [28] established a tradeoff between the sensing time and the secondary throughput (R_s) subject to a target detection probability (\bar{P}_d). This tradeoff is represented as

$$R_s(\tilde{\tau}_{sen}) = \max_{\tau_{sen}} R_s(\tau_{sen}) = \frac{T - \tau_{sen}}{T} \left[C_0(1 - P_{fa})\mathbb{P}(\mathcal{H}_0) + C_1(1 - P_d)\mathbb{P}(\mathcal{H}_1) \right], \quad (2.6)$$

$$\text{s.t. } P_d \geq \bar{P}_d, \quad (2.7)$$

$$\text{where } C_0 = \log_2 \left(1 + |h_s|^2 \frac{P_{Tx,ST}}{\sigma_w^2} \right) = \log_2 (1 + \gamma_s) \quad (2.8)$$

$$\begin{aligned} \text{and } C_1 &= \log_2 \left(1 + \frac{|h_s|^2 P_{Tx,ST}}{|h_{p,2}|^2 P_{Tx,PT} + \sigma_w^2} \right) \\ &= \log_2 \left(1 + \frac{|h_s|^2 P_{Tx,ST}}{P_{Rx,SR}} \right) = \log_2 \left(1 + \frac{\gamma_s}{\gamma_{p,2} + 1} \right), \end{aligned} \quad (2.9)$$

where $\mathbb{P}(\mathcal{H}_0)$ and $\mathbb{P}(\mathcal{H}_1)$ are the occurrence probabilities for the respective hypothesis, whereas $\gamma_{p,1}$ and γ_s represent the signal to noise ratio for the links PT-ST and ST-SR, respectively, and $\gamma_{p,2}$ corresponds to interference (from the PT) to noise ratio for the link PT-SR. Moreover, $P_{Tx,PT}$ and $P_{Tx,ST}$ represent the transmit power at the PT and the ST, whereas $P_{Rx,SR}$ corresponds to the received power (which includes the interference power from the PT and the noise power) at the SR. In addition, C_0 and C_1 represent the data rate without and with the interference from the PT. In other words, using (2.6), the ST determines a suitable sensing time $\tau_{sen} = \tilde{\tau}_{sen}$, such that the secondary throughput is maximized subject to a target detection probability, refer to (2.7). From the deployment perspective, the tradeoff depicted above has the following fundamental issues:

- Without the knowledge of the received power $P_{Rx,ST}$ over the sensing channel, it is not feasible to characterize P_d , refer to (4.2). This leaves the characterization of the throughput (2.6) impossible and the constraint defined in (2.7) inappropriate.

- Moreover, the knowledge of the interference and the access channels is required at the ST, refer to (4.8) and (4.9) for characterizing the throughput in terms of C_0 and C_1 at the SR.

Taking these issues into account, it is not feasible to employ the performance analysis depicted by this model (referred as ideal model, hereafter) for hardware implementation. In the subsequent section, an analytical framework (also referred as estimation model) that addresses the aforementioned issues, thereby including the estimation of the sensing channel at the ST, and the interference and the access channels at the SR is proposed. Based on the proposed approach, the performance of the IS in terms of the sensing-throughput tradeoff is investigated.

2.4.2 Proposed Approach

In order to overcome the difficulties discussed in Section 2.4.1, the following strategy is proposed.

1. As a first step, the estimation of the involved channels is considered. In order to characterize the detection probability, a received power-based estimation at the ST for the sensing channel is employed. This is done to ensure that the detection probability remains above a desired level. Further, a pilot-based estimation and a received power-based estimation for the access channel and the interference channel, respectively, are employed at the SR, to characterize the secondary throughput.
2. Next, the variations due to channel estimation in the estimated parameters, namely, received power (for the sensing and the interference channels) and the power gain (for the access channel) are characterized in terms of their cdfs.
3. In order to investigate the performance of the IS subject to the channel estimation, these variations in the performance parameters, which include the detection probability and the secondary throughput, are characterized in terms of their cdfs.
4. Finally, the derived cdfs are utilized to obtain the expressions of sensing-throughput tradeoff. Hence, based on these expressions, the impact of imperfect channel knowledge on the performance of the ISs is qualified, and subsequently the achievable secondary throughput at a suitable sensing time is determined.

Considering the channel estimation, it is well-known that systems with transmitter information (which includes the filter parameters, pilot symbols, modulation type and time-frequency synchronization) at the receiver acquire the channel knowledge by listening to the pilot data sent by the ST [42, 43, 52, 53]. Other systems, where the receiver possesses either no access to this information or limited by hardware complexity, procure channel knowledge indirectly by estimating a different parameter that entails the channel knowledge, for instance, received signal power [K5] or received signal to noise ratio [44, 45]. Recently, estimation techniques such as pilot-based estimation [54, 55] and received power-based estimation [K6] have been applied to obtain channel knowledge for the CR systems. However, the performance analysis has been limited to the underlay systems, where the emphasis has been given on modelling the interference at the PR.

Since the pilot-based estimation requires the knowledge of the PU signal at the secondary system, the versatility (in terms of PU signals) of the secondary system is compromised. On the other side, for the estimation of the received signal to noise ratio, Eigenvalue (which involves matrix operations) based approach [45] or iterative approaches such as expectation-maximization have been proposed [44]. Due to the complicated mathematical operations or the complexity of the iterative algorithms, such approaches tend to increase the hardware complexity of the ISs. In order to resolve these issues, a received power-based estimation for the sensing and the interference channels, and a pilot-based estimation for the access channel is employed. Similar to the energy based detection, since the received power-based estimation involves simple operations on the obtained samples such as magnitude squared followed by summation, the proposed estimation provides a reasonable tradeoff between complexity and versatility.

However, with the inclusion of this channel estimation, the system anticipates: (i) a performance loss in terms of temporal resources used and (ii) variations in the aforementioned performance parameters. A preliminary analysis of this performance loss was carried out in [K5], where it was revealed that in low signal to noise ratio regime, imperfect knowledge of received power corresponds to a large variation in the detection probability, hence, causes a severe degradation in the performance of the IS. However, this performance degradation was determined by means of lower and upper bounds. In this chapter, a more exact analysis is considered, whereby the variations in detection probability are captured by characterizing its cdf, and subsequently apply new probabilistic constraints on the detection probability, which allow ISs to operate at low signal to noise ratio regime.

In order to include channel estimation, a frame structure that constitutes estimation τ_{est} , sensing τ_{sen} and data transmission $T - \tau_{\text{sen}}$ is proposed, where τ_{est} and τ_{sen} correspond to time intervals and $0 < \tau_{\text{est}} \leq \tau_{\text{sen}} < T$, refer to Figure 4.2. Since the estimated values of the interacting channels are required for determining the suitable sensing time (the duration of the sensing phase), the sequence depicted in Figure 4.2, whereby estimation followed by sensing is reasonable for the hardware deployment. Particularly for the sensing channel, it is worthy to note that the samples used for estimation can be combined with the samples acquired for sensing³ such that the time resources within the frame duration can be utilized efficiently, as shown in the frame structure in Figure 4.2. To acquire the estimates for the interference and the access channels at the ST, a low-rate feedback channel from the SR to the ST is required for the proposed approach. In the following paragraphs, the estimation of the involved channels is considered.

Estimation of sensing channel ($h_{p,1}$)

Following the previous discussions, the ST acquires the knowledge of $h_{p,1}$ by estimating its received power. The estimated received power is required for the characterization of P_d , thereby evaluating the detector performance.

Under \mathcal{H}_1 , the received power-based estimated during the estimation phase at the ST is given as [33]

$$\hat{P}_{\text{Rx,ST}} = \frac{1}{\tau_{\text{est}} f_s} \sum_{n=1}^{\tau_{\text{est}} f_s} |y_{\text{ST}}[n]|^2. \quad (2.10)$$

$\hat{P}_{\text{Rx,ST}}$ determined in (2.10) using $\tau_{\text{est}} f_s$ samples follows a central chi-squared distribution χ^2 [49]. The cdf of $\hat{P}_{\text{Rx,ST}}$ is given by

$$F_{\hat{P}_{\text{Rx,ST}}}(x) = 1 - \Gamma\left(\frac{\tau_{\text{est}} f_s}{2}, \frac{\tau_{\text{est}} f_s x}{2 P_{\text{Rx,ST}}}\right). \quad (2.11)$$

Estimation of access channel (h_s)

The signal received from the ST undergoes matched filtering and demodulation at the SR, hence, it is reasonable to employ pilot-based estimation for h_s . Unlike received power-based estimation, pilot-based estimation renders a direct

³Therefore, the sensing phase incorporates the estimation phase, see Figure 4.2.

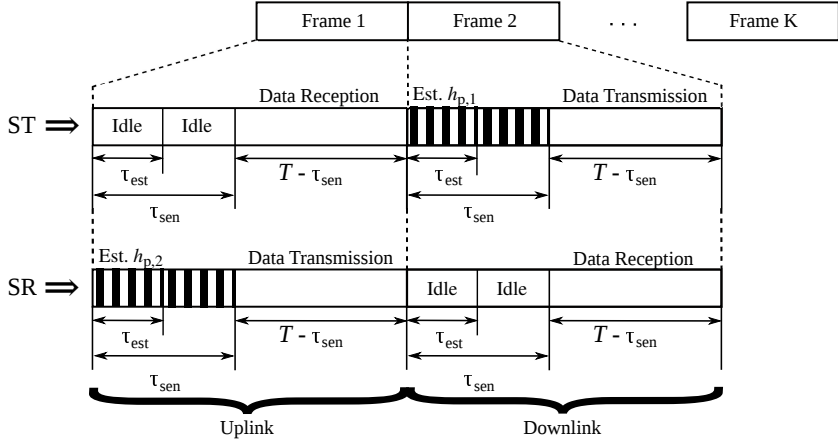


Figure 2.2: Frame structure of the IS illustrating the time allocation of the channel estimation, sensing and data transmission from the perspective of the ST and the SR. Corresponding to the uplink and the downlink, the sensing ($h_{p,1}$) and the interference channel ($h_{p,2}$) estimation occur at the ST and the SR, respectively. The estimation of the access channel (h_s) happens at the SR. Because of the employment of pilot-based channel estimation, the time resources allocated (number of sample used) for its estimation relatively less as compared to the previous two channels used for the channel estimation, it is not considered in the frame structure.

estimation of the channel. Now, to accomplish pilot-based estimation, the SR aligns itself to pilot symbols transmitted by the ST. Under \mathcal{H}_0 , the discrete and complex pilot symbols at the output of the demodulator is given by [43]

$$p[n] = \sqrt{E_s} h_s + w[n], \quad (2.12)$$

where E_s denotes the pilot energy. Without loss of generality, the pilot symbols are considered to be +1. The maximum likelihood estimate, representing a sample average of N_s pilot symbols, is given by [42]

$$h_s = \hat{h}_s + \underbrace{\frac{\sum_n^{N_s} p[n]}{2N_s}}_{\epsilon}, \quad (2.13)$$

where ϵ denotes the estimation error. The estimate \hat{h}_s is unbiased, efficient and

achieves a Cramér-Rao bound with equality, with variance $\mathbb{E} \left[|\hat{h}_s - h_s|^2 \right] = \sigma_w^2 / (2N_s)$ [43]. Consequently, \hat{h}_s conditioned on h_s follows a Gaussian distribution.

$$\hat{h}_s | h_s \sim \mathcal{N} \left(h_s, \frac{\sigma_w^2}{2N_s} \right). \quad (2.14)$$

As a result, the power gain $|\hat{h}_s|^2$ follows a non-central chi-squared (χ_1^2) distribution with 1 degree of freedom and non-centrality parameter $\lambda_s = \frac{2N_s|h_s|^2}{\sigma_w^2}$.

Estimation of interference channel ($h_{p,2}$)

Analog to the sensing channel, the SR performs received power-based estimation by listening to the transmission from the PT. The knowledge of $h_{p,2}$ is required to characterize the interference from the PT. Under \mathcal{H}_1 , the discrete signal model at the SR is given as

$$y_{SR}[n] = h_{p,2} \cdot x_{PT}[n] + w[n]. \quad (2.15)$$

The received power at the SR from the PT given by

$$\hat{P}_{Rx,SR} = \frac{1}{N_{p,2}} \sum_{n=1}^{N_{p,2}} |y_{SR}[n]|^2, \quad (2.16)$$

follows a χ^2 distribution, where $N_{p,2}$ corresponds to the number of samples used for the estimation.

2.4.3 Validation

It is now clear that the estimates $\hat{P}_{Rx,ST}$, $|\hat{h}_s|^2$ and $\hat{P}_{Rx,SR}$ exhibit the knowledge corresponding to the involved channels, however, it is essential to validate them, mainly $\hat{P}_{Rx,ST}$ and $\hat{P}_{Rx,SR}$. In this context, it is necessary to ensure the presence of the PU signal (\mathcal{H}_1) for that particular frame. In this direction, Chavali *et al.* [44] recently proposed a detection followed by the estimation of the signal to noise ratio, while [56] implemented a blind technique for estimating the signal power of non-coherent PU signals. In this thesis, a different

methodology is proposed, according to which, a coarse detection⁴ on the estimates $\hat{P}_{\text{Rx},\text{ST}}$, $\hat{P}_{\text{Rx},\text{SR}}$ at the end of the estimation phase τ_{est} is applied. Through an appropriate selection of the time interval τ_{est} (for instance, $\tau_{\text{est}} \in [1, 10]\text{ms}$) during the system design, the reliability of the coarse detection can be ensured. With the existence of a separate control channel such as cognitive pilot channel, the reliability of the coarse detection can be further enhanced by exchanging the detection results between the ST and the SR.

Since the estimation and the coarse detection processes in the proposed method are equivalent in terms of their mathematical operations (which include magnitude squared and summation), the validity of the channel estimates with certain reliability and without comprising the complexity of the estimators employed by the secondary system is considered. Moreover, by performing a joint estimation and (coarse) detection, an efficient way of utilizing the time resources within the frame duration is proposed. The ST considers these estimates to determine a suitable sensing time based on the sensing-throughput tradeoff such that the desired detector's performance is ensured. At the end of the detection phase, a fine detection⁵ of the PU signals is carried out, thereby improving the performance of the detector.

2.4.4 Assumptions and Approximations

To simplify the analysis and sustain analytical tractability for the proposed approach, several assumptions considered in the chapter are summarized as follows:

- All transmitted signals are subjected to distance dependent path loss and small scale fading gain. With no loss of generality, it is considered that the channel gains include distance dependent path loss and small scale gain. Moreover, the coherence time for the channel gain is considered to be greater than the frame duration⁶.
- Perfect knowledge of the noise power is assumed in the system, however, the uncertainty in noise power can be captured as a bounded interval [50]. Inserting this interval in the derived expressions, refer to Section 2.5, the

⁴For the coarse detection, an energy detection is employed whose threshold can be determined by means of a constant false alarm rate.

⁵In accordance with the proposed frame structure in Fig. 2, fine detection represents the main detection which also includes the samples acquired during the estimation phase.

⁶In the scenarios where the coherence time exceeds the frame duration, in such cases, the proposed characterization depicts a lower performance bound.

performance of the IS can be expressed in terms of the upper and the lower bounds.

- For all degrees of freedom, \mathcal{X}_1^2 distribution can be approximated by Gamma distribution [57]. The parameters of the Gamma distribution are obtained by matching the first two central moments to those of \mathcal{X}_1^2 .

2.5 Theoretical Analysis

2.5.1 Deterministic Channel

At first, the performance of the proposed framework in context to the deterministic channel is evaluated. It is evident that the variation due to the imperfect channel knowledge translates to the variations in the performance parameters \hat{P}_d , \hat{C}_0 and \hat{C}_1 , which are fundamental to sensing-throughput tradeoff. Below, these variations are captured by characterizing their cdfs $F_{\hat{P}_d}$, $F_{\hat{C}_0}$ and $F_{\hat{C}_1}$, respectively.

Lemma 1 The cdf of \hat{P}_d is characterized as

$$F_{\hat{P}_d}(x) = 1 - \Gamma\left(\frac{\tau_{\text{est}}f_s}{2}, \frac{\tau_{\text{est}}\tau_{\text{sen}}f_s^2\mu}{4P_{\text{Rx,ST}}\Gamma^{-1}(x, \frac{\tau_{\text{sen}}f_s}{2})}\right), \quad (2.17)$$

where $\Gamma^{-1}(\cdot, \cdot)$ is inverse function of regularized upper-incomplete Gamma function [51].

Proof: The cdf of \hat{P}_d is defined as

$$F_{\hat{P}_d}(x) = \mathbb{P}(\hat{P}_d \leq x). \quad (2.18)$$

Using (4.2)

$$= \mathbb{P}\left(\Gamma\left(\frac{\tau_{\text{sen}}f_s}{2}, \frac{\tau_{\text{sen}}f_s\mu}{2\hat{P}_{\text{Rx,ST}}}\right) \leq x\right), \quad (2.19)$$

$$= 1 - \mathbb{P}\left(\hat{P}_{\text{Rx,ST}} \geq \frac{\mu\tau_{\text{sen}}f_s}{2\Gamma^{-1}\left(x, \frac{\tau_{\text{sen}}f_s}{2}\right)}\right). \quad (2.20)$$

Replacing the cdf of $\hat{P}_{\text{Rx,ST}}$ in (2.20), an expression of $F_{\hat{P}_d}$ is obtained. ■

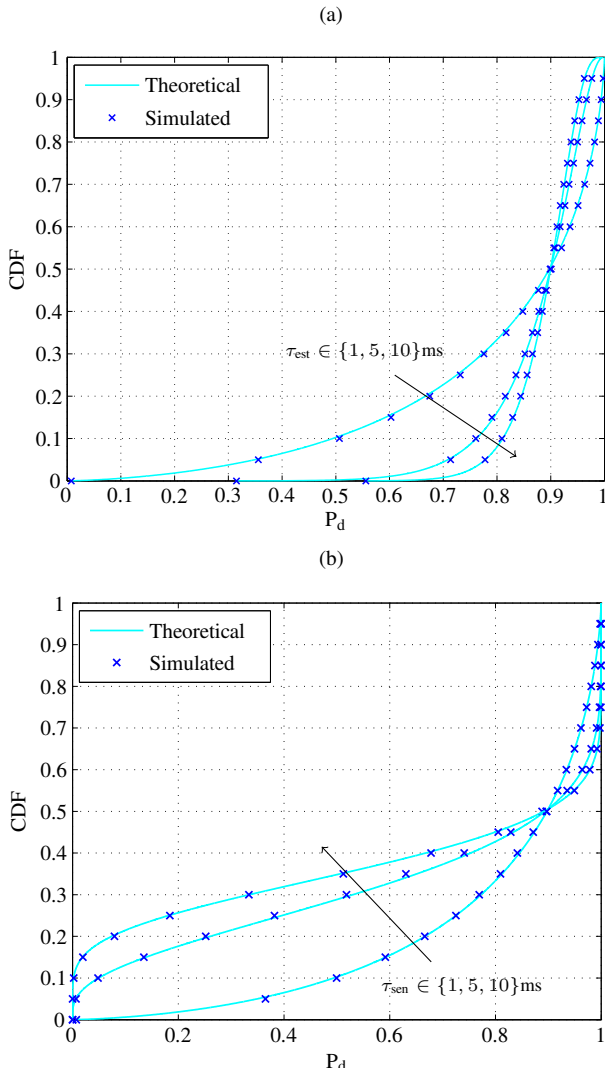


Figure 2.3: The cdf of \hat{P}_d for different τ_{est} and τ_{sen} . (a) $\tau_{\text{est}} \in \{1, 5, 10\} \text{ ms}$ and $\tau_{\text{sen}} = 1 \text{ ms}$, (b) $\tau_{\text{est}} = 1 \text{ ms}$ and $\tau_{\text{sen}} \in \{1, 5, 10\} \text{ ms}$.

Lemma 2 The cdf of \hat{C}_0 is defined as

$$F_{\hat{C}_0}(x) = \int_0^x f_{\hat{C}_0}(t)dt, \quad (2.21)$$

where

$$f_{\hat{C}_0}(x) = 2^x \ln 2 \frac{(2^x - 1)^{a_s - 1}}{\Gamma(a_s)b_s^{a_s}} \exp\left(-\frac{2^x - 1}{b_s}\right), \quad (2.22)$$

and

$$\begin{aligned} a_s &= \frac{\left(\frac{\sigma_w^4}{2N_s P_{Tx,ST}} + |h_s|^2\right)^2}{\frac{\sigma_w^4}{2N_s P_{Tx,ST}} \left(2\frac{\sigma_w^4}{2N_s P_{Tx,ST}} + 4|h_s|^2\right)} \text{ and} \\ b_s &= \frac{\frac{\sigma_w^4}{2N_s P_{Tx,ST}} \left(2\frac{\sigma_w^4}{2N_s P_{Tx,ST}} + 4|h_s|^2\right)}{\left(\frac{\sigma_w^4}{2N_s P_{Tx,ST}} + |h_s|^2\right)}. \end{aligned} \quad (2.23)$$

Proof: See Section 2.8.1 ■

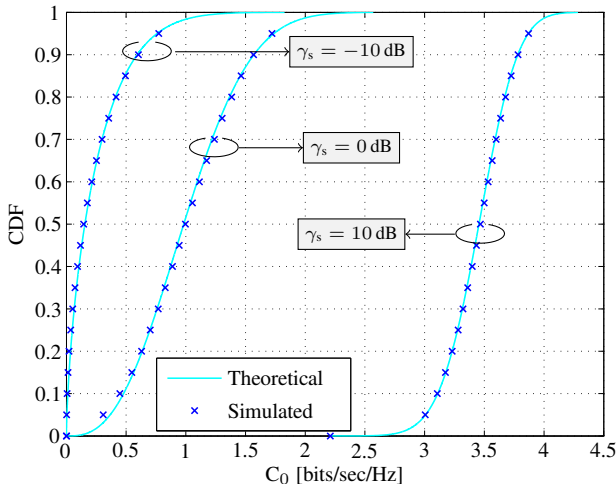


Figure 2.4: The cdf of \hat{C}_0 for different values of $\gamma_s \in \{-10, 0, 10\}$ dB.

Lemma 3 The cdf of \hat{C}_1 is given by

$$F_{\hat{C}_1}(x) = \int_0^x f_{\hat{C}_1}(t)dt, \quad (2.24)$$

where

$$f_{\hat{C}_1}(x) = 2^x \ln 2 \frac{(2^x - 1)^{a_s - 1} \Gamma(a_s + a_2)}{\Gamma(a_s) \Gamma(a_2) b_s^{a_s} b_2^{a_2}} \left(\frac{1}{b_2} + \frac{2^x - 1}{b_s} \right)^{(a_s + a_2)}, \quad (2.25)$$

and

$$a_2 = \frac{N_{p,2}}{2} \text{ and } b_2 = \frac{2P_{Rx,SR}}{\sigma_w^2 N_{p,2}}, \quad (2.26)$$

where a_s and b_s are defined in (2.23). ■

Proof: See Section 2.8.2 ■

The theoretical expressions of the cdfs depicted in Lemma 4, Lemma 5 and Lemma 6 are validated by means of simulations in Figure 2.3, Figure 2.4 and Figure 2.5, respectively, with different choices of system parameters, these include $\tau_{est} \in \{1, 5, 10\}$ ms, $\tau_{sen} = \{1, 5, 10\}$ ms, $\gamma_s \in \{-10, 0, 10\}$ dB and $\gamma_{p,2} \in \{-10, 0, 10\}$ dB.

Next, a sensing-throughput tradeoff for the estimation model is established that includes the estimation time and incorporates variations in the performance parameter. Most importantly, to restrain the harmful effect of the uncertain interference at the PR due to the variations in the detection probability, two new PU constraints at the PR, namely, an average constraint and an outage constraint on the detection probability are proposed. Based on these constraints, the sensing-throughput tradeoff for the IS is characterized.

Theorem 1 Subject to an average constraint on \hat{P}_d , the sensing-throughput tradeoff for the IS that employs channel estimation corresponding to the de-

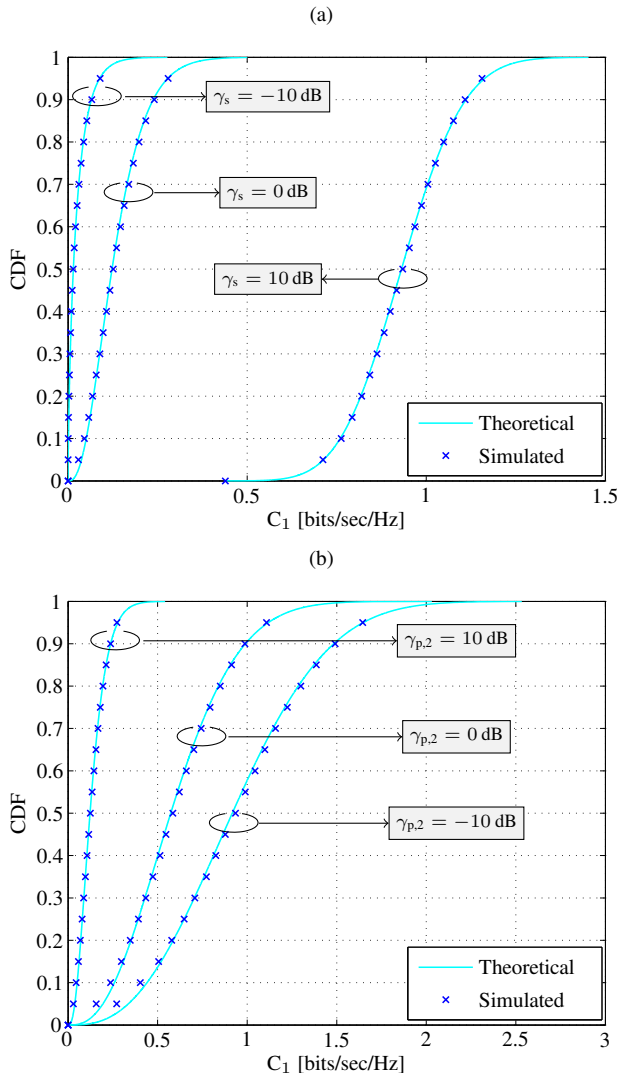


Figure 2.5: The cdf of \hat{C}_1 for different γ_s and $\gamma_{p,2}$. (a) $\gamma_s \in \{-10, 0, 10\} \text{ dB}$ and $\gamma_{p,2} = 10 \text{ dB}$, (b) $\gamma_s = 0 \text{ dB}$ and $\gamma_{p,2} \in \{-10, 0, 10\} \text{ dB}$.

deterministic behavior of the interacting channels, is given by

$$\begin{aligned} R_s(\tilde{\tau}_{\text{est}}, \tilde{\tau}_{\text{sen}}) &= \max_{\tau_{\text{est}}, \tau_{\text{sen}}} \mathbb{E}_{\hat{P}_d, \hat{C}_0, \hat{C}_1} [R_s(\tau_{\text{est}}, \tau_{\text{sen}})], \\ &= \frac{T - \tau_{\text{sen}}}{T} \left[\mathbb{E}_{\hat{C}_0} [\hat{C}_0] (1 - P_{\text{fa}}) \mathbb{P}(\mathcal{H}_0) + \right. \\ &\quad \left. \mathbb{E}_{\hat{C}_1} [\hat{C}_1] (1 - \mathbb{E}_{\hat{P}_d} [\hat{P}_d]) \mathbb{P}(\mathcal{H}_1) \right], \end{aligned} \quad (2.27)$$

$$\text{s.t. } \mathbb{E}_{\hat{P}_d} [\hat{P}_d] \geq \bar{P}_d, \quad (2.28)$$

$$\text{s.t. } 0 < \tau_{\text{est}} \leq \tau_{\text{sen}} \leq T,$$

where $\mathbb{E}_{\hat{P}_d} [\cdot]$ represents the expectation with respect to \hat{P}_d , $\mathbb{E}_{\hat{P}_d, \hat{C}_0, \hat{C}_1} [\cdot]$ denotes the expectation with respect to \hat{P}_d , \hat{C}_0 and \hat{C}_1 . Unlike (2.7), \bar{P}_d in (2.27) represents the constraint on expected detection probability.

Proof: See Section 2.8.3 For simplification, the proof of Theorem 5 is included in the proof of Theorem 2. \blacksquare

Theorem 2 Subject to an outage constraint on \hat{P}_d , the sensing-throughput trade-off for the IS that employs channel estimation corresponding to the deterministic behavior of the interacting channels, is given by

$$\begin{aligned} R_s(\tilde{\tau}_{\text{est}}, \tilde{\tau}_{\text{sen}}) &= \max_{\tau_{\text{est}}, \tau_{\text{sen}}} \mathbb{E}_{\hat{P}_d, \hat{C}_0, \hat{C}_1} [R_s(\tau_{\text{est}}, \tau_{\text{sen}})], \\ &= \frac{T - \tau_{\text{sen}}}{T} \left[\mathbb{E}_{\hat{C}_0} [\hat{C}_0] (1 - P_{\text{fa}}) \mathbb{P}(\mathcal{H}_0) + \right. \\ &\quad \left. \mathbb{E}_{\hat{C}_1} [\hat{C}_1] (1 - \mathbb{E}_{\hat{P}_d} [\hat{P}_d]) \mathbb{P}(\mathcal{H}_1) \right], \end{aligned} \quad (2.29)$$

$$\text{s.t. } \mathbb{P}(\hat{P}_d \leq \bar{P}_d) \leq \rho_d, \quad (2.30)$$

$$\text{s.t. } 0 < \tau_{\text{est}} \leq \tau_{\text{sen}} \leq T,$$

where ρ_d represents the outage constraint.

Proof: See Section 2.8.3 \blacksquare

In contrast to the ideal model, the sensing-throughput tradeoff investigated by the estimation model (refer to Theorems 5 and 2) incorporates the imperfect channel knowledge, in this context, the performance characterization considered by the proposed framework are closer to the realistic situations.

Remark 1 Herein, based on the estimation model, a fundamental relation between estimation time (regulates the variation in the detection probability according to the PU constraint), sensing time (represents the detector performance) and achievable throughput is established, this relationship is characterized as *estimation-sensing-throughput tradeoff*. Based on this tradeoff, a suitable estimation $\tau_{\text{est}} = \tilde{\tau}_{\text{est}}$ and a suitable sensing time $\tau_{\text{sen}} = \tilde{\tau}_{\text{sen}}$ that attains a maximum achievable throughput $R_s(\tilde{\tau}_{\text{est}}, \tilde{\tau}_{\text{sen}})$ for the IS is determined.

Corollary 1 Theorems 5 and 2 consider the optimization of the average throughput to incorporate the effect of variations due to the channel estimation, and subsequently determine the suitable sensing and the suitable estimation time. Here, an alternative approach to the optimization problem described in (2.6) is investigated to capture these variations, whereby for a certain estimation time τ_{est} , the suitable sensing time subject to the average constraint is determined as

$$\begin{aligned} \tilde{\tau}_{\text{sen}} &= \underset{\tau_{\text{sen}}}{\operatorname{argmax}} R_s(\tau_{\text{est}}, \tau_{\text{sen}}), \\ &= \frac{T - \tau_{\text{sen}}}{T} \left[\hat{C}_0(1 - P_{\text{fa}})\mathbb{P}(\mathcal{H}_0) + \hat{C}_1(1 - \hat{P}_{\text{d}})\mathbb{P}(\mathcal{H}_1) \right], \\ \text{s.t. } &\mathbb{E}_{\hat{P}_{\text{d}}} \left[\hat{P}_{\text{d}} \right] \geq \bar{P}_{\text{d}}, \\ \text{s.t. } &0 < \tau_{\text{est}} \leq \tau_{\text{sen}} \leq T. \end{aligned} \quad (2.31)$$

Similarly, the suitable sensing time subject to the outage constraint is determined as

$$\begin{aligned} \tilde{\tau}_{\text{sen}} &= \underset{\tau_{\text{sen}}}{\operatorname{argmax}} R_s(\tau_{\text{est}}, \tau_{\text{sen}}), \\ &= \frac{T - \tau_{\text{sen}}}{T} \left[\hat{C}_0(1 - P_{\text{fa}})\mathbb{P}(\mathcal{H}_0) + \hat{C}_1(1 - \hat{P}_{\text{d}})\mathbb{P}(\mathcal{H}_1) \right], \\ \text{s.t. } &\mathbb{P}(\hat{P}_{\text{d}} \leq \bar{P}_{\text{d}}) \leq \rho_{\text{d}}, \\ \text{s.t. } &0 < \tau_{\text{est}} \leq \tau_{\text{sen}} \leq T. \end{aligned} \quad (2.32)$$

In contrast to (2.27) and (2.29), the suitable sensing time evaluated in (2.31) and (2.32) entails the variations due to the channel estimation from the performance parameters $(\hat{P}_{\text{d}}, \hat{C}_0, \hat{C}_1)$. Hence, the secondary throughput subject to the average and the outage constraints captures the variations in the suitable sensing time and the performance parameters is determined as

$$\mathbb{E}_{\hat{P}_{\text{d}}, \hat{C}_0, \hat{C}_1, \tilde{\tau}_{\text{sen}}} [R_s(\tau_{\text{est}}, \tilde{\tau}_{\text{sen}})], \quad (2.33)$$

where $\mathbb{E}_{\hat{P}_d, \hat{C}_0, \hat{C}_1, \tilde{\tau}_{\text{sen}}} [\cdot]$ corresponds to an expectation over $\hat{P}_d, \hat{C}_0, \hat{C}_1, \tilde{\tau}_{\text{sen}}$. Following Remark 3, the average secondary throughput, defined in (2.33), are further optimized over the estimation time

$$R_s(\tilde{\tau}_{\text{est}}, \tilde{\tau}_{\text{sen}}) = \max_{\tau_{\text{est}}} \mathbb{E}_{\hat{P}_d, \hat{C}_0, \hat{C}_1, \tilde{\tau}_{\text{sen}}} [R_s(\tau_{\text{est}}, \tilde{\tau}_{\text{sen}})]. \quad (2.34)$$

In this way, an estimation-sensing-throughput tradeoff for the alternative approach is established that determines the suitable estimation time.

Remark 2 Complementing the analysis in [28], it is complicated to obtain a closed-form expression of $\tilde{\tau}_{\text{sen}}$, thereby rendering the analytical tractability of its cdf difficult. In view of this, the performance of the alternative approach is captured by means of simulations.

2.5.2 Random Channel

In this section, the purpose is to extend the performance analysis of the proposed framework, where the interacting channels encounter quasi-static block fading. In this view, the channel gains $|h_{p,1}|^2$, $|h_{p,2}|^2$ and $|h_s|^2$ according to Nakagami- m fading model are characterized. As a consequence, the power gains $|h_{p,1}|^2$, $|h_{p,2}|^2$ and $|h_s|^2$ follow a Gamma distribution [24], whose corresponding cdfs are defined as

$$F_{|h_{p,1}|^2}(x) = 1 - \Gamma\left(m_{p,1}, \frac{m_{p,1}x}{|h_{p,1}|^2}\right), \quad (2.35)$$

$$F_{|h_{p,2}|^2}(x) = 1 - \Gamma\left(m_{p,2}, \frac{m_{p,2}x}{|h_{p,2}|^2}\right), \quad (2.36)$$

$$F_{|h_s|^2}(x) = 1 - \Gamma\left(m_s, \frac{m_s x}{|h_s|^2}\right), \quad (2.37)$$

where $m_{p,1}$, $m_{p,2}$ and m_s represent the Nakagami- m parameter for $|h_{p,1}|^2$, $|h_{p,2}|^2$ and $|h_s|^2$, respectively, and $\Gamma(\cdot, \cdot)$ is a regularized upper-incomplete Gamma function [57].

Perfect Channel Knowledge

First a scenario (also represented as the ideal model for the random channels) that precludes channel estimation is considered, in other words, the ST assumes

the perfect knowledge of the interacting channels. In this context, the ST encounters variations caused due to the channel fading only. These variations translate to the variations in the detection probability, more specifically those variations that do not meet the desired detection probability (\bar{P}_d) results in uncertain interference⁷ at the PR. To overcome this issue, [39] proposed to employ an outage constraint over P_d , given as

$$\mathbb{P}(P_d \leq \bar{P}_d) \leq \rho_d, \quad (2.38)$$

where ρ_d represents the outage constraint. Using (2.38), the ST is able to regulate the uncertain interference at the PR. As a result, a decision threshold (μ) on the $P_{Rx,ST}$ is obtained such that it satisfies the constraint defined (2.38) for a certain value of τ_{sen} .

Besides the interference at the PR, the throughput at the SR is given by

$$R_s(\tau) = \frac{T - \tau_{sen}}{T} \mathbb{E}_{|h_s|^2 |h_{p,2}|^2} \left[\underbrace{\mathbb{P}(\mathcal{H}_0)(1 - P_{fa}) \log_2 \left(1 + \frac{|h_s|^2 P_{Tx,ST}}{\sigma_w^2} \right)}_{C_0} + \underbrace{\mathbb{P}(\mathcal{H}_1)(1 - P_d) \log_2 \left(1 + \frac{|h_s|^2 P_{Tx,ST}}{|h_{p,2}|^2 P_{Tx,PT} + \sigma_w^2} \right)}_{C_1} \right], \quad (2.39)$$

where C_0 and C_1 correspond to the data rate at the SR with and without interference from the PT. Since the detection probability and the secondary throughput are related through the sensing time, this relationship is exploited to determine a sensing-throughput tradeoff for the case with the perfect channel estimation.

Theorem 3 Subject to an outage constraint on P_d at the PR, the sensing-throughput tradeoff for the IS that considers the perfect channel estimation and the random behaviour of the interacting channels, is given by

$$R_s(\tilde{\tau}_{test}, \tilde{\tau}_{sen}) = \max_{\tilde{\tau}_{test}, \tilde{\tau}_{sen}} \mathbb{E}_{P_d, |h_s|^2, |h_{p,2}|^2} [R_s(\tau_{sen})], \quad (2.40)$$

$$\text{s.t. (2.38)}$$

$$\text{s.t. } 0 < \tau_{sen} \leq T.$$

⁷Please note that, for the case with perfect channel knowledge, the uncertainty is due to the variations in the channel gain.

Remark 3 It is worth noticing the fact the authors in [39] applied channel fading only to the sensing channel, however, according to Theorem 3, here, a more practical approach is considered, whereby, the channel fading also over the access and the interference channels is employed. Since the perfect channel knowledge scenario is employed to benchmark the performance of those ISs that employ channel estimation (discussed later in Section 2.5.2), the parameters such as threshold (which is used for evaluating P_d and P_{fa}) and the expected throughput are evaluated numerically.

Imperfect Channel Knowledge

Now, the estimation of the interacting channels in context to the channel fading is considered. To incorporate channel estimation, the similar frame structure depicted in Figure 4.2 is employed. In contrast to the deterministic channel, here the IS incorporates variations in the performance parameters (P_d and R_s) due to the channel estimation and the channel fading. The characterization of the estimated parameters $\hat{P}_{Rx,ST}$ and $\hat{P}_{Rx,SR}$ for the sensing and the interference channel, and $|\hat{h}_s|^2$ for the access channel in terms of their cdfs, for the deterministic case, has been determined in Section 2.5.1. In addition, the estimated parameters are used to estimate the performance parameters \hat{P}_d , \hat{C}_0 and \hat{C}_1 , their cdfs $F_{\hat{P}_d}$, $F_{\hat{C}_0}$ and $F_{\hat{C}_1}$ are characterized in Lemma 1, Lemma 2 and Lemma 3 of Section 2.5.1.

The outage constraint that jointly captures the variations due to channel estimation and channel fading, which result in uncertain interference at the PR, is defined as

$$\underbrace{\mathbb{E}_{|h_{p,1}|^2} \overbrace{[\mathbb{P}(P_d \leq \bar{P}_d)]}^{\text{Channel Estimation}}}_{\text{Channel fading}} \leq \rho_d, \quad (2.41)$$

where $\mathbb{E}_{|h_{p,1}|^2} [\cdot]$ represents the expectation over the sensing channel.

The variations due to the channel estimation only ($\mathbb{P}(P_d \leq \bar{P}_d)$) are characterized in terms of cdf in (4.22). It is worth noticing that $\mathbb{E}_{|h_{p,1}|^2} [\cdot]$ in (2.41) acts on $P_{Rx,ST}$, as $P_{Rx,ST}$ incorporates the variations due to fading in the sensing channel $|h_{p,1}|^2$.

Next, the expression of the secondary throughput for the random channel is characterized as

$$R_s(\tau_{\text{est}}, \tau_{\text{sen}}) = \mathbb{E}_{\hat{P}_d, \hat{C}_0, \hat{C}_1, |h_{p,1}|^2, |h_s|^2, |h_{p,2}|^2} \left[\frac{T - \tau_{\text{sen}}}{T} \times \right. \\ \left(\mathbb{P}(\mathcal{H}_0)(1 - P_{\text{fa}})\hat{C}_0 + \mathbb{P}(\mathcal{H}_1)(1 - \hat{P}_d)\hat{C}_1 \right) \Big] \quad (2.42) \\ = \frac{T - \tau_{\text{sen}}}{T} \left[\mathbb{P}(\mathcal{H}_0)(1 - P_{\text{fa}})\mathbb{E}_{\hat{C}_1, |h_s|^2} [\hat{C}_1] + \right. \\ \left. \mathbb{P}(\mathcal{H}_1)\mathbb{E}_{\hat{P}_d, |h_{p,1}|^2} [\hat{P}_d] \mathbb{E}_{\hat{C}_1, |h_s|^2, |h_{p,2}|^2} [\hat{C}_1] \right]$$

where $\mathbb{E}_{\hat{P}_d, \hat{C}_0, \hat{C}_1, |h_{p,1}|^2, |h_s|^2, |h_{p,2}|^2} [\cdot]$ corresponds to an expectation over the estimated parameters $(\hat{P}_d, \hat{C}_0, \hat{C}_1)$ and the channel fading ($|h_{p,1}|^2, |h_s|^2, |h_{p,2}|^2$). Please note that the channel fading is included in the system parameters \hat{P}_d, \hat{C}_0 and \hat{C}_1 , refer to (2.39).

Theorem 4 Subject to an outage constraint on P_d at the PR, the sensing-throughput tradeoff for the IS that considers the imperfect channel estimation and the random behaviour of the interacting channels, is given by

$$R_s(\tilde{\tau}_{\text{est}}, \tilde{\tau}_{\text{sen}}) = \max_{\tau_{\text{est}}, \tau_{\text{sen}}} \mathbb{E}_{\hat{P}_d, \hat{C}_0, \hat{C}_1, |h_{p,1}|^2, |h_s|^2, |h_{p,2}|^2} [R_s(\tau_{\text{est}}, \tau_{\text{sen}})], \quad (2.43) \\ \text{s.t. (2.41),} \\ \text{s.t. } 0 < \tau_{\text{est}} \leq \tau_{\text{sen}} \leq T.$$

Proof: In order to solve the constrained optimization problem, the following approach is considered. First the underlying constraint (2.41) is exploited to determine the decision threshold μ . Since it is complicated to obtain a closed form expression of μ , in this regard, its value is obtained numerically.

Using μ to determine \hat{P}_d and P_{fa} and evaluating an expectation over $\hat{P}_d, \hat{C}_0, \hat{C}_1, |h_{p,1}|^2, |h_s|^2, |h_{p,2}|^2$, the expected throughput as function of estimation and sensing time is determined. Finally, this function is used to determine the suitable estimation time ($\tilde{\tau}_{\text{est}}$) and sensing time ($\tilde{\tau}_{\text{sen}}$). ■

In contrast to the ideal model (refer to Theorem 3), the sensing-throughput tradeoff investigated by the proposed approach (refer to Theorem 4) incorporates the imperfect channel knowledge, in this context, the performance characterization considered by the proposed framework are closer to the realistic situations.

Remark 4 Similar to the deterministic channel, the expression $R_s(\tau_{\text{est}}, \tau_{\text{sen}})$ derived by the estimation model (referred as the proposed approach) establishes a fundamental relation between estimation time, sensing time and achievable throughput characterized as estimation-sensing-throughput tradeoff for the random channel that incorporates channel estimation. Based on this tradeoff, a suitable estimation $\tau_{\text{est}} = \tilde{\tau}_{\text{est}}$ and a sensing time $\tau_{\text{sen}} = \tilde{\tau}_{\text{sen}}$ that attains a maximum achievable throughput $R_s(\tilde{\tau}_{\text{est}}, \tilde{\tau}_{\text{sen}})$ for the IS is determined.

2.6 Numerical Results

Here, the performance of the IS based on the proposed approach is investigated. In this regard: (i) the simulations are performed to validate the expressions obtained, (ii) the performance degradation incurred due to the channel estimation is evaluated and analyzed. In this regard, the ideal model is considered to benchmark and evaluate the performance loss, (iii) the mathematical justification to the considered approximations is established. Although the expressions derived in this chapter depicting the sensing-throughput analysis are general and applicable to all CR systems, the parameters are selected in such a way that they closely relate to the deployment scenario described in Figure 5.1. Unless stated explicitly, the choice of the parameters given in Table 4.1 is considered for the analysis.

2.6.1 Deterministic Channel

At first, the performance of the IS in terms of sensing-throughput tradeoff corresponding to the ideal model (IM) and estimation model (EM) for a fixed $\tau_{\text{est}} = 5$ ms is analyzed, refer to Figure 2.6. In contrast to constraint on P_d for the ideal model, the average constraint (EM-AC) and the outage constraint (EM-OC) for the proposed estimation model are employed. With the inclusion of received power-based estimation in the frame structure, the ST achieves no throughput at the SR for the interval τ_{est} . For the given cases, namely, IM, EM-AC and EM-OC, a suitable sensing time that results in a maximum throughput $R_s(\tau_{\text{est}} = 5 \text{ ms}, \tilde{\tau}_{\text{sen}})$ is determined. Apart from that, a performance degradation is depicted in terms of the achievable throughput, refer to Figure 2.6. For $\rho_d = 0.05$, it is observed that the outage constraint is more sensitive to the performance loss in comparison to the average constraint. It is clear that the

Table 2.1: Parameters for Numerical Analysis

Parameter	Value
f_s	1 MHz
$ h_{p,1} ^2, h_{p,2} ^2$	-100 dB
$ h_s ^2$	-80 dB
T	100 ms
\bar{P}_d	0.9
ρ_d	0.05
σ_w^2	-100 dBm
$\gamma_{p,1}$	-10 dB
$\gamma_{p,2}$	-10 dB
γ_s	10 dB
$\sigma_s^2 = P_{Tx,PT}$	-10 dBm
$P_{Tx,ST}$	-10 dBm
$\mathbb{P}(\mathcal{H}_1) = 1 - \mathbb{P}(\mathcal{H}_0)$	0.2
τ_{est}	5 ms
N_s	10
$N_{p,2}$	1000

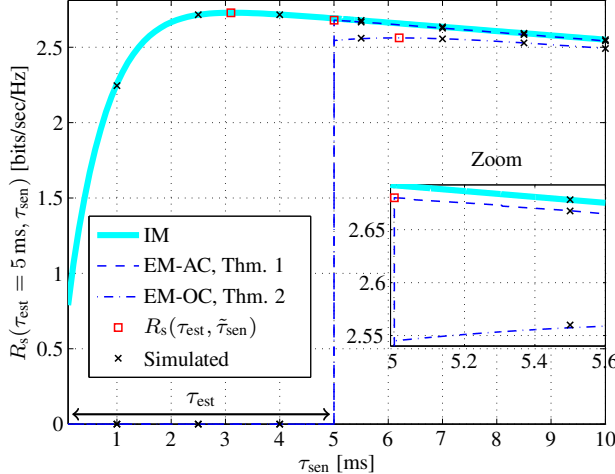


Figure 2.6: Sensing-throughput tradeoff for the ideal model (IM) and estimation model (EM), $\gamma_{p,1} = -10$ dB, $\tau_{\text{est}} = 5$ ms and $\rho_d = 0.05$.

analysis illustrated in Figure 2.6 is obtained for a certain choice of system parameters, particularly $\gamma_{p,1} = -10$ dB, $\tau_{\text{est}} = 5$ ms and $\rho_d = 0.05$. To acquire more insights, the effect of variation of these parameters on the performance of the IS is considered, subsequently.

Hereafter, the theoretical expressions are considered for the analysis, in addition, the suitable sensing time is chosen to be as an operation point. Next, the variation in the achievable throughput $R_s(\tau_{\text{est}}, \tilde{\tau}_{\text{sen}})$ against the received signal to noise ratio $\gamma_{p,1}$ at the ST with $\tau_{\text{est}} = 5$ ms is considered, refer to Figure 2.7. For $\gamma_{p,1} < -10$ dB, the estimation model incurs a significant performance loss. This clearly reveals that the ideal model overestimates the performance of the ISs. From the previous discussion, it is concluded that the inclusion of the average and the outage constraints (depicted by the proposed framework) precisely tackles the uncertainty in the interference at the PR arising due to channel estimation without considerably degrading the performance of the IS.

Upon maximizing the secondary throughput, it is interesting to analyze the variation of the achievable throughput with the estimation time. Corresponding to the estimation model, Figure 2.8 illustrates a tradeoff among the estimation time, the sensing time and the secondary throughput, refer to Remark 3. From Figure 2.8, it can be noticed that the function $R_s(\tau_{\text{est}}, \tau_{\text{sen}})$ is well-behaved in

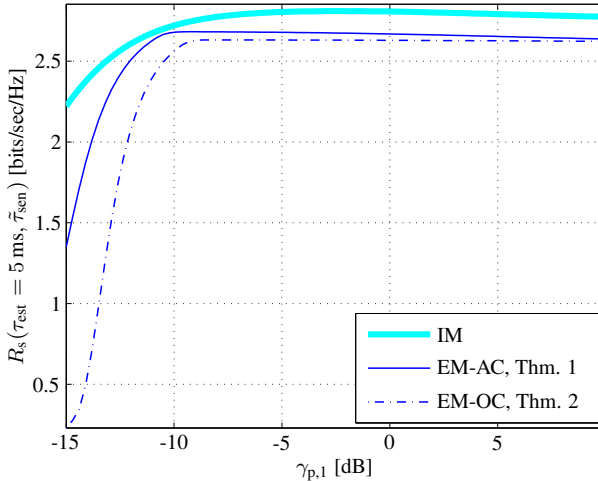


Figure 2.7: Achievable secondary throughput versus $\gamma_{p,1}$ with $\tau_{\text{est}} = 5$ ms for the deterministic channel.

the region $0 < \tau_{\text{est}} \leq \tau_{\text{sen}} \leq T$ and consists of a global maximum. This tradeoff depicted by the proposed framework, further presented in Figure 2.9, can be explained from the fact that low values of the estimation time result in large variations in \hat{P}_d . To counteract and satisfy the average and the outage constraints, the corresponding thresholds shift to a lower value. This causes an increase in P_{fa} , thereby increasing the sensing-throughput curvature. As a result, the suitable sensing time is obtained at a higher value. However, beyond a certain value ($\tilde{\tau}_{\text{est}}$), a further increase in the estimation time slightly contributes to the performance improvement and largely consumes the time resources. As a consequence to the estimation-sensing-throughput tradeoff, the suitable estimation time that yields an achievable throughput $R_s(\tilde{\tau}_{\text{est}}, \tilde{\tau}_{\text{sen}})$ is determined.

Besides that, the variation in the achievable throughput for different values of the outage constraint is illustrated, refer to Figure 2.9. It is observed that for the selected choice of ρ_d , the outage constraint is severe as compared to the average constraint, hence, results in a lower throughput or achieves greater performance degradation. Thus, depending on the nature of the policy (aggressive or conservative) followed by the regulatory bodies towards the interference at the primary system, it is possible to define ρ_d accordingly during the system design. Moreover, it is observed that the alternative approach proposed in Corollary 1 does not present any noticeable performance difference depicted in terms of the achievable throughput corresponding to the one characterized

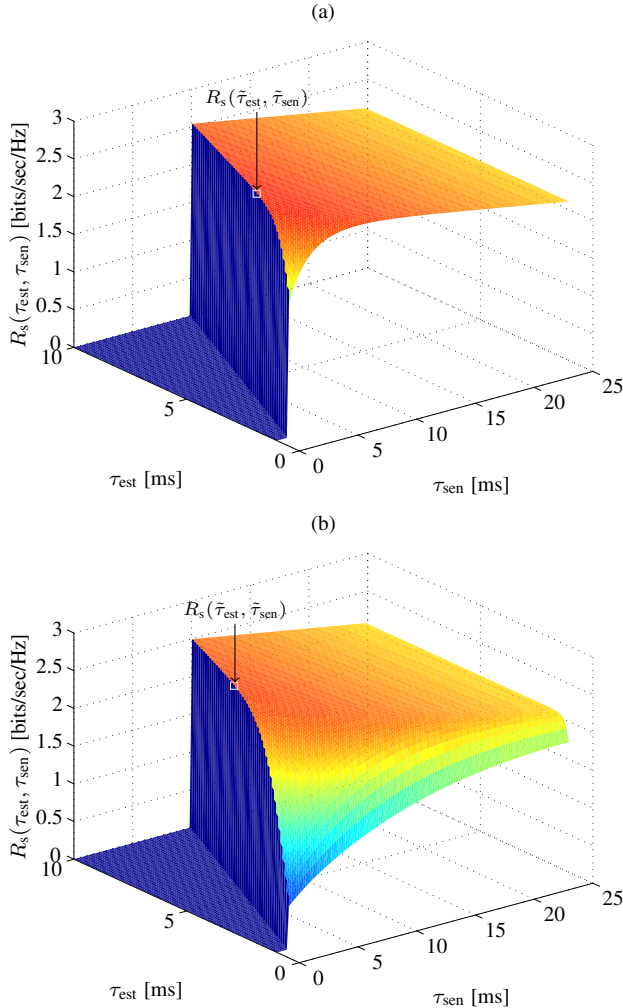


Figure 2.8: Estimation-sensing-throughput tradeoff for the estimation model for (a) average constraint and (b) outage constraint with $\rho_d = 0.05$.

in Theorems 5 and 2.

To procure further insights, the variations of expected P_d and P_{fa} with the esti-

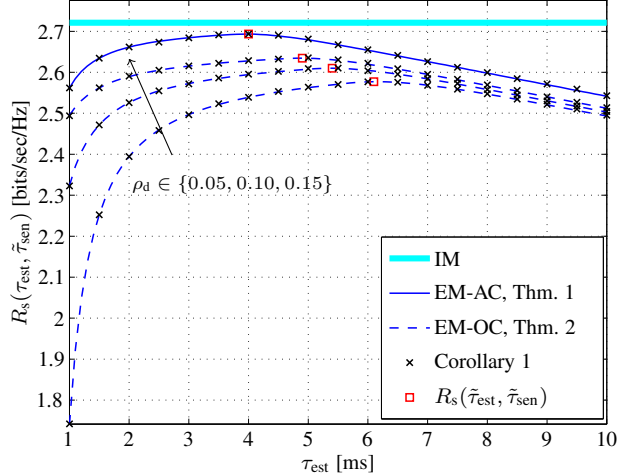


Figure 2.9: Estimation-sensing-throughput tradeoff for the average and the outage constraints with $\gamma_{p,1} = -10$ dB, where the throughput is maximized over the sensing time, $R_s(\tau_{\text{est}}, \tilde{\tau}_{\text{sen}})$. The estimation-sensing-throughput tradeoff is utilized to determine a suitable estimation time $\tilde{\tau}_{\text{est}}$ that maximizes the throughput, $R_s(\tilde{\tau}_{\text{est}}, \tilde{\tau}_{\text{sen}})$.

mation time are studied. From Figure 2.10, it is observed that the expected P_d corresponding to the outage constraint is strictly above the desired level \bar{P}_d for all values of the estimation time, however, for lower values of estimation time, this margin reduces. This is based on the fact that lower estimation time shifts the probability mass of P_d to a lower value, refer to Figure 2.3a. According to Figure 2.11, the system notices a considerable improvement in P_{fa} at small values of τ_{est} , which saturates for a certain period and falls drastically beyond a certain value. To understand this, it is important to study the dynamics between the estimation and the sensing time. Low τ_{est} increases the variations in the detection probability, these variations are compensated by an increase in the suitable sensing time, and vice versa. The performance improves until a maximum $(\tilde{\tau}_{\text{est}}, \tilde{\tau}_{\text{sen}})$ is reached, beyond this, the time resources (allocated in terms of the sensing and the estimation time) contribute more in improving the detector's performance (in terms of P_{fa} as P_d is already constrained) and less in reducing the variations due to the channel estimation.

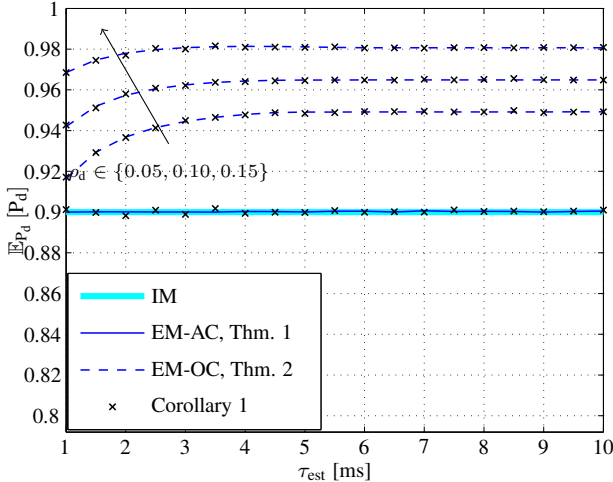


Figure 2.10: Variation of $\mathbb{E}_{P_d} [P_d]$ versus the τ_{est} , where the secondary throughput is maximized over the sensing time, $R_s(\tau_{\text{est}}, \tilde{\tau}_{\text{sen}})$.

2.6.2 Random Channel

In contrast to the deterministic scenario, the choice of the system parameters is slightly modified, $\gamma_{p,1} = 0 \text{ dB}$, $\gamma_{p,2} = 0 \text{ dB}$, $\gamma_s = 10 \text{ dB}$, $\sigma_s^2 = P_{\text{Tx,PT}} = 0 \text{ dBm}$, $P_{\text{Tx,ST}} = -10 \text{ dBm}$, $\mathbb{P}(\mathcal{H}_1) = 1 - \mathbb{P}(\mathcal{H}_0) = 0.2$, $\tau_{\text{est}} = 1 \text{ ms}$ and $N_s = \tau_{\text{est}}$. This is done to illustrate the effectiveness of the proposed approach for the random channel. In addition, the performance of the IS under the following fading scenarios is evaluated: (i) severe fading $m = 1$ (Rayleigh fading), and (ii) mild fading $m = 1.5$.

First, the sensing-throughput tradeoff for a certain value of estimation time $\tau_{\text{est}} = 1 \text{ ms}$ is studied, corresponding to the IM and the EM that represent the perfect and the imperfect channel estimation, respectively, refer to Figure 2.12. Again like the deterministic channel, it is observed that with the inclusion of τ_{est} in the frame structure, the EM procure no throughput at the SR for the time interval τ_{est} . Furthermore, it is noticed that the suitable sensing time increases with severity in the fading. To further understand the effect of the channel fading on the performance of the IS, the variation of other parameters on the performance of the IS are considered.

After maximizing the secondary throughput for a certain estimation time, the

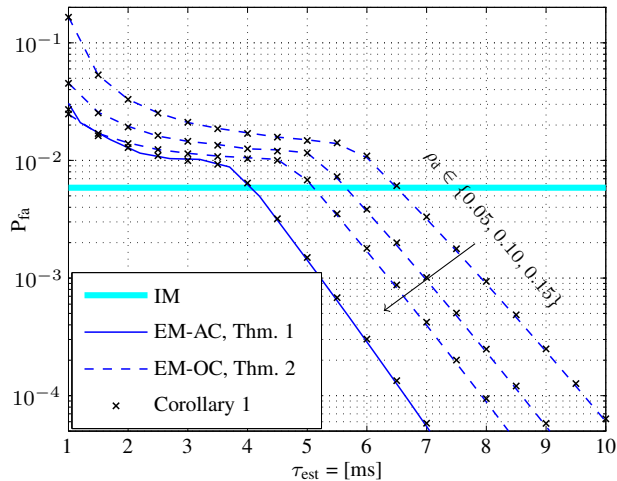


Figure 2.11: Variation of P_{fa} versus the τ_{est} , where the secondary throughput is maximized over the sensing time, $R_s(\tau_{est}, \tilde{\tau}_{sen})$.

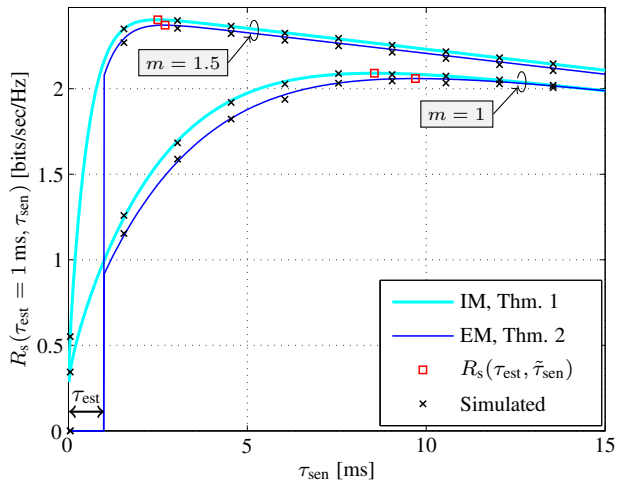


Figure 2.12: Sensing-throughput tradeoff for the ideal model (IM) and estimation model (EM), $\gamma_{p,1} = 0$ dB, $\tau_{est} = 1$ ms and $\rho_d = 0.05$.

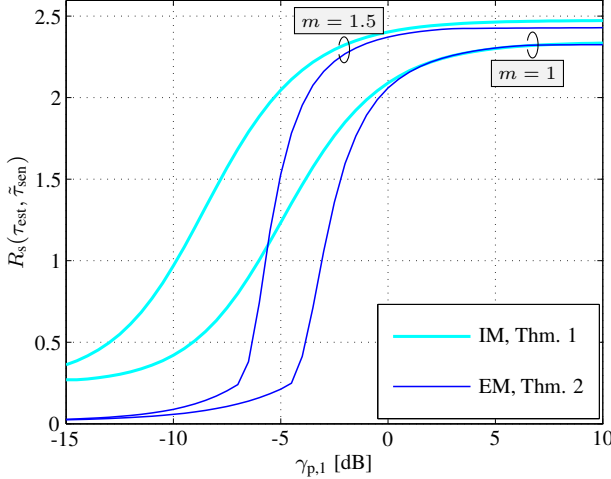


Figure 2.13: Achievable secondary throughput versus $\gamma_{p,1}$ with $\tau_{est} = 1$ ms for the random channel.

variation of $R_s(\tau_{est}, \tilde{\tau}_{sen})$ along the received signal to noise ratio for the different choice of the aforementioned fading scenarios is analyzed. From Figure 2.13, it is evident that for a certain choice of estimation time, the performance degrades severely below $\gamma_{p,1} = 0$ dB. More specifically, the performance degradation decreases with the severity in the fading. This concludes that the scenarios with mild fading and low $\gamma_{p,1}$ are more sensitive to the choice of estimation time. Complementing the analysis for the deterministic channel depicted in Figure 2.8, Figure 2.14 presents the variation of the secondary throughput along the estimation and the sensing time. In contrast to the deterministic channel, Figure 2.14 jointly incorporates the variations due to channel estimation and channel fading. It is clearly noticed that the mild fading scenario are sensitive to the performance degradation around the suitable estimation and the suitable sensing time.

Next, the variation of $R_s(\tau_{est}, \tilde{\tau}_{sen})$ along the estimation time is examined, refer to Figure 2.15. It is noticed that $R_s(\tau_{est}, \tilde{\tau}_{sen})$ increases for low values of τ_{est} and then decreases beyond $\tilde{\tau}_{est}$. This can be explained as follows, low τ_{est} increases the variations in \hat{P}_d , shifting the threshold to lower values, which subsequently increases P_{fa} , hence, degrading the achievable secondary throughput. Beyond $\tilde{\tau}_{est}$, the variations are largely dominated by the channel fading,

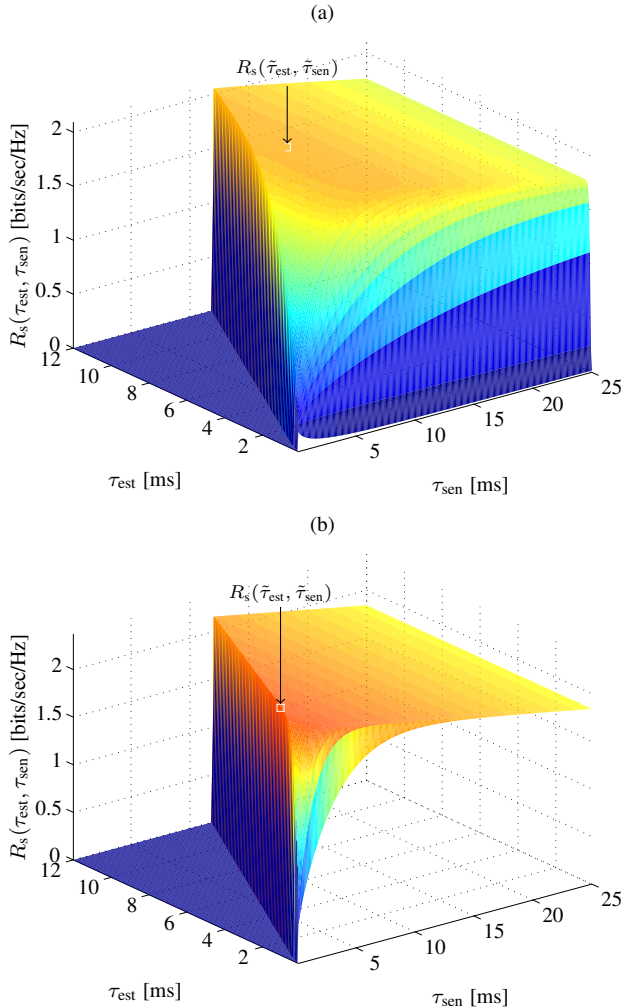


Figure 2.14: Estimation-sensing-throughput tradeoff for the estimation model for different fading scenarios (a) $m = 1$ (b) $m = 1.5$.

therefore, the IS observes no improvement by increasing τ_{est} . From the analysis, it is again depicted that the mild fading scenarios are more sensitive to the performance degradation in terms of the achievable secondary throughput.

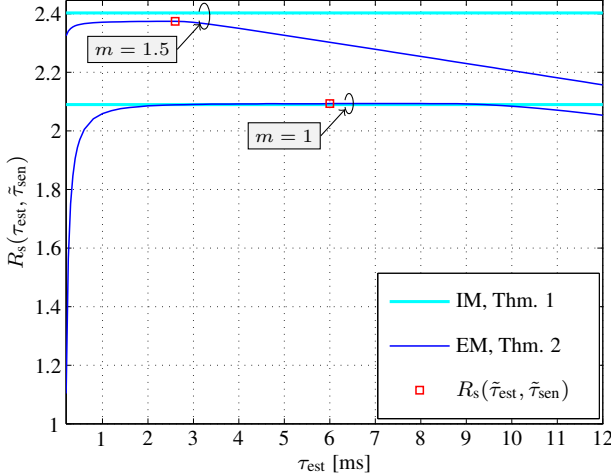


Figure 2.15: Estimation-sensing-throughput tradeoff subject to the random channel with $\gamma_{p,1} = 0 \text{ dB}$, where the throughput is maximized over the sensing time, $R_s(\tilde{\tau}_{\text{est}}, \tilde{\tau}_{\text{sen}})$. Estimation-sensing-throughput tradeoff is utilized to determine a suitable estimation time $\tilde{\tau}_{\text{est}}$ that maximizes the throughput, $R_s(\tilde{\tau}_{\text{est}}, \tilde{\tau}_{\text{sen}})$.

Figure 2.16 presents the variation of expected detection probability against τ_{est} . It is indicated that the EM compensates for the variations due to the channel estimation and the channel fading to satisfy the outage constraint. Subsequently, Figure 2.16 illustrates the performance in terms of the false alarm probability. The random channel case encounters a similar behaviour as depicted by the deterministic channel, where P_{fa} severely reduces beyond a certain τ_{est} . Since $1 - P_{\text{fa}} \approx 1$ beyond the aforementioned τ_{est} , this reduction in P_{fa} does not influence the performance of the IS in terms of secondary throughput.

Lastly, the performance degradation in terms of achievable secondary throughput $R_s(\tilde{\tau}_{\text{est}}, \tau_{\text{sen}})$ versus the Nakagami- m parameter (that accounts for severity in the fading) is investigated, refer to Figure 2.18. For both scenarios, i.e., perfect (IM) and imperfect channel estimation (EM), the performance decreases with the severity in fading. In addition, by comparing the IM and the EM, it can be concluded that, for situations where the variations in the system are largely dominated by the channel estimation, the EM notices a greater performance degradation.

2 Interweave System

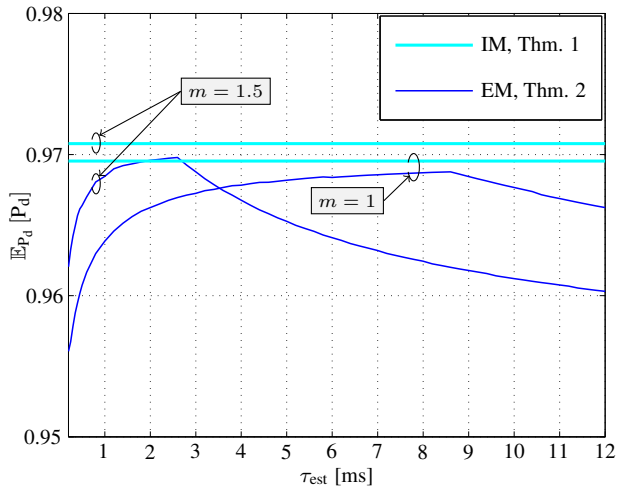


Figure 2.16: Expected detection probability versus estimation time.

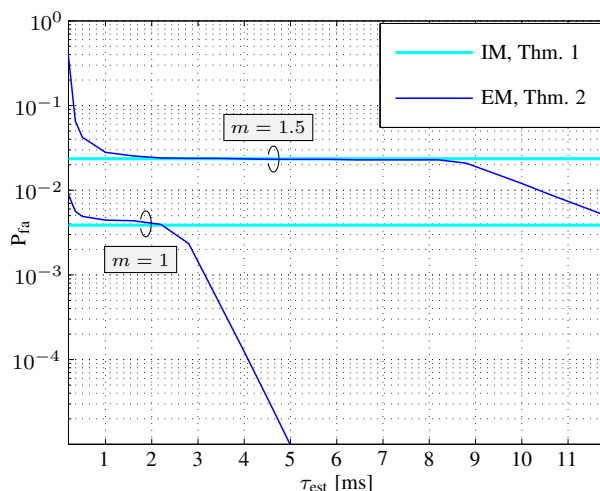


Figure 2.17: False alarm probability versus estimation time.

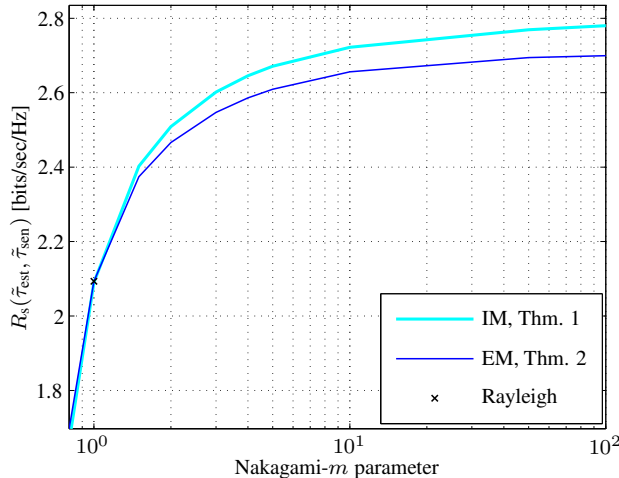


Figure 2.18: Variation of the achievable throughput $R(\tilde{\tau}_{\text{est}}, \tilde{\tau}_{\text{sen}})$ with Nakagami- m parameter for $\gamma_{p,1} = 0$ dB.

2.7 Summary

In this chapter, the performance of cognitive radio as an interweave system from a deployment perspective is investigated. It has been argued that the knowledge of the interacting channels is a key aspect that enables the performance characterization of the interweave system in terms of the sensing-throughput tradeoff. In this regard, a novel framework that facilitates channel estimation and captures the effect of channel estimation in the system model has been proposed. As a major outcome of the analysis, it has been justified that the existing model, illustrating an ideal scenario, overestimates the performance of the interweave system, hence, less suitable for deployment. Moreover, it has been clearly stated that the variations induced in the system, specially in the detection probability cause uncertain interference. Unless controlled, this uncertain interference may severely degrade the performance of the primary system. To overcome this situation, average and outage constraints as primary user constraints have been employed. As a consequence, for the proposed estimation model, novel expressions for the sensing-throughput tradeoff based on the mentioned constraints have been established. More importantly, by analyzing the estimation-sensing-throughput tradeoff, the suitable estima-

tion time and the suitable sensing time that maximize the secondary throughput have been determined.

In addition to this, the performance of the interweave systems that incorporate imperfect knowledge of the involved channels, where these channels are subject to Nakagami- m fading is characterized. In this context, an outage constraint that jointly captures the variations in the IS due to channel estimation and channel fading has been employed. Subject to this constraint, a sensing-throughput tradeoff that incorporates channel estimation and channel fading that yields a maximum secondary throughput at a suitable estimation and a sensing time has been characterized. Finally through numerical analysis, it has been concluded that the suitable choice of the estimation time is essential for controlling the performance degradation in terms of the achievable secondary throughput, particularly for scenarios that encounter less severe (mild) fading.

2.8 Proofs

2.8.1 Proof of Lemma 5

Proof: Following the probability density function (pdf) of $|\hat{h}_s|^2$ in (2.14), the pdf $f_{|\hat{h}_s|^2 P_{\text{Tx,ST}}} \frac{P_{\text{Tx,ST}}}{\sigma_w^2}$ is given by

$$f_{|\hat{h}_s|^2 P_{\text{Tx,ST}}} \left(x \right) = \frac{2N_s P_{\text{Tx,ST}}}{\sigma_w^4} \frac{1}{2} \exp \left[-\frac{1}{2} \left(x \frac{\sigma_w^4}{2N_s P_{\text{Tx,ST}}} + \lambda_s \right) \right] \times \\ \left(\frac{x}{\lambda_s} \frac{\sigma_w^4}{2N_s P_{\text{Tx,ST}}} \right)^{\frac{N_s}{4} - \frac{1}{2}} I_{\frac{N_s}{2} - 1} \left(\sqrt{\lambda_s x \frac{\sigma_w^4}{2N_s P_{\text{Tx,ST}}}} \right),$$

where $I_{(\cdot)}(\cdot)$ represents the modified Bessel function of first kind [51]. Approximating $\mathcal{X}_1^2(\cdot, \cdot)$ with Gamma distribution $\Gamma(a_s, b_s)$ [57] gives

$$f_{|\hat{h}_s|^2 P_{\text{Tx,ST}}} \approx \frac{1}{\Gamma(a_s)} \frac{x^{a_s - 1}}{b_s^{a_s}} \exp \left(-\frac{x}{b_s} \right), \quad (2.44)$$

where the parameters a_s and b_s in (2.44) are determined by comparing the first two central moments of the two distributions. Finally, by substituting the expression of C_0 in (4.8) yields (4.24). ■

2.8.2 Proof of Lemma 6

Proof: For simplification, the expression $\left(\frac{|\hat{h}_s|^2 P_{\text{Tx,ST}}}{\hat{P}_{\text{Rx,SR}}}\right)$ in (4.9) is decomposed as $E_1 = \left(\frac{|\hat{h}_s|^2 P_{\text{Tx,ST}}}{\sigma_w^2}\right)$ and $E_2 = \left(\frac{\hat{P}_{\text{Rx,SR}}}{\sigma_w^2}\right)$, where $C_1 = \log_2 \left(1 + \frac{E_1}{E_2}\right)$. The pdf of the expression E_1 is determined in (2.44).

Following the characterization $\hat{P}_{\text{Rx,SR}}$ in (2.16), the pdf of E_2 is determined as

$$f_{\frac{\hat{P}_{\text{Rx,SR}}}{\sigma_w^2}} = \frac{N_{p,2}\sigma_w^2}{P_{\text{Rx,SR}}} \frac{1}{2^{\frac{N_{p,2}}{2}} \Gamma\left(\frac{N_{p,2}}{2}\right)} \left(x \frac{N_{p,2}\sigma_w^2}{P_{\text{Rx,SR}}}\right)^{\frac{N_{p,2}}{2}-1} \times \\ \exp\left(-x \frac{N_{p,2}\sigma_w^2}{2P_{\text{Rx,SR}}}\right). \quad (2.45)$$

Using the characterizations of pdfs $f_{\frac{|\hat{h}_s|^2 P_{\text{Tx,ST}}}{\sigma_w^2}}$ and $f_{\frac{\hat{P}_{\text{Rx,SR}}}{\sigma_w^2}}$, Mellin transform [58] is applied to determine the pdf of $\frac{E_1}{E_2}$ as

$$f_{\frac{|\hat{h}_s|^2 P_{\text{Tx,ST}}}{\sigma_w^2} / \frac{\hat{P}_{\text{Rx,SR}}}{\sigma_w^2}}(x) = \frac{x^{a_s-1} \Gamma(a_s + a_2)}{\Gamma(a_s)\Gamma(a_2)b_s^{a_s}b_2^{a_2}} \left(\frac{1}{b_2} + \frac{x}{b_s}\right)^{(a_s+a_2)}. \quad (2.46)$$

Finally, substituting the expression $\frac{E_1}{E_2}$ in C_1 yields (4.26). ■

2.8.3 Proof of Theorems 5 and 2

Proof: In order to solve the constrained optimization problems illustrated in Theorem 5 and Theorem 2, the following approach is considered. As a first step, the underlying constraint is employed to determine μ as a function of the τ_{sen} and τ_{est} .

For the average constraint, the expression $\mathbb{E}_{P_d} [P_d]$ in (2.28) did not lead to a closed form expression, consequently, no analytical expression of μ is obtained. In this context, μ for the average constraint is procured numerically from (2.28).

Next, μ based on the outage constraint is determined. This is accomplished by combining the expression of $F_{\hat{P}_d}$ in (4.22) with the outage constraint (2.30)

$$P(P_d \leq \bar{P}_d) = F_{\hat{P}_d}(\bar{P}_d) \leq \rho_d. \quad (2.47)$$

Rearranging (2.47) gives

$$\mu \geq \frac{4P_{\text{Rx,ST}}\Gamma^{-1}\left(1 - \rho_d, \frac{\tau_{\text{est}}f_s}{2}\right)\Gamma^{-1}\left(\bar{P}_d, \frac{\tau_{\text{sen}}f_s}{2}\right)}{\tau_{\text{est}}\tau_{\text{sen}}(f_s)^2}. \quad (2.48)$$

Clearly, the random variables $P_d(\hat{P}_{\text{Rx,ST}})$, and $C_0(|\hat{h}_s|^2)$ and $C_1(|\hat{h}_s|^2, \hat{P}_{\text{Rx,SR}})$ are functions of the independent random variables $\hat{P}_{\text{Rx,ST}}$, and $|\hat{h}_s|^2$ and $\hat{P}_{\text{Rx,SR}}$, respectively. In this context, the independence property on P_d , C_0 and C_1 is applied to obtain

$$\begin{aligned} \mathbb{E}_{P_d, C_0, C_1} [C_0(1 - P_{fa}) + C_1(1 - P_d)] &= \mathbb{E}_{C_0} [C_0] (1 - P_{fa}) + \\ &\quad \mathbb{E}_{C_1} [C_1] \mathbb{E}_{P_d} [(1 - P_d)] \end{aligned}$$

in (2.27) and (2.29). Upon replacing the respective thresholds in P_d and P_{fa} and evaluating the expectation over P_d , C_0 and C_1 using the cdfs characterized in Lemma 4, Lemma 5 and Lemma 6, the expected throughput as a function of sensing and estimation time is determined. ■

CHAPTER 3

Underlay System

CHAPTER 4

Hybrid Systems

This chapter¹ studies the performance of hybrid cognitive radio systems. A hybrid system combines the benefits of the interweave and the underlay systems by employing a spectrum sensing and a power control mechanism at the ST. Like the previous two chapters, it is examined that the existing baseline models considered for performance analysis of the HSs assume perfect knowledge of the involved channels at the ST. However, analog to the interweave and the underlay scenarios investigated in chapters 2 and 3, such situations hardly exist in practical deployments. Motivated by this fact, a novel approach that incorporates channel estimation at the ST is proposed. By doing this, the performance characterization of the HSs under realistic scenarios is significantly enhanced. In order to overcome the impact of imperfect channel knowledge that mainly consists of the uncertain interference at the primary system, outage constraints on the detection probability at the ST and on the interference power received at the primary receiver are proposed. The analysis reveals that the baseline model overestimates the performance of the HS in terms of achievable secondary user throughput. In this chapter, corresponding to the HSs, an estimation-sensing-throughput tradeoff is established to determine a suitable estimation and a sensing durations that effectively capture the effect of imperfect channel knowledge and subsequently enhance the achievable secondary user throughput.

¹That primarily features the performance analysis conducted in [K11].

4.1 Related Work

From the previous chapters, it can be easily comprehended that the USs employ several techniques such as power control, interference alignment, beamforming that allow CR systems to mitigate the interference at the primary systems [31]. More particularly, the USs tend to operate below a certain level defined as the IT. In the context of an IS, the interference is avoided by sensing a licensed spectrum or PU signal at the ST. Spectrum sensing can be performed by employing various techniques such as energy detection, matched filter based detection, cyclostationary based detection [32]. Due to its versatility towards the unknown primary user signal, energy detection is considered for performing spectrum sensing. In this view, the performance of ISs depend on the detector's performance, which is characterized in terms of detection probability and false alarm probability. As a result, to ensure that the interference is restricted below a certain level, it is essential to operate the detector in such a way that the detection probability stays above a desired level. Besides that, the performance of the secondary system can be characterized in terms of throughput achieved at the SR, which is generally influenced by the false alarm probability. In this context, a fundamental relationship between the sensing and the secondary throughput has been investigated by Liang *et al.* [28].

However, the IS does not account for the severity of the interference power received at the PR, which in most cases can be tolerated by the primary systems and in other cases can lead to outage at the PR, thereby resulting in serious performance degradation of the primary system. In contrast to the ISs, the detection incapability of US forbids them to transmit with full power, specially during the periods when the primary system remains inactive. By addressing these issues one can significantly enhance the spectral efficiency of the CR systems. In this context, a joint solution that precisely utilizes the interference tolerance capability of the USs and the agility of ISs to detect spectrum holes, defined as HS, has been considered in [29, 59–65].

Kang *et al.* [59] established a frame structure for HSs, whereby the ST first senses a PU channel in order to decide its operation mode (interweave or underlay) based on the detection result. Further, to decide upon a suitable operation mode, appropriate strategies that maximize the secondary system's throughput have been investigated by [60–63]. Besides that, Jiang *et al.* employed a double detection threshold, which enables dynamic switching between full and partial access modes. Whereas Filippou *et al.* [65] analyzed the performance of the HSs when a Multiple Input Multiple Output antenna system is deployed at the

ST. Lastly, a sensing-throughput tradeoff to characterize the performance of the HS has been investigated by Sharma *et al.* [29]. Considering the fact that most of the existing models [29, 59–65] used for performance analysis assume the perfect knowledge of the involved channels at the ST. This assumption is however not viable for practical implementations, thereby rendering the performance analysis carried out using these models inaccurate. In this context, the performance analysis of the HS that incorporates channel estimation is an interesting research problem. Motivated by this fact, this chapter establishes a fundamental framework that considers the estimation of the involved channels and analyze the impact of channel estimation on performance of those CR systems that employ hybrid technique for accessing the licensed spectrum.

4.2 Contributions

More specifically, this chapter provides the following contributions:

4.2.1 Analytical framework

A novel analytical framework for the HS that constitutes the estimation of interacting channels, namely: (i) sensing channel, (ii) interference channels and (iii) access channel is established. Clearly, due to incorporation of channel estimation, the variations induced in the performance parameters (which include the interference received at the PR and the throughput at the SR) can lead to violation of the existing constraints. As a result, with the inclusion of channel estimation, the primary system observes an uncertainty in the interference (defined as uncertain interference). In order to combat this uncertain interference, outage constraints on the detection probability at the ST and on the interference power received at the PR are employed. Consequently, the performance of the HS in terms of the achievable secondary throughput is analyzed.

4.2.2 Estimation-sensing-throughput tradeoff

The performance of the proposed framework that incorporates channel estimation is analyzed by considering a fundamental tradeoff between estimation time, sensing time and achievable throughput. This tradeoff is exploited to determine suitable estimation and sensing durations that achieve a maximum

performance for the HS in terms of the secondary throughput. From a system design perspective, this tradeoff provides the necessary tools for evaluating the performance degradation encountered by the HSs due to inappropriate selection of the estimation time. This degradation (depicted in terms of secondary throughput) is determined by comparing the proposed framework to those scenarios that consider perfect channel knowledge (Ideal Model).

4.3 System Model

4.3.1 Deployment Scenario and Medium Access

Considering that the spectrum sensing and the power control mechanisms are employed at the CSC-BS, the CSC deployment is transformed into a hybrid scenario, by which the CSC-BS and the MS represent ST and SR, respectively. As an extension to the existing models depicted in [29, 59], a slotted medium access for the HS, where the time axis is segmented into frames of length T is considered, according to which, the ST employs periodic sensing. In this view, each frame consists of a sensing time interval τ_{sen} followed by data transmission ($T - \tau_{\text{sen}}$). Depending on the outcome of the sensing, the data transmission takes place with or without power control.

4.3.2 Signal Model

As illustrated in chapter 2 the primary and the secondary systems employ Orthogonal Frequency Division Multiplex (OFDM) signal to carry out their transmissions. As a result, OFDM signals transmitted by the primary system are modelled as zero mean Gaussian signals by the secondary system, and vice versa.

Subject to the underlying hypothesis, illustrating the presence \mathcal{H}_1 and the absence \mathcal{H}_0 of the primary signal, the discrete and complex received signal is given by

$$y_{\text{ST}}[n] = \begin{cases} h_{\text{p},1} \cdot x_{\text{PT}}[n] + w[n] & : \mathcal{H}_1 \\ w[n] & : \mathcal{H}_0 \end{cases}, \quad (4.1)$$

where $x_{\text{PT}}[n]$ corresponds to a discrete and complex sample transmitted by the PT, $|h_{\text{p},1}|^2$ represents the power gain of the sensing channel for a given frame

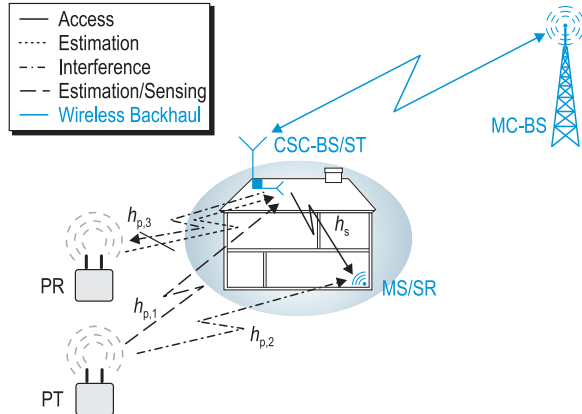


Figure 4.1: A cognitive small cell scenario demonstrating: (i) the hybrid paradigm, (ii) the associated network elements, which constitute Cognitive Small Cell-Base Station/Secondary Transmitter (CSC-BS/ST), Mobile Station/Secondary Receiver (MS/SR), Macro Cell-Base Station (MC-BS) and Primary Transmitter (PT), (iii) the interacting channels: sensing ($h_{p,1}$), interference ($h_{p,2}, h_{p,3}$) and access (h_s) channels.

and $w[n]$ is circularly symmetric additive white Gaussian noise at the ST. The mean and variance for the signal and the noise are determined as: $\mathbb{E}[x_{\text{PT}}[n]] = 0$, $\mathbb{E}[w[n]] = 0$, $\mathbb{E}[|x_{\text{PT}}[n]|^2] = P_{\text{Rx,ST},h_{p,1}} = \sigma_s^2$ and $\mathbb{E}[|w[n]|^2] = \sigma_w^2$. The channel $h_{p,1}$ is considered to be independent of $x_{\text{PT}}[n]$ and $w[n]$, thus, $y_{\text{ST}}[n]$ is also an independent and identically distributed (i.i.d.) random process.

Following the conventional frame structure, ST performs periodic sensing for a duration of τ_{sen} . The test statistics $T(\mathbf{y})$ at the ST is evaluated as $T(\mathbf{y}) = \frac{1}{\tau_{\text{sen}} f_s} \sum_{n=1}^{\tau_{\text{sen}} f_s} |y_{\text{ST}}[n]|^2 \geq_{\mathcal{H}_0} \mu$, where μ is the decision threshold and \mathbf{y} is a vector with $\tau_{\text{sen}} f_s$ samples. $T(\mathbf{y})$ represents a random variable, whereby the characterization of the cdf depends on the underlying hypothesis. With regard to the OFDM signal transmissions that correspond to a Gaussian signal model, $T(\mathbf{y})$ follows a central chi-squared (χ^2) distribution for both hypotheses \mathcal{H}_0 and \mathcal{H}_1 [49]. Consequently, the detection probability (P_d) and the false alarm

probability (P_{fa}) are determined as [50]

$$P_d(\mu, \tau_{\text{sen}} f_s, P_{\text{Rx,ST}, h_{p,1}}) = \Gamma \left(\frac{\tau_{\text{sen}} f_s}{2}, \frac{\tau_{\text{sen}} f_s \mu}{2P_{\text{Rx,ST}, h_{p,1}}} \right), \quad (4.2)$$

$$P_{fa}(\mu, \tau_{\text{sen}} f_s) = \Gamma \left(\frac{\tau_{\text{sen}} f_s}{2}, \frac{\tau_{\text{sen}} f_s \mu}{2\sigma_w^2} \right), \quad (4.3)$$

where $P_{\text{Rx,ST}, h_{p,1}}$ is the power received over the sensing channel and $\Gamma(\cdot, \cdot)$ represents a regularized upper-incomplete Gamma function [51].

Similar to (4.1), the discrete and complex received signal at the SR conditioned on the sensing outcome is given by

$$y_{\text{SR}}[n] = \begin{cases} h_s \cdot x_{\text{ST}}[n] + h_{p,2} \cdot x_{\text{PT}}[n] + w[n] & : 1 - P_d \\ h_s \cdot x_{\text{ST}}[n] + w[n] & : 1 - P_{fa} \\ h_s \cdot x_{\text{ST,cont}}[n] + h_{p,2} \cdot x_{\text{PT}}[n] + w[n] & : P_d \\ h_s \cdot x_{\text{ST,cont}}[n] + w[n] & : P_{fa} \end{cases}, \quad (4.4)$$

where $x_{\text{ST}}[n]$ and $x_{\text{ST,cont}}[n]$ present the discrete and complex samples with full transmit power $P_{\text{Tx,ST,full}}$ and controlled transmit power $P_{\text{Tx,ST,cont}}$, respectively. Additionally, $|h_s|^2$ and $|h_{p,2}|^2$ represent the power gains for the access and the interference channels, cf. Figure 5.1.

Besides that, an interference signal from the ST is encountered at the PR across the channel $h_{p,3}$ only for the cases where the PT is transmitting, i.e., $(1 - P_d, P_d)$, cf. (4.4). In this regard, the received signal at the PR is given by

$$y_{\text{PR}}[n] = \begin{cases} h_{p,3} \cdot x_{\text{ST,cont}}[n] + w[n] & : P_d \\ h_{p,3} \cdot x_{\text{ST}}[n] + w[n] & : 1 - P_d \end{cases}. \quad (4.5)$$

4.3.3 Problem Description

To employ a power control mechanism, the ST is required to control its transmit power in such a way that the interference power received at the PR is below a certain interference threshold (θ_I). In reference to the HS, constraints on interference power received at the PR are defined as

$$\mathbb{P}(\mathcal{H}_1) \cdot P_d \cdot |h_{p,3}|^2 P_{\text{Tx,ST,cont}} \leq \theta_I \quad (4.6)$$

and

$$\mathbb{P}(\mathcal{H}_1) \cdot (1 - P_d) \cdot |h_{p,3}|^2 P_{Tx,ST,full} \leq \theta_I, \quad (4.7)$$

where $\mathbb{P}(\mathcal{H}_1)$ ($= 1 - \mathbb{P}(\mathcal{H}_0)$) represents the occurrence probability of the hypothesis \mathcal{H}_1 . According to [29], (4.7) is usually handled by the regulatory bodies. In this regard, using (4.6) and the knowledge of θ_I , the controlled power is computed as $\frac{\theta_I}{\mathbb{P}(\mathcal{H}_1) \cdot P_d \cdot |h_{p,3}|^2}$.

Next, the throughput received at the SR corresponding to the cases illustrated in (4.4) is characterized. Subject to the sensing outcome $1 - P_{fa}$, $1 - P_d$, P_{fa} , P_d , the corresponding throughputs at the SR are defined as

$$R_0(\tau_{sen}) = \frac{T - \tau_{sen}}{T} \cdot \overbrace{\log_2 \left(1 + |h_s|^2 \frac{P_{Tx,ST,full}}{\sigma_w^2} \right)}^{C_0} \times (1 - P_{fa}) \cdot \mathbb{P}(\mathcal{H}_0), \quad (4.8)$$

$$R_1(\tau_{sen}) = \frac{T - \tau_{sen}}{T} \overbrace{\log_2 \left(1 + \frac{|h_s|^2 P_{Tx,ST,full}}{|h_{p,2}|^2 P_{Tx,PT} + \sigma_w^2} \right)}^{C_1} \times (1 - P_d) \cdot \mathbb{P}(\mathcal{H}_1), \quad (4.9)$$

$$R_2(\tau_{sen}) = \frac{T - \tau_{sen}}{T} \overbrace{\log_2 \left(1 + |h_s|^2 \frac{P_{Tx,ST,cont}}{\sigma_w^2} \right)}^{C_2} \times P_{fa} \cdot \mathbb{P}(\mathcal{H}_0), \quad (4.10)$$

$$R_3(\tau_{sen}) = \frac{T - \tau_{sen}}{T} \overbrace{\log_2 \left(1 + \frac{|h_s|^2 P_{Tx,ST,cont}}{|h_{p,2}|^2 P_{Tx,PT} + \sigma_w^2} \right)}^{C_3} \times P_d \cdot \mathbb{P}(\mathcal{H}_1), \quad (4.11)$$

where C_0, C_1, C_2 and C_3 represent the data rates.

In order to highlight the dependency of the uncertain interference and the secondary throughput that characterizes the performance of the HS, Sharma *et al.* [29] established a tradeoff between the sensing time and secondary throughput (R_s) subject to a target detection probability (\bar{P}_d). This tradeoff is repre-

sented as

$$R_s(\tilde{\tau}_{\text{sen}}) = \max_{\tau_{\text{sen}}} R_s(\tau_{\text{sen}}) \quad (4.12)$$

$$\begin{aligned} &= R_0(\tau_{\text{sen}}) + R_1(\tau_{\text{sen}}) + R_2(\tau_{\text{sen}}) + R_3(\tau_{\text{sen}}) \\ \text{s.t. } &P_d \geq \bar{P}_d, \\ &\text{s.t. (4.7).} \end{aligned} \quad (4.13)$$

As a consequence, the tradeoff depicted in (4.12) determines a suitable sensing time $\tilde{\tau}_{\text{sen}}$ that achieves the maximum secondary throughput. However, the system model depicted above has the following fundamental issues:

- Without the knowledge of the received power (sensing channel, $h_{p,1}$), the characterization of P_d is not possible, cf. (4.2). This leaves the constraint defined in (4.13) inappropriate.
- Without the knowledge of the interference channel towards the PR ($h_{p,3}$), the power control mechanism cannot be employed at the ST.
- Along with the above mentioned channels, the knowledge of the access (h_s) and interference channel ($h_{p,2}$) to the SR, from the PT, is required at the ST for characterizing the secondary throughput.

With these issues, it is not reasonable to consider the performance analysis depicted by the ideal model (described as the baseline model) for hardware implementation. In order to address these issues, an analytical framework that includes the estimation of these channels and characterizes the performance of the HS in terms of the sensing-throughput tradeoff is proposed in this chapter.

4.4 Proposed Approach

4.4.1 Frame Structure

In order to incorporate the estimation of the involved channels, a novel frame structure is proposed in Figure 4.2, according to which, $\tau_{\text{est}, h_{p,1}}$ and $\tau_{\text{est}, h_{p,2}}$ are utilized for estimating $h_{p,1}$ and $h_{p,2}$ by the ST and the SR², respectively. Besides that, $\tau_{\text{est}, h_{p,3}}$ is used for estimating the $h_{p,3}$. Also, the ST considers

²In order to accomplish this, it is assumed that both the ST and the SR align themselves to the control-based transmission from the PT.

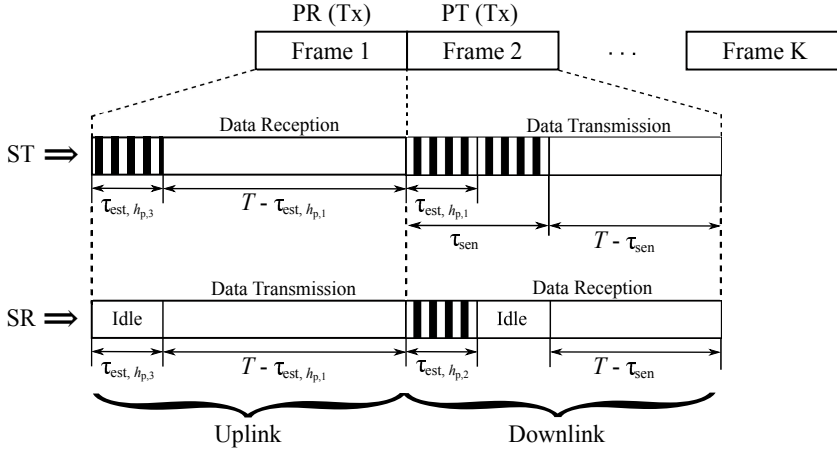


Figure 4.2: Frame structure of HSs illustrating the time allocation for channel estimation, sensing and data transmission from the perspective of a ST and a SR.

the estimation based on the pilot symbols transmitted by the ST. Considering the fact that the pilot-based estimation allocate a negligible amount of samples compared to the received power-based estimation. In this context, time resources are allocated for the estimation of h_s are omitted in the frame structure. In simple words, time allocation for the pilot based-estimation have little impact on the secondary throughput. But, it causes variations in the performance, leading to uncertain interference. As a result, these variations are accounted in the analytical framework.

Apart from this, it is possible that the time interval between two control-based transmissions is large as compared to T . Under such conditions, the frame structure followed by the secondary system can be adapted from the one proposed in Figure 4.2 in such a way that channel estimation is restricted to particular frames and the remaining frames follow the conventional structure, i.e., sensing followed by data transmission. Hence, the proposed frame structure presents a general framework and is adaptable to different control-based configurations followed by various primary systems. For scenarios, where the PT and the PR represent a single entity, i.e., interchangeably act as transmitter and receiver, the first two slots $\tau_{est, h_{p,1}}$ and $\tau_{est, h_{p,3}}$ of the ST can be combined into one, cf. Figure 4.2.

4.4.2 Channel Estimation

Here, the estimation of the interacting channels is revisited. In this chapter, a similar approach for the channel estimation to the one described in chapters 2 and 3, according to which, it is logical to employ a received power-based estimation for the sensing and the interference channels, and a pilot-based estimation for the access channel.

Sensing Channel ($h_{p,1}$)

The ST estimates the sensing channel by estimating the received power from the PT during $\tau_{\text{est}, h_{p,1}}$. With $\tau_{\text{est}, h_{p,1}} f_s$ samples used for estimation, the estimated received power $\hat{P}_{\text{Rx,ST}, h_{p,1}} = \sum_{n=1}^{\tau_{\text{est}, h_{p,1}} f_s} |h_{p,1} x_{\text{PT}}[n] + w[n]|^2$ follows a χ^2 distribution. The cumulative distribution function (cdf) of $\hat{P}_{\text{Rx,ST}, h_{p,1}}$ is characterized as

$$F_{\hat{P}_{\text{Rx,ST}, h_{p,1}}} (x) = 1 - \Gamma \left(\frac{\tau_{\text{est}, h_{p,1}} f_s}{2}, \frac{\tau_{\text{est}, h_{p,1}} f_s x}{2P_{\text{Rx,ST}, h_{p,1}}} \right). \quad (4.14)$$

In order to improve the detector's performance, the samples $f_s \tau_{\text{est}, h_{p,1}}$ considered for the estimation can also be utilized for the sensing $f_s \tau_{\text{sen}}$ as illustrated in Figure 4.2. In this sense, hereafter, the characterization of the detector incurs the time interval $\tau_{\text{est}, h_{p,1}}$.

Access Channel (h_s)

The pilot signal received from the SR undergoes matched filtering and demodulation at the ST, hence, a pilot-based estimation at the ST is employed to acquire the knowledge of the access channel. The maximum-likelihood estimate of \hat{h}_s presented by [43] is unbiased, efficient, i.e., achieves a Cramér-Rao bound with equality and asymptotic variance $\mathbb{E} [|h_s - \hat{h}_s|^2] = \frac{\sigma_w^2}{2N_s}$, where N_s denotes the number of pilot symbols. As a result, \hat{h}_s conditioned on h_s follows a Gaussian distribution $\hat{h}_s | h_s \sim \mathcal{N} \left(h_s, \frac{\sigma_w^2}{2N_s} \right)$. Consequently, the estimated power gain $|\hat{h}_s|^2$ follows a non-central chi-squared $\mathcal{X}_1^2(\lambda_s, 1)$ distribution with 1 degree of freedom and non-centrality parameter $\lambda_s = \frac{2N_s |h_s|^2}{\sigma_w^2}$. For analytical tractability, the following approximation is considered.

Approximation 1 For all degrees of freedom, the \mathcal{X}_1^2 distribution can be approximated by a Gamma distribution [57]. The parameters of the Gamma distribution are obtained by matching the first two central moments to those of \mathcal{X}_1^2 .

Following Approximation 1, the cdf of $|\hat{h}_s|^2$ is characterized as

$$F_{|\hat{h}_s|^2}(x) \approx 1 - \Gamma\left(a, \frac{x}{b}\right), \quad (4.15)$$

$$\text{where } a = \frac{(1 + \lambda_s)^2}{2 + 4\lambda_s} \text{ and } b = \frac{\sigma_w^2(2 + 4\lambda_s)}{(1 + \lambda_s)}. \quad (4.16)$$

Interference Channel ($h_{p,2}$)

Besides the access channel, the knowledge of the interference channel to the SR from the PT is required for determining the secondary throughput. It is worthy to note that the expression $|h_{p,2}|^2\sigma_s^2 + \sigma_w^2$ in R_1 and R_3 , cf. (4.9) and (4.11), which corresponds to the interference and the noise power, represents $P_{Rx,SR}$. Hence, by estimating $\hat{P}_{Rx,SR}$, it is possible to jointly characterize the interference and the noise, and consequently characterize R_1 and R_3 . In this view, the SR estimates received power by listening to the control-based transmission from the PT, cf. Figure 4.2. Similar to the sensing channel, the cdf of the estimated interference power received $\hat{P}_{Rx,SR}$ at the ST is characterized as

$$F_{\hat{P}_{Rx,SR}}(x) = 1 - \Gamma\left(\frac{\tau_{est, h_{p,2}} f_s}{2}, \frac{\tau_{est, h_{p,2}} f_s x}{2P_{Rx,SR}}\right). \quad (4.17)$$

Interference Channel ($h_{p,3}$)

Lastly, the estimation of the interference channel between the ST and the PR is essential for employing power control at the ST. Like the sensing channel, the ST estimates $|h_{p,3}|^2$ by listening to the control-transmission from the PR. The received power estimated ($P_{Rx,ST,h_{p,3}}$) from $\tau_{est, h_{p,3}} f_s$ samples follows \mathcal{X}^2 distribution and its cdf is given by

$$F_{\hat{P}_{Rx,ST,h_{p,3}}}(x) = 1 - \Gamma\left(\frac{\tau_{est, h_{p,3}} f_s}{2}, \frac{\tau_{est, h_{p,3}} f_s x}{2P_{Rx,ST,h_{p,3}}}\right). \quad (4.18)$$

4.4.3 Characterization of performance parameters

It is clear that the estimation of the involved channels translates to the variations in the performance parameters, which include detection probability \hat{P}_d at the ST, power received $\hat{P}_{Rx,PR}$ at the PR (which includes the interference and noise power) and secondary throughput \hat{R}_s at the SR. In particular, the variations in \hat{P}_d and $\hat{P}_{Rx,PR}$ lead to uncertain interference to the primary system, if not captured, it can seriously degrade the performance of CR systems. Such aspect concerning the uncertain interference has been left aside in the outage constraints (please consider, (4.6) and (4.7) determined by the ideal model. This renders the existing constraints defined by the ideal model inaccurate. Motivated by this fact, the uncertain interference is captured by proposing new outage constraints ρ_d and ρ_{cont} on the \hat{P}_d and $\hat{P}_{Rx,PR}$, respectively, as PU constraints for the HS. These constraints are defined as

$$\mathbb{P}(\hat{P}_d \leq \bar{P}_d) \leq \rho_d, \quad (4.19)$$

$$\mathbb{P}(\hat{P}_{Rx,PR} \geq \theta_1) \leq \rho_{cont}. \quad (4.20)$$

In contrast to the ideal model, which captures the interference received individually for the corresponding sensing outcomes P_d and $1 - P_d$, refer to (4.6) and (4.7), the proposed framework considers an outage over the two constraints jointly (by combining the corresponding sensing outcomes) in terms of the aggregate interference power received at the PR, $\hat{P}_{Rx,PR}$. In this regard, (4.20) is written as

$$\mathbb{E}_{\hat{P}_d} \left[\mathbb{P} \left(\mathbb{P}(\mathcal{H}_1) \cdot \overbrace{\left(\frac{\hat{P}_{Rx,ST,h_{p,3}} - \sigma_w^2}{\sigma_s^2} \right)}^{|\hat{h}_{p,3}|^2} \geq ((1 - \hat{P}_d)P_{Tx,ST,\text{full}} + \hat{P}_d P_{Tx,ST,\text{cont}}) \geq \theta_1 \right) \right] \leq \rho_{cont}, \quad (4.21)$$

where $\mathbb{E}_{\hat{P}_d} [\cdot]$ and $\mathbb{P}(\cdot)$ (that represents the cdf of $\hat{P}_{Rx,PR}$) capture the variations due to \hat{P}_d and $\hat{P}_{Rx,PR}$. To proceed further, the cdf of \hat{P}_d , $\hat{P}_{Rx,PR}$ and \hat{R}_s are characterized. This is done by transforming the cdfs of the estimated parameters, characterized previously in (4.14), (4.15), (4.17) and (4.18). To begin with, the cdf of the \hat{P}_d is evaluated to characterize the constraint on the detection probability defined in (4.19).

Lemma 4 The cdf of P_d is characterized as (see chapter for proof 2)

$$F_{\hat{P}_d}(x) = 1 - \Gamma\left(\frac{\tau_{\text{est}, h_{p,1}} f_s}{2}, \frac{\tau_{\text{est}, h_{p,1}} f_s \tau_{\text{sen}} f_s \mu}{4 P_{\text{Rx,ST}, h_{p,1}} \Gamma^{-1}\left(\frac{\tau_{\text{sen}}}{2}, x\right)}\right), \quad (4.22)$$

where $\Gamma^{-1}(\cdot, \cdot)$ is inverse function of regularized upper-incomplete Gamma function [51].

Along with $F_{\hat{P}_d}$ defined in (4.22), the cdf of the $P_{\text{Rx,PR}}$ is characterized in order to characterize the outage constraint defined in (4.20).

Lemma 5 The cdf of $\hat{P}_{\text{Rx,PR}}$ is characterized as

$$\begin{aligned} F_{\hat{P}_{\text{Rx,PR}}}(x) &= \\ &\int_0^1 \Gamma\left(\frac{\tau_{\text{est}, h_{p,3}} f_s}{2}, \left(\frac{x \sigma_s^2}{h_{p,1} \cdot ((1 - P_d) P_{\text{Tx,ST,full}} + P_d P_{\text{Tx,ST,cont}})} + \sigma_w^2\right) \times \right. \\ &\left. \frac{\tau_{\text{est}, h_{p,3}} f_s}{2 P_{\text{Rx,ST}, h_{p,3}}} \right) dF_{\hat{P}_d}. \end{aligned} \quad (4.23)$$

Besides that, since the variations in \hat{P}_d , $\hat{P}_{\text{Rx,ST}, h_{p,1}}$, $|\hat{h}_s|^2$ and $\hat{P}_{\text{Rx,ST}, h_{p,3}}$ translate to the variations in \hat{R}_s , these variations are captured in terms of the expected secondary throughput. More specifically, the variations in $\hat{P}_{\text{Rx,ST}, h_{p,1}}$, $|\hat{h}_s|^2$ and $\hat{P}_{\text{Rx,ST}, h_{p,3}}$ result in variations in capacities \hat{C}_0 , \hat{C}_1 , \hat{C}_2 and \hat{C}_3 , cf. (4.8), (4.9), (4.10) and (4.11). In this view, we characterize the probability density functions (pdfs) for \hat{C}_0 , \hat{C}_1 , \hat{C}_2 and \hat{C}_3 in the following Lemmas.

Lemma 6 The pdf of \hat{C}_0 is defined as (refer to chapter 2)

$$f_{\hat{C}_0}(x) = 2^x \ln 2 \frac{(2^x - 1)^{a_1 - 1}}{\Gamma(a_1) b^{a_1}} \exp\left(-\frac{2^x - 1}{b_1}\right), \quad (4.24)$$

$$\text{where } a_0 = a \text{ and } b_0 = \frac{P_{\text{Tx,ST,full}}}{\sigma_w^2} b, \quad (4.25)$$

where a and b are defined in (4.16).

Lemma 7 The pdf of \hat{C}_1 is defined as (refer to chapter 2)

$$f_{\hat{C}_1}(x) = 2^x \ln 2 \frac{(2^x - 1)^{a_0-1} \Gamma(a_0 + a_1)}{\Gamma(a_0) \Gamma(a_1) b_0^{a_0} b_1^{a_1}} \left(\frac{1}{b_1} + \frac{2^x - 1}{b_0} \right), \quad (4.26)$$

$$\text{where } a_1 = \frac{N_{p,2}}{2} \text{ and } b_1 = \frac{2P_{Rx,SR}}{\sigma_w^2 N_{p,2}}, \quad (4.27)$$

and a_0, b_0 are defined in (4.25).

Following the characterization of the pdfs for C_0 and C_1 , the pdfs for C_2 and C_3 can be obtained by substituting $P_{Tx,ST,cont}$ for $P_{Tx,ST,full}$ in (4.24) and (4.26).

Lemma 8 The pdf of \hat{C}_2 is defined as

$$f_{\hat{C}_2}(x) = 2^x \ln 2 \frac{(2^x - 1)^{a_2-1}}{\Gamma(a_2) b^{a_2}} \exp \left(-\frac{2^x - 1}{b_2} \right), \quad (4.28)$$

$$\text{where } a_2 = \frac{(1 + \lambda_s)^2}{2 + 4\lambda_s} \text{ and } b_2 = \frac{P_{Tx,ST,cont}}{\sigma_w^2} \frac{\sigma_w^2 (2 + 4\lambda_s)}{(1 + \lambda_s)}. \quad (4.29)$$

Lemma 9 The pdf of \hat{C}_3 is defined as

$$f_{\hat{C}_3}(x) = 2^x \ln 2 \frac{(2^x - 1)^{a_2-1} \Gamma(a_2 + a_1)}{\Gamma(a_2) \Gamma(a_1) b_2^{a_2} b_1^{a_1}} \left(\frac{1}{b_1} + \frac{2^x - 1}{b_2} \right), \quad (4.30)$$

where a_1, b_1 and a_2, b_2 are defined in (4.27) and (4.29), respectively.

Subsequently, the variations arising due to \hat{P}_d are captured by considering $F_{\hat{P}_d}$ characterized in Lemma 4. As a result, the expected throughput is given by (4.31), where $\mathbb{E}_\Omega [\cdot]$ denotes the expectation over Ω , where $\Omega \in \{\hat{P}_d, \hat{C}_0, \hat{C}_1, \hat{C}_2, \hat{C}_3\}$

$$\begin{aligned} \mathbb{E}_\Omega [R_s(\tau_{sen})] &= \frac{T - \tau_{est, h_{p,3}} - \tau_{sen}}{T} \times \\ &\left[(1 - P_{fa}) \cdot \mathbb{P}(\mathcal{H}_0) \cdot \mathbb{E}_{\hat{C}_0} [\hat{C}_0] + (1 - \mathbb{E}_{\hat{P}_d} [\hat{P}_d]) \cdot \mathbb{P}(\mathcal{H}_1) \cdot \mathbb{E}_{\hat{C}_1} [\hat{C}_1] \right. \\ &+ P_{fa} \cdot \mathbb{P}(\mathcal{H}_0) \cdot \mathbb{E}_{\hat{C}_2} [\hat{C}_2] + \mathbb{E}_{\hat{P}_d} [\hat{P}_d] \cdot \mathbb{P}(\mathcal{H}_1) \cdot \mathbb{E}_{\hat{C}_3} [\hat{C}_3] \left. \right]. \end{aligned} \quad (4.31)$$

The random variables \hat{P}_d and \hat{C}_1, \hat{C}_3 are functions of independent random variables $\hat{P}_{Rx,ST}$ and, $|\hat{h}_s|^2$ and $\hat{P}_{Rx,SR}$, respectively. In this context, the independence property is applied to carry out the expectation on \hat{P}_d , \hat{C}_1 and \hat{C}_3 in (4.31) individually.

4.4.4 Sensing-Throughput Tradeoff

Here, a sensing-throughput tradeoff for the proposed approach that incorporates variations in the performance parameters is established.

Theorem 5 The expected achievable secondary throughput subject to an outage constraint on detection probability at the ST and an outage constraint on interference power at the PR given by

$$R_s(\tilde{\tau}_{est, h_{p,1}}, \tilde{\tau}_{est, h_{p,2}}, \tilde{\tau}_{est, h_{p,3}}, \tilde{\tau}_{sen}) = \max_{\substack{\tau_{est, h_{p,1}}, \tau_{est, h_{p,2}}, \tau_{est, h_{p,3}}, \\ \tau_{sen}, P_{Tx,ST,cont}}} \mathbb{E}_{\Omega} [R_s(\tau_{sen})] \quad (4.32)$$

s.t. (4.19), (4.21).

Proof: In order to solve the constrained optimization problem, the following assumptions are considered: (i) for the simplicity of the analysis, the estimation times $(\tau_{est, h_{p,1}}, \tau_{est, h_{p,2}}, \tau_{est, h_{p,3}})$ are optimized jointly, i.e., $\tau_{est, h_{p,1}} = \tau_{est, h_{p,2}} = \tau_{est, h_{p,3}}$, (ii) it is assumed that the primary system attains sufficient protection when high detection probability is achieved by the ST. In this sense, it is reasonable to consider first the constraint on the detection probability with desired \bar{P}_d and ρ_d , cf. (4.19). These assumptions are used to obtain an expression of μ (refer to chapter 2)

$$\mu \geq \frac{4P_{Rx,ST,h_{p,1}}\Gamma^{-1}\left(1 - \rho_d, \frac{\tau_{est, h_{p,1}}f_s}{2}\right)\Gamma^{-1}\left(\bar{P}_d, \frac{\tau_{sen}f_s}{2}\right)}{\tau_{est, h_{p,1}}\tau_{sen}(f_s)^2}. \quad (4.33)$$

Next, using the constraint (4.21), the controlled transmit power at the SR is determined as

$$\mathbb{E}_{\hat{P}_d} \left[F_{\hat{P}_{Rx,PR}}(\hat{P}_d, \theta_1) \right] \geq \rho_{cont}. \quad (4.34)$$

Solving numerically (5.9) yields $P_{Tx,ST,cont}$ for the HS. Finally, by substituting μ and $P_{Tx,ST,cont}$ computed in (5.9) and (4.33), and using the pdfs of \hat{P}_d , \hat{C}_0 , \hat{C}_1 , \hat{C}_2 and \hat{C}_3 determined in Lemma 4, Lemma 6, Lemma 7, Lemma 8 and Lemma 9

yield an expression of $\mathbb{E}_{\Omega} [R_s]$ as a function of $\tau_{\text{est}, h_{p,1}}, \tau_{\text{est}, h_{p,2}}, \tau_{\text{est}, h_{p,3}}$ and τ_{sen} , cf. (4.31). Solving numerically $\mathbb{E}_{\Omega} [R_s]$ delivers $\tilde{\tau}_{\text{est}, h_{p,1}}, \tilde{\tau}_{\text{est}, h_{p,2}}, \tilde{\tau}_{\text{est}, h_{p,3}}$ and $\tilde{\tau}_{\text{sen}}$ that achieves the maximum expected secondary throughput. ■

Remark 5 Herein, using the estimation model, a fundamental relation between estimation time (regulates the variations in the detection probability and interference power received at the PR according to the PU constraint), sensing time (represents the detector's performance) and secondary throughput is established, this relationship is characterized as an estimation-sensing-throughput tradeoff. Based on this tradeoff, suitable estimation and suitable sensing time intervals are determined that yields an optimum performance for the HS in terms of achievable secondary throughput.

4.5 Numerical Analysis

In this section, the performance of the proposed approach is evaluated. In this view, simulations are performed: (i) to validate the expressions obtained in the previous section, (ii) to analyze the performance loss incurred due to channel estimation. In order to illustrate the performance degradation, the ideal model is considered to benchmark the performance of the proposed approach. Unless stated explicitly, the choice of parameters given in Table 4.1 is considered for analysis. First the performance of the HS is analyzed in terms of a sensing-throughput tradeoff, cf. Theorem 5, corresponding to the Ideal Model (IM) and Estimation Model (EM) by fixing $\tau_{\text{est}, h_{p,1}} = \tau_{\text{est}, h_{p,2}} = \tau_{\text{est}, h_{p,3}} = 1 \text{ ms}$, cf. Figure 4.3. With the inclusion of channel estimation in the frame structure, the ST procures no throughput at the SR for the interval $\tau_{\text{est}, h_{p,1}}$. As indicated by the margin between the IM and the EM, a certain performance degradation is witnessed by the EM due to the incorporation of channel estimation. Moreover, the sensing-throughput tradeoff yields a suitable sensing time $\tilde{\tau}_{\text{sen}}$ that achieves the maximum performance in terms of secondary throughput $R_s(\tilde{\tau}_{\text{sen}})$. Hereafter, the theoretical expressions are considered for the analysis. In addition, the proposed EM operates at the suitable sensing time.

Following the previous discussions, it is well-known that the combination of interweave and underlay systems is intended to enhance the performance of the HS, hence, it is worthy to acquire insights on the performance gain in terms of the achievable secondary throughput due to the association of the underlay and the interweave techniques in the HS. In this regard, it is essential to observe the

Table 4.1: Parameters for Numerical Analysis

Parameter	Value
f_s	1 MHz
T	100 ms
$\tau_{\text{est}}, h_{p,1}$	1 ms
$\tau_{\text{est}}, h_{p,2}$	1 ms
$\tau_{\text{est}}, h_{p,3}$	1 ms
$ h_{p,1} ^2$	-120 dB
$ h_{p,2} ^2$	-120 dB
$ h_{p,3} ^2$	-100 dB
$ h_s ^2$	-80 dB
θ_I	-110 dBm
ρ_{cont}	0.1
ρ_d	0.1
σ_w^2	0 dBm
N_s	10

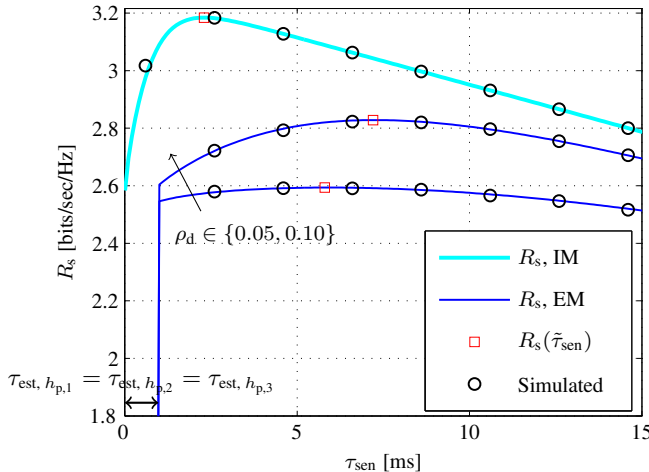


Figure 4.3: Sensing-throughput tradeoff for the Ideal Model and Estimation Model (EM) for $\tau_{\text{est}, h_{p,1}} = \tau_{\text{est}, h_{p,2}} = \tau_{\text{est}, h_{p,3}} = 1 \text{ ms}$.

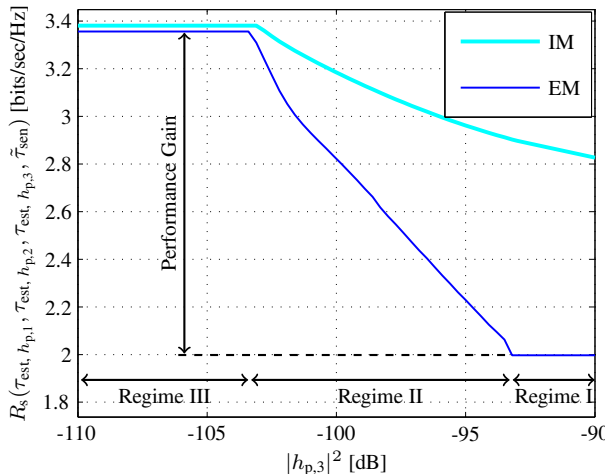


Figure 4.4: Achievable secondary throughput versus path loss $|h_{p,3}|^2$ where the system is operating at $\tilde{\tau}_{\text{sen}}$ and the estimation time is fixed to $\tau_{\text{est}, h_{p,1}} = \tau_{\text{est}, h_{p,2}} = \tau_{\text{est}, h_{p,3}} = 1 \text{ ms}$.

variation of the achievable secondary throughput corresponding to the interfer-

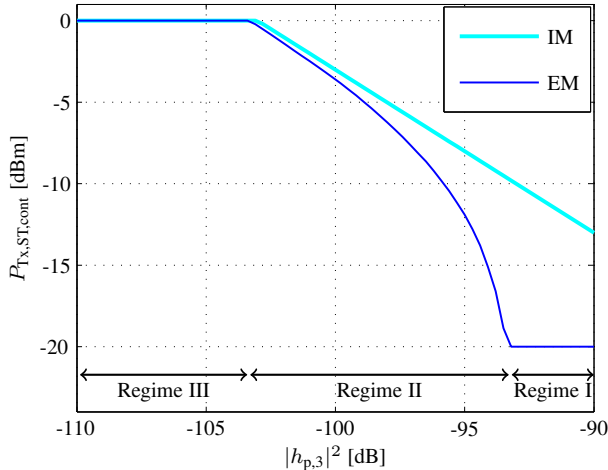


Figure 4.5: Optimum power control versus path loss $|h_{p,3}|^2$ where the system is operating at $\tilde{\tau}_{sen}$ and the estimation time is fixed to $\tau_{est}, h_{p,1} = \tau_{est}, h_{p,2} = \tau_{est}, h_{p,3} = 1 \text{ ms}$.

ence channel from the ST to the PR, cf. Figure 5.1. Before proceeding with the analysis, it is essential to understand that the performance of the underlay system decreases with the increase in the channel gain $|h_{p,3}|^2$. To simplify the analysis, the channel gain $|h_{p,3}|^2 \in [-110, -90] \text{ dBm}$ is categorized in three different regimes: (i) Regime I, (ii) Regime II and (iii) Regime III, cf. Figure 4.4. Under Regime I, large channel gain $|h_{p,3}|^2 > -93 \text{ dB}$ causes control power to fall below a certain level $P_{\text{Tx,ST,cont}} \leq -20 \text{ dBm}$, cf. Figure 4.5, for the considered value of the channel gain $|h_s|^2 = -80 \text{ dB}$ over the access channel, such a low power transmission do not translate to an effective performance gain to the HS. As a result, no benefits are attained from the underlay system while operating in this regime, hence, the HS operates as an IS. In contrast to that, the Regime II ($-103 \text{ dB} < |h_{p,3}|^2 < -93 \text{ dB}$) witnesses a significant performance gain as HS procures benefits from the US and the IS. Moreover, it is observed that, no performance gain is attained below a certain channel gain $|h_{p,3}|^2 < -103 \text{ dB}$ (Regime III). This is due to the fact that the ST is limited by the maximum transmit power, i.e., beyond -103 dB , $P_{\text{Tx,ST,full}}$ operates at $P_{\text{Tx,ST,full}}$, as illustrated in Figure 4.5. From this discussion, it can be concluded that the interference tolerance capability of the US and the detection capability of the IS incorporated by the HS can be transformed into significant performance gain only in situations where the channel gain between the ST

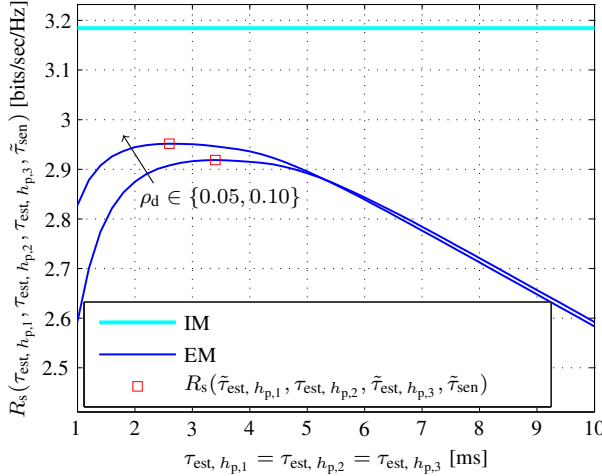


Figure 4.6: Achievable secondary throughput versus the estimation time $\tau_{\text{est}, h_{p,1}} = \tau_{\text{est}, h_{p,2}} = \tau_{\text{est}, h_{p,3}}$ operating at the suitable sensing time $\tilde{\tau}_{\text{sen}}$.

and the PR goes below a certain level, for instance $|h_{p,3}|^2 < -93 \text{ dBm}$ for the considered case.

Besides maximizing the secondary throughput over the sensing time, it is interesting to observe the variation of the achievable throughput with the estimation time. As proposed in Theorem 5, $\tau_{\text{est}, h_{p,1}} = \tau_{\text{est}, h_{p,2}} = \tau_{\text{est}, h_{p,3}}$ is considered for the analysis. Corresponding to the estimation model, Figure 4.6 reveals the estimation-sensing-throughput tradeoff, cf. Remark 5. This effect can be explained as follows, the variations due to the estimation of $|h_{p,1}|^2$ and $|h_{p,3}|^2$ causes variations in \hat{P}_d and $\hat{P}_{\text{RX,PR}}$, these variations are captured using the outage constraints, hence, a small increase in $\tau_{\text{est}, h_{p,1}}$ ($= \tau_{\text{est}, h_{p,2}} = \tau_{\text{est}, h_{p,3}}$) leads to a significant performance improvement in terms of secondary throughput, however, by increasing the estimation time beyond $\tilde{\tau}_{\text{est}, h_{p,1}}$ ($= \tilde{\tau}_{\text{est}, h_{p,2}} = \tilde{\tau}_{\text{est}, h_{p,3}}$) slightly contributes to the performance improvement and largely consumes the time resources, which leads to performance degradation. Moreover, it is noticed that performance degradation of the secondary system evaluated in terms of $R_s(\tau_{\text{est}, h_{p,1}} = \tau_{\text{est}, h_{p,2}} = \tau_{\text{est}, h_{p,3}}, \tilde{\tau}_{\text{sen}})$ becomes more sensitive to the estimation time $\tilde{\tau}_{\text{est}, h_{p,1}}$ ($= \tilde{\tau}_{\text{est}, h_{p,2}} = \tilde{\tau}_{\text{est}, h_{p,3}}$) as ρ_d decreases. From this analysis, it can be concluded that a suitable choice of estimation time becomes

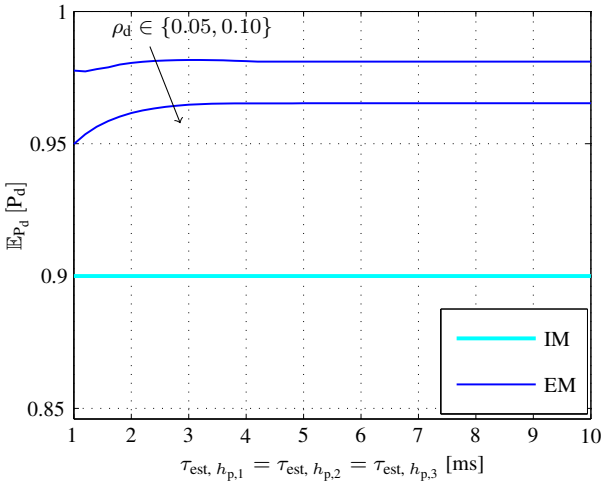


Figure 4.7: Detection probability versus $\tau_{\text{est}, h_{p,1}} = \tau_{\text{est}, h_{p,2}} = \tau_{\text{est}, h_{p,3}}$ operating at the suitable sensing time $\tilde{\tau}_{\text{sen}}$.

significant, specially for those HSs that are pertained to the aggressive policies provided by the primary systems or regulatory bodies.

To procure further insights, the variation of the detector's performance with the estimation time is analyzed. For the EM, it is observed that, for all values of the estimation time, expected detection probability $\mathbb{E}_{\hat{P}_d} [\hat{P}_d]$ strictly stays above \bar{P}_d , cf. Figure 4.7. This indicates that the proposed approach yields a reasonable performance of the detector incorporated in the HS. It is further noticed that the expected detection probability slightly degrades for low values of the estimation time. This is due to the fact that low values of $\tau_{\text{est}, h_{p,1}}$ shifts the probability mass of \hat{P}_d towards lower values, thus, a small value of $\mathbb{E}_{\hat{P}_d} [\hat{P}_d]$ is attained.

Finally, the variation of P_{fa} along the estimation time is illustrated in Figure 4.8. From the HS's perspective, it is worthy to note that low P_{fa} is beneficial only if the HS procures its large contribution of the performance when operating in interweave mode, refer to (4.31). From Figure 4.8, it is noticed that the P_{fa} improves with estimation time, particularly $\tau_{\text{est}, h_{p,1}}$. It is important to note the detector's performance is similar to one depicted by the ISs in chapter 2, according to which, the estimation time and the sensing time jointly controls the

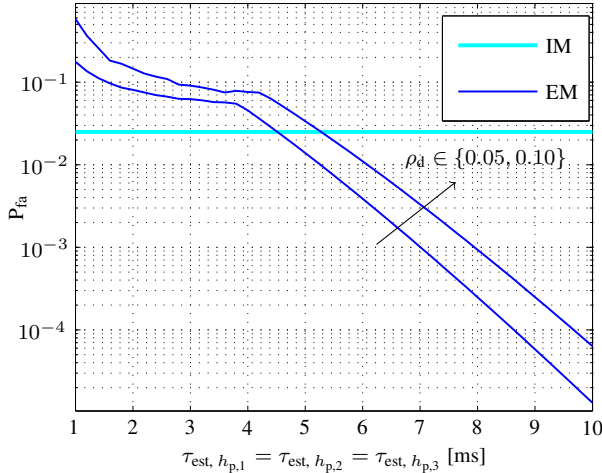


Figure 4.8: False alarm probability versus $\tau_{est, h_{p,1}} = \tau_{est, h_{p,2}} = \tau_{est, h_{p,3}}$ operating at the suitable sensing time $\tilde{\tau}_{sen}$.

variations due to the channel estimation and the performance of the detector. Beyond $\tilde{\tau}_{est, h_{p,1}}, \tilde{\tau}_{sen}$, the time resources contribute only to improve the detector's performance, therefore lead to the performance degradation in terms of the secondary throughput. Since \hat{P}_d is constrained, the improvement in the detector's performance is noticed in P_{fa} , cf. Figure 4.8

4.6 Summary

In this chapter, the performance of cognitive radio as a hybrid system that exploits the benefits of both underlay and interweave paradigms from a deployment perspective is investigated. It has been argued that the lack of knowledge of the involved channels renders the existing models unsuitable for the performance characterization. In this view, an analytical framework that incorporates channel estimation, and subsequently captures the effect of imperfect channel knowledge has been established. More importantly, a fundamental tradeoff among the estimation time, sensing time and the secondary throughput is proposed that jointly captures the effect of the channel estimation (in terms of the time resources allocated for the channel estimation and the uncertain in-

4 Hybrid Systems

terference due to the imperfect knowledge of the involved channels) and the performance of the primary and the secondary systems. Based on this tradeoff, the proposed analytical framework, a suitable estimation time and a suitable sensing time that yields the achievable secondary throughput is determined.

CHAPTER 5

Hardware Validation and Demonstration

Previous chapters (chapter 2, chapter 3 and chapter 4) focused on characterizing the performance of different CR systems jointly in terms of the interference power received by the PR and the throughput at the SR by taking the estimation of the involved channels into account. In addition, it has been motivated that the low complexity and the versatility towards unknown primary user signals requirements can be satisfied only if unconventional channel estimation techniques such as received power-based estimation are employed for acquiring the knowledge of the interacting channels, particularly for the channels between the primary and the secondary systems, which corresponds to different systems. However, the aforementioned analysis in the previous chapters has been limited to the theoretical expressions. With regard to the analytical expressions that are necessary for the performance analysis, it is essential as well-as challenging to depict the hardware realizability of CR systems.

Motivated by this fact, this chapter, which is based on [K6, K12], reconciles between the theory established in the previous chapters and the hardware feasibility of the CSC. As a result, it complements the performance analysis by deploying the CR techniques on a hardware. By doing this, the applicability of the assumptions considered while deriving the analytical expressions can be examined. These investigations are essential to facilitate the evolution of the

proposed analytical framework. Without any specific argumentation, an US is considered for the deployment.

This chapter provides the following contributions:

- Empirical validation: The performance of the USs in accordance to the received power-based estimation employed for the channel between the PR and the ST is validated by means of a hardware deployment. The variations (induced due to incorporation of channel estimation) in the system parameters are validated by comparing their probability density functions obtained from the measurements to those computed analytically. Moreover, the joint performance of the underlay system is validated in terms of an estimation-throughput tradeoff proposed in chapter 3.
- Demonstrator: Upon validating the theoretical expressions, a hardware demonstrator following the guidelines of an US is deployed. In this context, the applicability of the proposed framework in realistic scenarios can be justified. A graphical user interface is designed to procure insights to the working of the demonstrator.

5.1 System Model

5.1.1 Simplifications

In contrast to the framework presented in chapter 3, the following simplifications and modifications are considered for the hardware implementation.

- The channel estimation (received power-based) is only deployed for the link between the PR and the ST, which is associated with the interference (power) received at the PR. In order to simplify the deployment, the interference from the PTs at the SR is neglected¹. In addition, perfect knowledge of the access channel between the ST and the SR that employs the pilot-based channel estimation is considered².

¹Although the interference from the PTs plays an significant role in characterizing the throughput at the SR, the interference at the PR is more critical for the PU or the regulatory bodies.

²Since the effect due to the pilot-based channel estimation in terms of time allocated within the frame structure and the amount of variations induced has negligible effect on the performance degradation of the CR system, perfect channel estimation for access channel presents a reasonable assumption.

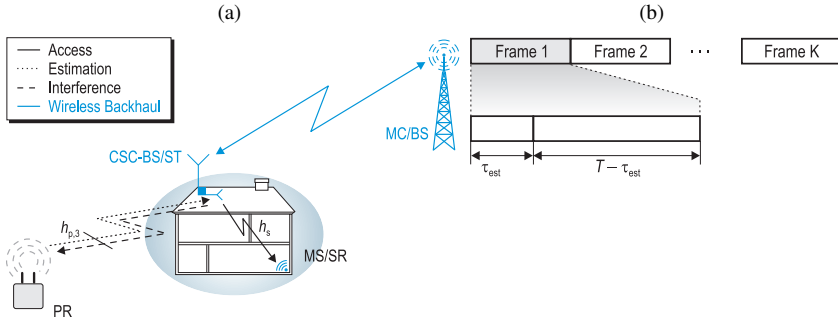


Figure 5.1: A simplified (with respect to the chapter 3) illustration of (a) the CSC scenario demonstrating an underlay paradigm. (b) Frame structure from the perspective of the ST that presents a time duration (τ_{est}) allocated within the frame duration for the estimation of the interference channel.

- The measurements taken to perform the validation and the demonstration for the proposed deployment scenario consider the deterministic behaviour of the interference channel.
- As an alternative to the outage constraint proposed in chapter 3, a confidence probability constraint is employed for capturing the variations due to channel estimation around the interference temperature.
- Lastly, in contrast to the OFDM signal considered in chapter 3, in this chapter all transmit signals (which include pilot and data signals) at the primary and the secondary systems are modeled as a PSK signal.

In accordance to these simplifications and the modifications, the system model for the US depicted in chapter 3 is slightly modified.

5.1.2 Underlay Scenario and Medium Access

Figure 5.1 depicts a CSC deployment consisting of a CSC-BS, a MS, a PR and a MC-BS. Analog to the previous scenarios, the CSC-BS and the MS represent a ST and a SR. The channels between the PR and the ST and between the ST and SR are designated as the interference and the access channels with channel gains $h_{p,3}$ and h_s , respectively. A power control mechanism is employed at

the ST to ensure that interference received at the PR is below a certain level. In order to exercise power control mechanism, it is necessary to acquire the knowledge of the channel between the ST and the PR. As proposed in chapter 3, the ST can retrieve this information by listening to a pilot or beacon signal transmitted by the PR.

A slotted medium access is implemented at the ST with a frame duration of T . The knowledge of the interference channel is acquired by employing channel reciprocity over the link PR-ST. Besides, T is selected such that the channel can be assumed to remain constant for the frame duration. In order to incorporate channel estimation in context to the power control mechanism, the frame interval is divided in two phases, namely estimation and data transmission, refer to Figure 5.1. During the estimation phase τ_{est} (also referred as estimation time), the ST measures the received power of the signal³ transmitted by the PR. Based on this received power, the ST estimates $|h_{\text{p},3}|^2$ and control its transmit power for the secondary link in order to satisfy a certain constraint on the interference power (interference) received by the PR. During the data transmission phase $T - \tau_{\text{est}}$, the ST transmits data with the controlled power to the SR.

5.1.3 Signal Model

The discrete and complex signal received at the ST is given by

$$y_{\text{ST}}[n] = h_{\text{p},3} \cdot x_{\text{PR}}[n] + w[n], \quad (5.1)$$

where $x_{\text{PR}}[n]$ corresponds to a discrete constant power signal transmitted by the PR, $|h_{\text{p},3}|^2$ represents the power gain for the channel PR-ST and $w[n]$ is circularly symmetric Additive White Gaussian Noise (AWGN) at the ST. $P_{\text{Tx,PR}}$ corresponds to the transmit power at the PR and $w[n]$ is an independent identically distributed (i.i.d.) Gaussian random process with mean $\mathbb{E}[w[n]] = 0$ and variance $\mathbb{E}[|w[n]|^2] = \sigma_w^2$. By the listening to the transitions from the PR, the estimated received power at the ST, computed using $\tau_{\text{est}}f_s$ samples, is given as

$$\hat{P}_{\text{Rx,ST}} = \frac{1}{\tau_{\text{est}}f_s} \sum_{n=1}^{\tau_{\text{est}}f_s} |h_{\text{p},3}x_{\text{PR}}[n] + w[n]|^2, \quad (5.2)$$

³This signal can be a data or a pilot signal with known transmit power

where f_s denotes the sampling frequency. After implementing the power control ($P_{\text{Tx,ST,cont}}$) at the ST, the received signal at the PR, during the data transmission, is given by

$$y_{\text{PR}}[n] = h_{\text{p,3}} \cdot x_{\text{ST,cont}}[n] + w[n], \quad (5.3)$$

and on the other side, the received signal at the SR follows

$$y_{\text{SR}}[n] = h_s \cdot x_{\text{ST,cont}}[n] + w[n], \quad (5.4)$$

where $x_{\text{ST,cont}}[n]$ is an i.i.d. random process. The controlled power at the ST is determined as

$$\hat{P}_{\text{Tx,ST,cont}} = \frac{1}{(T - \tau_{\text{est}})f_s} \sum_{n=1}^{(T - \tau_{\text{est}})f_s} |x_{\text{ST,cont}}[n]|^2 \quad (5.5)$$

Further, $|h_{\text{p,3}}|^2$ and $|h_s|^2$ represent the power gains for the channels ST-PR and ST-SR, respectively, cf. Figure 5.1. The received powers at the PR and the SR are evaluated as

$$\hat{P}_{\text{Rx,PR}} = \frac{1}{(T - \tau_{\text{est}})f_s} \sum_{n=1}^{(T - \tau_{\text{est}})f_s} |y_{\text{PR}}[n]|^2 \quad (5.6)$$

and

$$\hat{P}_{\text{Rx,SR}} = \frac{1}{(T - \tau_{\text{est}})f_s} \sum_{n=1}^{(T - \tau_{\text{est}})f_s} |y_{\text{SR}}[n]|^2, \quad (5.7)$$

respectively. Likewise (5.1), $w[n]$ represents circularly symmetric AWGN at the PR and the ST with zero mean and variance $\mathbb{E}[|w[n]|^2] = \sigma_w^2$ and $\mathbb{E}[|w[n]|^2] = \sigma_w^2$, correspondingly.

After utilizing τ_{est} for channel estimation, the throughput at the SR (secondary throughput) over the access channel is given by

$$\hat{R}_s = \frac{T - \tau_{\text{est}}}{T} \log_2 \left(1 + \frac{|h_s|^2 \hat{P}_{\text{Tx,ST,cont}}}{\sigma_w^2} \right). \quad (5.8)$$

All transmitted signals are subjected to distance dependent path loss and small scale fading gains depicted as $h_{\text{p,3}}, h_s$. In the analysis, the coherence time of the channels $\approx T$ is considered. But, there will be scenarios where the coherence time exceeds T , in such cases the expressions derived in this chapter depicts a lower performance bound.

5.2 Theoretical Analysis

In order establish a close relationship between the analytical framework and the hardware implementation, the sequence of events depicted by the underlay scenario in Figure 5.1 are summarized as follows:

1. The ST estimates the power received $\hat{P}_{\text{Rx,ST}}$ (receiver power-based estimation) by listening to the pilot signal received from the PR over the interference channel. In the context of the hardware implementation, an unmodulated sinusoidal signal is sent as a pilot or beacon signal⁵.
2. With the knowledge of the $P_{\text{Tx,PR}}$ and the estimate $\hat{P}_{\text{Rx,ST}}$, the ST indirectly acquires the knowledge of $|h_{p,3}|^2$. Upon acquiring this knowledge, a power control is employed at the ST. Using $\hat{P}_{\text{Rx,ST}}$, $\hat{P}_{\text{Tx,ST,cont}}$ is determined as

$$\hat{P}_{\text{Tx,ST,cont}} = \frac{\theta_I K}{\hat{P}_{\text{Rx,ST}}}, \quad (5.9)$$

where K represents a scaling factor. The scaling factor is required at the ST to hold $\mathbb{E}[\hat{P}_{\text{Rx,PR}}]$ at θ_I . It is defined as

$$K = \frac{1}{\mathbb{E}_{\hat{P}_{\text{Rx,ST}}} \left[\frac{h_{p,3}}{\hat{P}_{\text{Rx,ST}}} \right]}, \quad (5.10)$$

where, $\mathbb{E}_{\hat{P}_{\text{Rx,ST}}} [\cdot]$ represents the expectation over $\hat{P}_{\text{Rx,ST}}$.

3. The ST transmits data to the SR with $\hat{P}_{\text{Tx,ST,cont}}$. The estimated power ($\hat{P}_{\text{Rx,ST}}$) over the interference channel induces variations in controlled power defined as $\hat{P}_{\text{Tx,ST,cont}}$. Following the relation between the controlled power at the ST and the received power at the PR

$$\hat{P}_{\text{Rx,PR}} = |h_{p,3}|^2 \hat{P}_{\text{Tx,ST,cont}}, \quad (5.11)$$

the variations in $\hat{P}_{\text{Tx,ST,cont}}$ translate to the variations in $P_{\text{Rx,PR}}$ (defined as $\hat{P}_{\text{Rx,PR}}$) around θ_I , which result in uncertain interference at the PR. Unless captured, these variations may severely degrade the performance of

⁵The sinusoidal signal is mathematically equivalent to the constant power signal sent by the PR, which resembles a constant phase modulated signal or a perfectly downsampled (by choosing the sampling point appropriately, thereby satisfying the Nyquist criterion) PSK signal [K13].

the US. Besides this, due to the relationship between the controlled power and the secondary throughput defined in (5.8), a certain amount of the variations are further translated to the secondary throughput. These variations in the system parameters ($\hat{P}_{\text{Rx,ST}}$, $\hat{P}_{\text{Tx,ST,cont}}$, $\hat{P}_{\text{Rx,PR}}$ and \hat{R}_s) are characterized in terms of their probability density functions (pdfs).

4. In particular, the pdf of $\hat{P}_{\text{Rx,PR}}$ is utilized to employ an interference constraint (also referred as confidence probability constraint) in terms of confidence probability P_c at the ST such that the uncertain interference at the PR can be effectively regulated. In addition, by utilizing the pdf of \hat{R}_s , the performance of the access channel is determined in terms of the expected secondary throughput. Finally, subject to the interference constraint on the confidence probability the performance of the US is jointly characterized in terms of a tradeoff between the estimation time and the secondary throughput tradeoff.

5.2.1 Characterization of the System Parameters

In order to capture the variations induced due to channel estimation, the pdfs of the aforementioned system parameters ($\hat{P}_{\text{Rx,ST}}$, $\hat{P}_{\text{Tx,ST,cont}}$, $\hat{P}_{\text{Rx,PR}}$, \hat{R}_s) are characterized, subsequently.

In accordance to the employed signal model, $P_{\text{Rx,ST}}$ is modeled as a non-central chi-squared distribution \mathcal{X}_1^2 , whose pdf is characterized as [66]

$$f_{\hat{P}_{\text{Rx,ST}}}(x) = \frac{\tau_{\text{est}} f_s}{2\sigma_p^2} \left(\frac{\tau_{\text{est}} f_s x}{\lambda} \right)^{\frac{\tau_{\text{est}} f_s - 2}{4}} \exp \left(-\frac{\tau_{\text{est}} f_s x + \lambda}{2\sigma_p^2} \right) \times I_{\frac{\tau_{\text{est}} f_s}{2} - 1} \left(\frac{\sqrt{\tau_{\text{est}} f_s x \lambda}}{\sigma_p^2} \right), \quad (5.12)$$

where $\tau_{\text{est}} f_s$ is the degree of freedom and also the number of samples used for the estimation, σ_w^2 is the noise variance of the in-phase or quadrature-phase component of the received pilot signal ($y_{\text{ST}}[n]$, refer to 5.1), and $I_{\frac{\tau_{\text{est}} f_s}{2} - 1}(\cdot)$ is the modified Bessel function of the first kind of order $\frac{\tau_{\text{est}} f_s}{2} - 1$ [67]. Furthermore, the non-centrality parameter is defined as

$$\lambda = \sum_{n=1}^{\tau_{\text{est}} f_s} \mathbb{E}[|y_{\text{ST}}[n]|^2] = \tau_{\text{est}} f_s \times A^2 \quad (5.13)$$

The simplification in (5.13) is explained as follows: a sinusoidal signal that represents a pilot signal consists of a constant amplitude, which is down-converted by an I/Q demodulator at the ST. In this regard, the complex samples $y_{\text{ST}}[n]$ have a constant envelope of value A .

Corresponding to (5.9), $\hat{P}_{\text{Tx,ST,cont}}$ follows an inverse non-central chi-squared distribution. The pdf for $\hat{P}_{\text{Tx,ST,cont}}$ is given by

$$f_{\hat{P}_{\text{Tx,ST,cont}}}(x) = \frac{\tau_{\text{est}} f_s K \theta_I}{2 \sigma_w^2 x^2} e^{-\frac{\tau_{\text{est}} f_s}{2 \sigma_w^2} \left(\frac{K \theta_I}{x} + h_{p,3} P_{\text{Tx,PR}} \right)} \left(\frac{K \theta_I}{x h_{p,3} P_{\text{Tx,PR}}} \right)^{\frac{\tau_{\text{est}} f_s}{4} - \frac{1}{2}} \times \\ I_{\frac{\tau_{\text{est}} f_s}{2} - 1} \left(\frac{\tau_{\text{est}} f_s}{\sigma_w^2} \sqrt{\frac{K \theta_I h_{p,3} P_{\text{Tx,PR}}}{x}} \right). \quad (5.14)$$

Following the relation in (5.11) and substituting $f_{\hat{P}_{\text{Tx,ST,cont}}}(x)$ defined in (5.14), the pdf of $\hat{P}_{\text{Rx,PR}}$ is determined as

$$f_{\hat{P}_{\text{Rx,PR}}}(x) = \frac{h_{p,3} \tau_{\text{est}} f_s K \theta_I}{2 \sigma_w^2 x^2} e^{-\frac{\tau_{\text{est}} f_s h_{p,3}}{2 \sigma_w^2} \left(\frac{K \theta_I}{x} + P_{\text{Tx,PR}} \right)} \left(\frac{K \theta_I}{x P_{\text{Tx,PR}}} \right)^{\frac{\tau_{\text{est}} f_s}{4} - \frac{1}{2}} \times \\ I_{\frac{\tau_{\text{est}} f_s}{2} - 1} \left(\frac{\tau_{\text{est}} f_s h_{p,3}}{\sigma_w^2} \sqrt{\frac{K \theta_I P_{\text{Tx,PR}}}{x}} \right). \quad (5.15)$$

Consequently, the cumulative distribution function (cdf) of $\hat{P}_{\text{Rx,PR}}$ is given by

$$F_{\hat{P}_{\text{Rx,PR}}}(x) = Q_{\frac{\tau_{\text{est}} f_s}{2}} \left(\sqrt{\frac{\tau_{\text{est}} f_s P_{\text{Tx,PR}} h_{p,3}}{\sigma_w^2}}, \sqrt{\frac{\tau_{\text{est}} f_s h_{p,3} \theta_I K}{\sigma_w^2 x}} \right), \quad (5.16)$$

where $Q_{\frac{\tau_{\text{est}} f_s}{2}}(\cdot)$ is the Marcum Q-function [67].

Next, the pdf of the secondary throughput R_s is determined as

$$f_{\hat{R}_s}(x) = \frac{T}{T - \tau_{\text{est}}} \frac{\tau_{\text{est}} f_s K \theta_I h_s \ln 2}{2 \sigma_w^2 \sigma_w^2} \left(\frac{p(x) + 1}{[p(x)]^2} \right) e^{-\frac{\tau_{\text{est}} f_s}{2 \sigma_w^2} \left(\frac{K \theta_I \alpha_s}{p(x) \sigma_w^2} + h_{p,3} P_{\text{Tx,PR}} \right)} \quad (5.17)$$

$$\times \left(\frac{K\theta_1 h_s}{p(x) h_{p,3}} P_{Tx,PR} \sigma_w^2 \right)^{\frac{\tau_{est} f_s}{4} - \frac{1}{2}} I_{\frac{\tau_{est} f_s}{2} - 1} \left(\frac{\tau_{est} f_s}{\sigma_p^2} \sqrt{\frac{K\theta_1 h_{p,3} P_{Tx,PR} h_s}{p(x) \sigma_w^2}} \right),$$

with $p(x) = 2^{\frac{T_x}{T-\tau_{est}}} - 1$.

5.2.2 Estimation-Throughput Tradeoff

Following the estimation theory, it is clear that small τ_{est} results in large variations for the $\hat{P}_{Rx,PR}$, and subsequently results in the deviation of $\hat{P}_{Rx,PR}$ from θ_I . If not considered, these variations may affect the performance of the US. To capture these variations, an interference constraint defined in terms of a confidence probability P_c and an accuracy β^6 is proposed. In order to restrict the uncertain interference due to channel estimation, it is important to restrain P_c above a certain desired level \bar{P}_c for a fixed value of β . In this regard, the interference constraint is defined as

$$P_c = F_{\hat{P}_{Rx,PR}}((1 + \beta)\theta_I) - F_{\hat{P}_{Rx,PR}}((1 - \beta)\theta_I) \geq \bar{P}_c, \quad (5.18)$$

where $((1 + \beta)\theta_I)$ and $((1 - \beta)\theta_I)$ represent the confidence interval around θ_I . According to (5.18), the confidence probability can be computed by inserting confidence interval in $F_{\hat{P}_{Rx,PR}}(x)$, which is defined in (5.16). It is worthy to note that P_c depends on τ_{est} , through $F_{\hat{P}_{Rx,PR}}(x)$. Besides this, $\mathbb{E}_{\hat{R}_s}[\hat{R}_s]$ is also related to the estimation time. Hence, from the design perspective, it is essential to select the estimation time appropriately such that the maximum secondary throughput is achieved over the access link and the interference constraint is satisfied at the ST simultaneously. This relationship, characterized as estimation-throughput tradeoff, is given by

$$\mathbb{E}_{\hat{R}_s}[\hat{R}_s(\tilde{\tau}_{est})] = \max_{\tau_{est}} \mathbb{E}_{\hat{R}_s}[\hat{R}_s(\tau_{est})] \quad (5.19)$$

s.t.(5.18).

According to this tradeoff, there exists a suitable estimation time $\tilde{\tau}_{est}$ that satisfies the interference constraint and maximizes the expected secondary throughput.

⁶In order to scale the confidence interval relative to θ_I .

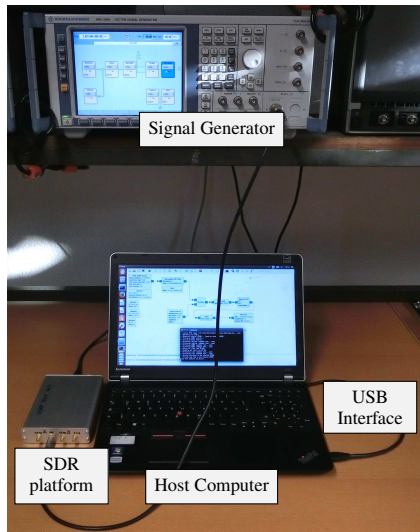


Figure 5.2: An illustration of the measurement setup required for the calibration and the validation process, consisting of: (i) Signal Generator (Rhode & Schwarz 200A), (ii) Software defined radio platform (USRP B210), (iii) USB interference to the host computer and (iv) host computer.

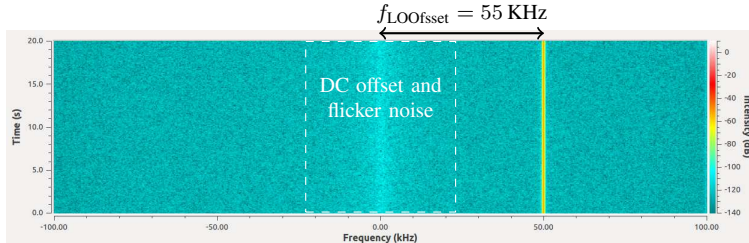
5.3 Validation

This section illustrates the validation of the theoretical expression derived in the previous section. The measurements necessary for the validation is carried out by means of a Software Defined Radio (SDR) platform. The experimental setup for acquiring the measurements is presented, subsequently.

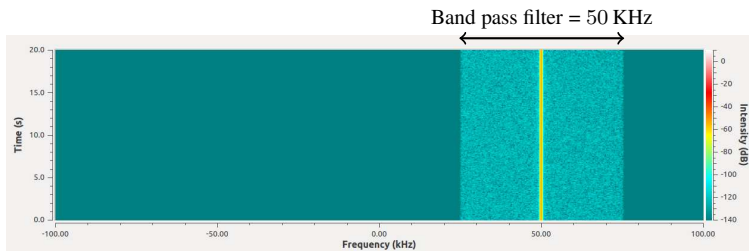
5.3.1 Experimental Setup

Figure 5.2 depicts the experimental setup deployed for performing the validation. It has been previously claimed that the experimental validation considers the deterministic behaviour of the channel. With the employment of the trans-

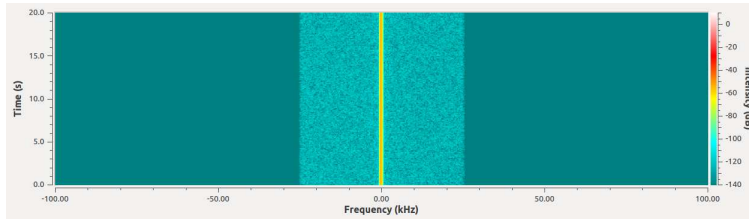
(a) Signal with oversampling, where the local oscillator is tuned at $f_{\text{LOOffset}} = 50 \text{ KHz}$



(b) Signal after bandpass filtering, filter bandwidth = 50 KHz



(c) Signal after digital down conversion



(d) Signal after decimation

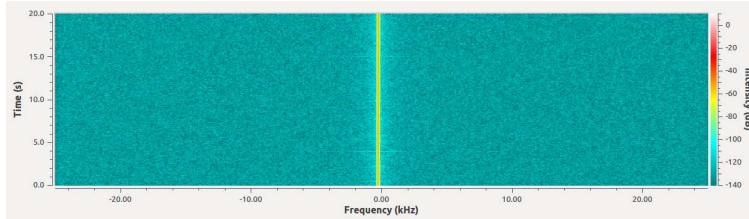


Figure 5.3: An illustration of the signal processing steps carried out at the host computer to preclude the spurious effects such as the DC offset and the flicker noise on the signal received at the ST.

mit and the receive antennas the interference signal received⁷ at the ST can influence the measurements, thereby resulting in the deviation of the empirical results from their analytical counterpart. To avoid this issue, the interference channel is implemented by means of a coaxial cable. In addition, attenuators are used to realize different values of $\gamma_{p,3}$. The use of the coaxial cable is limited to the validation process. For the deployment of the demonstrator later in Section 5.4, the coaxial cable is replaced with antennas.

The CSC-BS or the ST is emulated using a Universal Software Radio Peripheral (USRP) B210, a SDR platform from Ettus Research [68] and a host computer, which is connected to the USRP by means of a USB cable. The host computer performs the following tasks: (i) it enables the access to the USRP by controlling certain Radio frequency (RF) parameters such as, center frequency and sampling frequency, (ii) it allows the baseband processing over the complex samples. The PR, which transmits the pilot signal, is realized using a Rhode & Schwarz 200A vector signal generator (again, for the implementation of the demonstrator later in Section 5.4, the signal generator emulating the PR is replaced with an USRP and a host computer, like the ST). The signal generator is used instead of a USRP for excluding any kind of discrepancy in the transmit signal that may degrade the validation process. Since the USRP employs a homodyne receiver⁸, spurious effects such as DC offset, flicker noise ($1/f$) and I/Q imbalance arising from the analog front-end can affect the accuracy of the analytical expressions, thereby influencing the validation process. These spurious effects, particularly, the DC offset and the flicker noise become significant at low signal to noise ratio.

In order to retrieve the complex samples close to the one obtained while characterizing the system model (which does not take such spurious effects into account), following signal processing is proposed at the host computer.

- The received signal is oversampled with sampling frequency 200 KHz. In order to filter out the spurious effects, the local oscillator is tuned at a certain offset frequency defined as $f_{\text{LoOffset}} = 50 \text{ KHz}$, refer to Figure 5.3a.
- Subsequently, a bandpass filter (with bandwidth = 50 KHz, this corresponds to a oversampling factor = 4) is employed to obtain the desired

⁷The experiments were performed over the ISM bands with center frequency fixed at 2.45 GHz, an interference signal from the operational wireless LAN was observed within the band of interest (in-band) or as an out-of-band emissions from the neighbouring channels.

⁸A homodyne receiver implements a direct down conversion of the bandpass to the baseband signal.

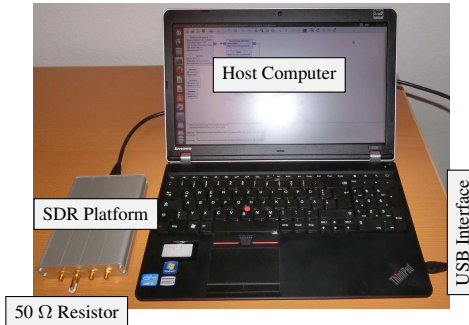


Figure 5.4: A measurement setup for acquiring the noise power, consisting of:
 (i) 50Ω resistor connected to the SMA port of the USRP,
 (ii) Software defined radio platform (USRP B210),
 (iii) USB interference to the host computer and
 (iv) host computer.

bandpass signal at the f_{LOOffset} . This filters out the DC offset and the flicker noise present at low frequencies, cf. Figure 5.3b.

- In order to obtain the low pass equivalent of the desired signal, a digital down conversion⁹ of the bandpass filtered signal is performed, cf. Figure 5.3c.
- In the end, decimation filter is applied (decimation factor = 4) over the down converted signal, cf. Figure 5.3d. This is done to reduce the correlation between the samples due to oversampling, since the proposed framework considers independent and identically distributed samples while characterizing the pdfs of the corresponding systems parameters.

5.3.2 Knowledge of Noise Power

Besides these spurious effects, it is challenging to accurately determine the noise power (σ_w^2), which characterizes the theoretical expressions. In this regard, an approximate value of σ_w^2 is determined using the variance of the envelope of $y_{\text{ST}}[n]$. This is done because the value of the noise power evaluated during the calibration (that involves no signal transmission, refer to Figure 5.4)

⁹Multiplying with a complex sinusoid with frequency f_{LOOffset} .

Table 5.1: Values of the parameters determined while performing the experiments.

Parameter	Value
$\gamma_{p,3}$	22 dB
N	100
τ_{est}	2 ms
θ_I	-110 dBm
T	100 ms
$ h_s ^2$	1
σ_w^2	-96.74 dBm

differed from the one determined while performance the measurements for different values of signal to noise ratio $\gamma_{p,3}$ received at the ST over the interference channel. It is noticed that the latter approach (as presented later in Section 5.3.3) provided a closer fit to the analytical expressions.

Finally, to complement the validation process, the measurement data is analyzed offline using Matlab.

5.3.3 Validation of System Parameters

Since the stochastic model is the basis of the performance analysis of the proposed framework. It is reasonable to first validate the pdfs of the system variables $\hat{P}_{\text{Rx,ST}}$, $\hat{P}_{\text{Tx,ST,cont}}$, $\hat{P}_{\text{Rx,PR}}$, and \hat{R}_s derived in Section 5.2. To this end, measurements with the setup illustrated in Figure 5.2 is performed. The measurement data is plotted in terms of histograms and scaled such that it represents the relative frequency ($f_{\text{hist}}(x)$, a discrete function), which are evaluated over a certain set of bins $x \in \mathcal{X}_{\text{bins}}$. Figure 5.5 compares the histograms from the measurements and the pdfs determined using the analytical expressions for a certain set of system parameters depicted in Table 5.1. The plots show that the theoretical expressions are valid and can be employed for capturing the performance of the CR systems over the hardware.

The experiments were repeated for different values of $\gamma_{p,3}$. It was observed that for a considerable range of $\gamma_{p,3} \in (4, 30)$ dB, the theoretical expressions

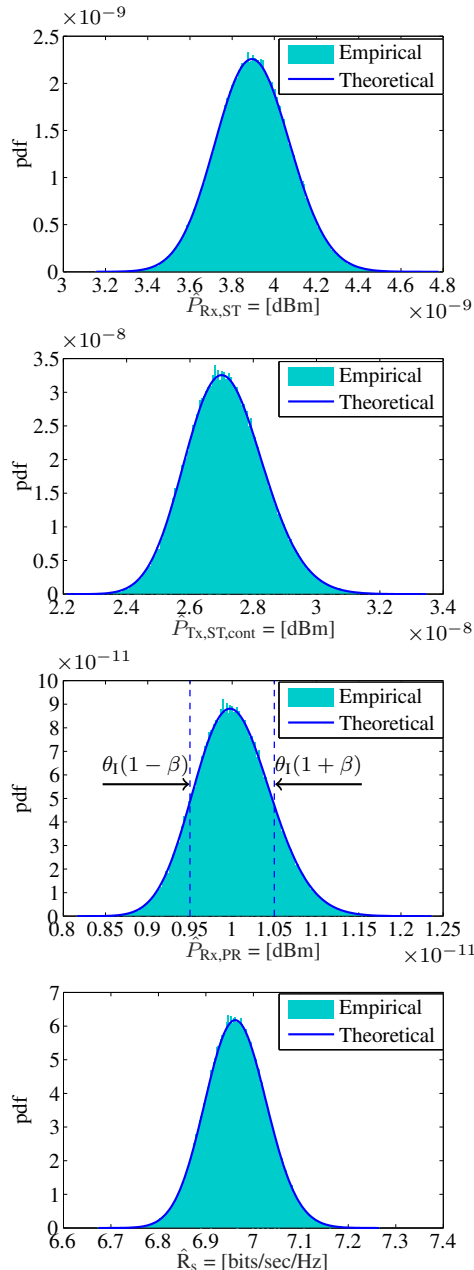


Figure 5.5: Validating the theoretical expressions of the pdf and the experimental results with a certain choice of the system parameters depicted in Table 5.1.

Table 5.2: ϵ for different values of $\gamma_{p,3}$

$\gamma_{p,3}/[\text{dB}]$	ϵ
4.08	0.0568
9.10	0.0601
14.11	0.0522
19.12	0.0437
24.09	0.0506
29.09	0.0634
34.03	0.1179
39.38	0.0800
45.08	0.1695

depicted a significant accuracy to the experimental data, refer to Table 5.2. The accuracy was quantified in terms of a relative error (ϵ) defined as

$$\epsilon = \frac{1}{|\mathcal{X}_{\text{bins}}|} \times \sum_{x \in \mathcal{X}_{\text{bins}}} \frac{f_{\hat{P}_{\text{Rx,ST}}}(x) - f_{\text{hist}}(x)}{f_{\text{hist}}(x)}, \quad (5.20)$$

$|\mathcal{X}_{\text{bins}}|$ represents the cardinality of $\mathcal{X}_{\text{bins}}$, which excludes the bins with $f_{\text{hist}}(x) \neq 0$. Different values of $\gamma_{p,3}$ corresponds to the different channel conditions, hence, this observation further concludes that the proposed framework is robust to the fluctuations in the channel gain.

5.3.4 Validation of the Estimation-Throughput Tradeoff

Following the validation of the pdfs that captures the variations in the system parameters, it is interesting to validate the performance of the CR system in terms of the estimation-throughput tradeoff, characterized in (5.19). Thus, the feasibility of the optimization problem that respects the interference constraint on P_c to determine a suitable estimation time and achieve a maximum secondary throughput is validated. As discussed previously, a large τ_{est} improves the performance of the primary system by reducing the variations in $\hat{P}_{\text{Rx,PR}}$, depicted by observing an increase in P_c , cf. Figure 5.6. Conversely, from the

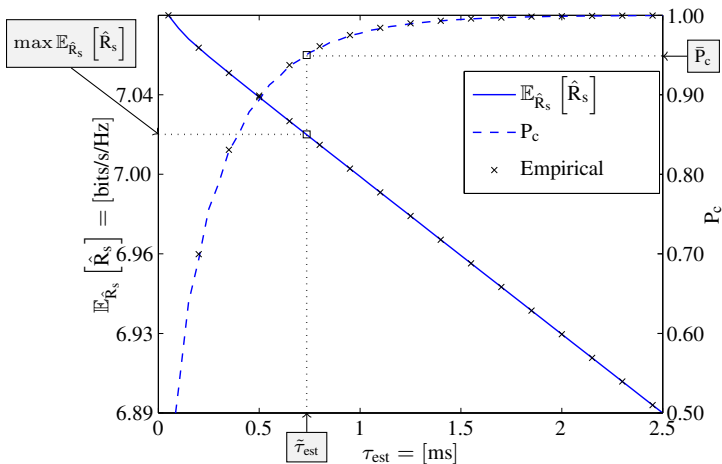


Figure 5.6: Validating the estimation-throughput tradeoff for the choice of parameters depicted in Table 5.1. The figure illustrates the suitable estimation time $\tilde{\tau}_{\text{est}}$ at which the confidence probability is satisfied, see the projection of \square on the curve P_c , at the same time achieves the maximum expected secondary throughput, see the projection of \square on the curve $E_{\hat{R}_s} [\hat{R}_s]$.

perspective of the secondary system, the increase in τ_{est} reduces the achievable secondary throughput. These variations of the expected throughput $\mathbb{E}_{\hat{R}_s} [\hat{R}_s]$ and the confidence probability P_c versus the estimation time τ_{est} are depicted Figure 5.6, which illustrates a joint validation of the performance of a underlay CR system. Again, the validation is achieved by comparing the measurements of the performance parameters ($\mathbb{E}_{\hat{R}_s} [\hat{R}_s]$ and P_c) with their analytical expressions for different τ_{est} . In contrast to the analytical framework presented in Section 5.2, the measurements of P_c are determined by computing a numerical integration in the region within the confidence interval $(1 \pm \beta)\theta_1$, cf. Figure 5.5.

After performing the validation described in this section, following conclusions can be outlined:

- The accuracy of the derived expressions and the feasibility of the received power-based estimation (proposed and investigated in this and previous chapters) have been justified by means of the hardware.
- Furthermore, the applicability of the simplifications and solutions proposed, cf. Section 5.1.1, to perform the validation process has been accounted.

Hence, the analytical framework proposed is capable of illustrating the underlay principle by means of a demonstrator.

5.4 Implementation of a Demonstrator

Although the validation is an important part of the system design, it considers an offline verification of the proposed approach. From a deployment perspective, it is interesting to demonstrate the online operation of the underlay paradigm on the hardware. This section provides insights and outline the involved challenges while deploying the proposed approach in the form of a demonstrator. In the thesis, the operation of CR systems at a suitable estimation time that is associated with the maximum secondary throughput has been analyzed, which represents the optimum performance of a CR system. However, in practice, it is difficult to determine the value of this parameter while the system is operating (*on the fly*). In this regard, the subsequent section discusses this challenging task and proposes a heuristic approach of determining the estimation time.

5.4.1 Estimation Time

The analytical expression (5.19) and Figure 5.6 illustrate a dependency of the performance parameters (P_c and $\mathbb{E}_{\hat{R}_s}[\hat{R}_s]$) on the estimation time τ_{est} . This dependency (depicted as the estimation-throughput tradeoff) is utilized to determine the suitable estimation time $\tilde{\tau}_{est}$ that achieves the maximum secondary throughput. However, $\tilde{\tau}_{est}$ can be determined for a certain value of the $\gamma_{p,3}$ (for a given channel gain). In practice, the mobility of the ST or the PR, or the surroundings objects can affect the channel gain, and consequently the received $\gamma_{p,3}$. Under this situation, it is challenging to select $\tilde{\tau}_{est}$ such that the system adheres to the interference constraint and still achieves the maximum secondary throughput for the corresponding values of $\gamma_{p,3}$. To approach this issue, the variation of $\tilde{\tau}_{est}$ for a certain range of $\gamma_{p,3}$ and different values of the confidence probability constraint $\bar{P}_c \in \{0.90, 0.95, 0.99\}$ is investigated¹⁰, cf. Figure 5.7. Thus, the maximum value of the suitable estimation time for a certain range of $\gamma_{p,3}$ and \bar{P}_c is selected as the estimation time for the demonstrator, given by, $\tau_{est}^* = \max\{\tilde{\tau}_{est} | \gamma_{p,3} \in (-10, 20)\text{dB}; \text{and } P_c = \bar{P}_c\}$ ¹¹. By doing this, it is assured that the interference constraint is satisfied for different realizations of the channel gain, which correspond to $\gamma_{p,3} \in (-10, 20)\text{dB}$.

From Figure 5.7, it is further observed that $\tilde{\tau}_{est}$ decreases with $\gamma_{p,3}$ and attains saturation below a certain $\gamma_{p,3}$. This behaviour can be explained as follows: For large values of $\gamma_{p,3}$, $P_{Tx,ST,cont}$ is low, this reduces the variations of $\hat{P}_{Rx,PR}$ around θ_l . As a result, a lower value of $\tilde{\tau}_{est}$ that is needed to maintain these variations within the confidence interval. On the other hand, the signal received with low $\gamma_{p,3}$, which correspond to a higher $P_{Tx,ST,cont}$. Considering the limited number of samples used for the estimation process and the sensitivity of the deployed hardware (USRP), it is difficult to distinguish these signals from the noise. This is why, $\tilde{\tau}_{est}$ saturates below a certain $\gamma_{p,3}$. However, upon increasing the number of samples for the channel estimation or selecting a hardware with higher sensitivity, the saturation region can be reduced to the lower $\gamma_{p,3}$.

Consequently, the analysis in Figure 5.7 is used for determining the estimation time τ_{est}^* for the demonstrator. For a certain value of the confidence probability constraint $\bar{P}_c = 0.95$, the estimation time allocated for the channel estimation is determined to be $\tau_{est}^* = 24\text{ ms}$, cf. Figure 5.7. With this, the interference

¹⁰Such investigations can be performed during the validation process, which is normally included at the system design.

¹¹Since the τ_{est}^* is not optimal for all $\gamma_{p,3}$, it is different from $\tilde{\tau}_{est}$. Hence, a different notation is assigned to it.

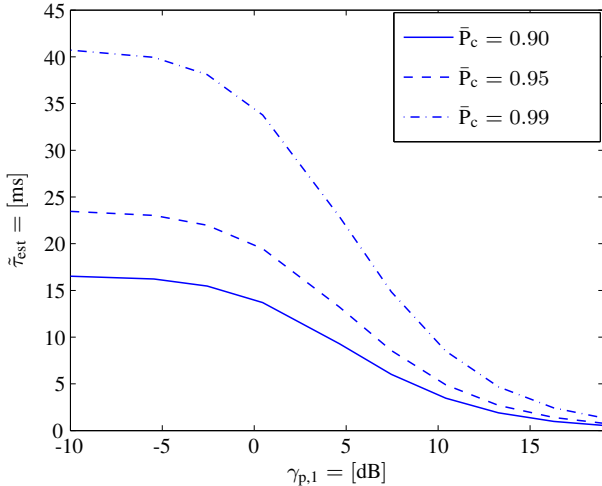


Figure 5.7: The variation of the suitable estimation time ($\tilde{\tau}_{\text{est}}$) versus the received signal to noise ratio at ST ($\gamma_{p,3}$) for different values of confidence probability constraint $\bar{P}_c \in \{0.90, 0.95, 0.99\}$.

constraint is satisfied for all $\gamma_{p,3} \in (-10, 20)$ dB at the cost of a decreased performance in expected secondary throughput, particularly for the situation with high $\gamma_{p,3}$ that achieves the suitable estimation time at a lower value.

5.4.2 Simplifications

In order to successfully deploy the demonstrator, in addition to the simplifications proposed for the hardware validation in Section 5.4.2, following simplifications are accounted in the system model:

1. The controlled power, according to the proposed framework, can be evaluated using (5.9). However, this requires knowledge of the scaling parameter K . According to (5.10), K can be computed by averaging the received power $\hat{P}_{\text{Rx,ST}}$, which corresponds to the expected received power $\mathbb{E}_{\hat{P}_{\text{Rx,ST}}} [\hat{P}_{\text{Rx,ST}}]$. As the antennas are mounted at the ST and the PR, the channel gain can vary over several measurements. These changes make it difficult to carry out such a computation while the system is operating. To resolve this issue, the control power is computed based on a

single realization of the $\hat{P}_{\text{Rx,ST}}$ for the demonstrator. Such a simplification, however, increases the variation in the system. As a result, a certain deviation in the performance depicted by the demonstrator (in terms of the confidence probability and expected secondary throughput) from the one computed using the theoretical expression is expected. In this regard, the estimated channel gain, evaluated from $\hat{P}_{\text{Rx,ST}}$, is determined as

$$|h_{\text{p,3}}|^2 = \frac{\mathbb{E}_{\hat{P}_{\text{Rx,ST}}} [\hat{P}_{\text{Rx,ST}}] - \sigma_w^2}{P_{\text{Tx,PR}}} \approx \frac{\hat{P}_{\text{Rx,ST}} - \sigma_w^2}{P_{\text{Tx,PR}}}. \quad (5.21)$$

As σ_w^2 is negligible compared to $\hat{P}_{\text{Rx,ST}}$, (5.21) can be further simplified as

$$|h_{\text{p,3}}|^2 = \frac{\hat{P}_{\text{Rx,ST}} - \sigma_w^2}{P_{\text{Tx,PR}}} \approx \frac{\hat{P}_{\text{Rx,ST}}}{P_{\text{Tx,PR}}}. \quad (5.22)$$

2. Furthermore, in order to exercise channel reciprocity, the analytical framework employs a TDD across the primary and secondary system. Hence, a perfect frame synchronization between the PR and the ST is needed. Since, the synchronization between two different systems is challenging¹². To simplify this matter, Frequency Division Duplexing between the PR and the ST is proposed. This simplification is described as follows: The signals are transmitted and received using two different frequencies (2.422 GHz and 2.423 GHz) over two separate antennas, as illustrated in Figure 5.8. With this technique, the channel reciprocity may be compromised.

In order to realize these simplifications, it is utmost necessary to observe the impact of these simplifications on the performance of the demonstrator, specially, in terms of the violation of the interference constraint.

In this regard, the principle operation of the underlay paradigm described in Section 5.1.2 is mapped onto the hardware and the above mentioned simplifications are applied. The signal flow illustrating the working of the hardware demonstrator is presented in Figure 5.8. The graphical interface and the different CR techniques such as the channel estimation (received power-based estimation), the power control mechanism, the interference constraint are implemented over the host computer using GNU Radio.

¹²For the preliminary analysis, it is cumbersome to deploy two different system and realize TDD.

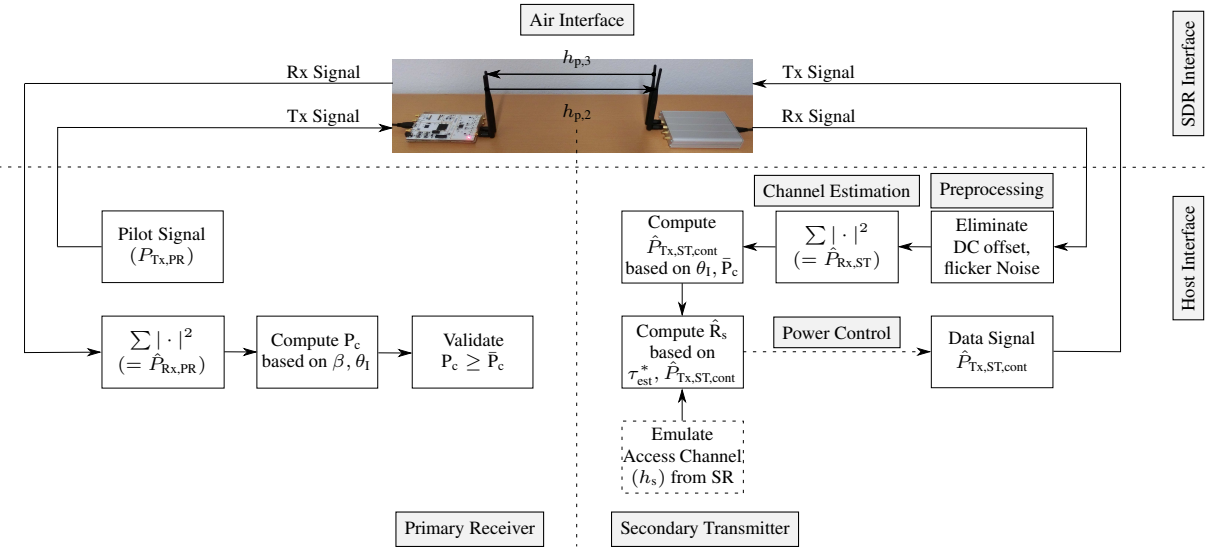


Figure 5.8: Setup and block diagram of the deployed demonstrator.

5.4.3 User Interaction and Observations

Figure 5.9 presents the graphical user interfaces of the demonstrator that provides insights to the parameters evaluated at the PR (which include, $P_{Rx,PR}$ and P_c) and the ST (which include, $\hat{P}_{Rx,ST}$, $\hat{P}_{Tx,ST,cont}$, and \hat{R}_s). A hardware calibration of the demonstrator is performed to provide physical significance to the digital values obtained from the USRPs. Because the SR has not been implemented over the hardware, a slider to modify the gain for the access channel (h_s) has been employed to demonstrate the effect of variations in the h_s on the performance of the system.

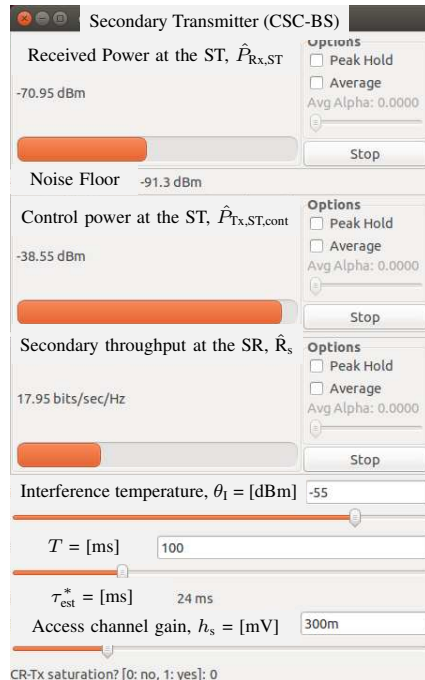
As expected, upon changing the value of θ_1 at the ST causes the variations (in the measurements of $\hat{P}_{Rx,PR}$ at the PR) to shift approximately to the same value. This indicates the expected receiver power $\mathbb{E}_{P_{Rx,PR}}[P_{Rx,PR}]$ is fixed to the interference temperature, as proposed in the analytical framework. A snapshot of this phenomenon is presented in Figure 5.9. In addition, due to the modification of the interference constraint¹³, the ST adapts its $P_{Tx,ST,cont}$ according to the new parameters that define the interference constraint. A change in the $P_{Tx,ST,cont}$ further changes the expected secondary throughput $\mathbb{E}_{\hat{R}_s}[\hat{R}_s]$. These observations demonstrate that the received power-based estimation (which enables the ST to procure the channel knowledge) implemented at the ST by listening to the pilot signal transmitted by the PR to perform the power control mechanism is operating in accordance to the underlay principle. Finally, the response of the demonstrator to the dynamic conditions can be analyzed by varying the distance, which consequently varies the channel gain for the link between the PR and the ST. The effect can be captured by observing the changes in $\hat{P}_{Rx,ST}$ and other corresponding parameters that depend on $h_{p,3}$. As the distance is increased beyond a certain value, the ST operates at its maximum transmit power. Such events during which the ST operates at the maximum transmit power are interesting to understand the behaviour of the demonstrator, hence, included in the graphical the user interface of the ST.

Conversely, for the given accuracy $\beta = 0.05$, it is observed that the demonstrator fails to achieve the target value of the confidence probability constraint $\bar{P}_c = 0.95$. Certainly, this issue is largely caused due to the simplifications undertaken in Section 5.4.2. Another possible reason for this kind of behaviour can be speculated as follows: Since a pilot signal produced by a signal generator has been used for the hardware validation, which offers a higher signal quality than the one produced by a USRP in the demonstrator. In order to tackle

¹³Changing the interference temperature changes the confidence interval.

5 Hardware Validation and Demonstration

(a) User interface to the ST



(b) User interface to the PR

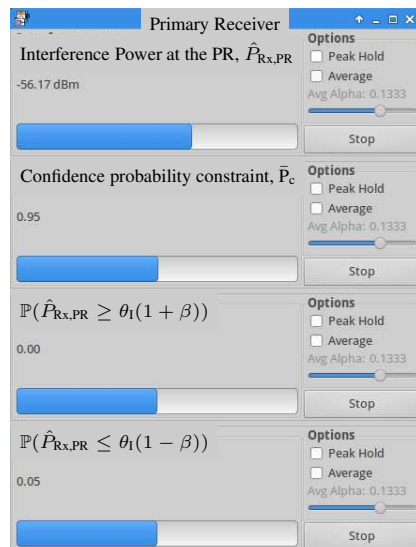


Figure 5.9: A snapshot of the performance parameters displayed in the graphical user interface.

this issue, the proposed interference constraint can be sustained by increasing the tolerance limit to $\beta = 0.20$. To demonstrate a preliminary working of a CR system, these simplifications presents a reasonable solution at this stage, however, it is important to relax these simplifications in the future. As a result, the confidence probability reaches the target value $P_c = 0.95$, thereby satisfying the interference constraint, refer to Figure 5.9 the PR interface. Despite this deviation from the theoretical behaviour, it can be concluded that the USRPs considered for the deployment of the demonstrator represent the viable choice for signal transmissions. To wrap up the discussions, the key observations while deploying the demonstrator for the US are summarized as follows:

- With the incorporation of channel estimation, the deployed hardware demonstrates the principle operation of an US that employs a power control mechanism at the ST and limits the uncertain interference at the PR by employing an interference constraint. This signifies the necessity of the channel knowledge for the operation of a CR system in a more practical situation.
- It further illustrates the capability of adapting to the changes in the environment in terms of channel between the ST and the PR.

5.5 Summary

In this chapter, the performance of an underlay system from a deployment perspective has been analyzed. To this end, an analytical framework has been validated by means of hardware measurements. While investigating the deployment process, it has been argued that the knowledge of the interacting channels play a crucial role in the hardware realization of the CR systems, the main aspect outlined in the thesis. Following the validation process, it has been indicated that the proposed framework that incorporates the channel estimation technique, which includes the received power-based estimation for the links between the primary and the secondary systems, is significant for supporting the hardware feasibility of a CR system by facilitating low complexity and the versatility towards unknown primary user signals. Based on the experimental validation, a hardware demonstrator that depicts the principle working of the underlay system has been examined. More importantly, in this chapter, the major challenges considered while deploying the demonstrator have been discussed, and consequently, the corresponding solutions and simplifications to overcome these challenges have been proposed.

CHAPTER 6

Conclusion

Acronyms and Abbreviation

AC	Average Constraint
AWGN	Additive White Gaussian Noise
BS	Base Station
CSC	Cognitive Small Cell
CSC-BS	Cognitive Small Cell-Base Station
DC	Direct Current
EM	Estimation Model (Proposed Approach)
FDD	Frequency Division Duplexing
HS	Hybrid System
IS	Interweave System
MC-BS	Macro Cell-Base Station
MS	Mobile Station
OC	Outage Constraint
OFDM	Orthogonal Frequency Division Multiplexing
OS	Overlay System
PR	Primary Receiver
PSK	Phase Shift Keying
PU	Primary User
PT	Primary Transmitter

Acronyms and Abbreviation

QoS/QoE	Quality of Service/Quality of Experience
RF	Radio Frequency
SC	Small Cell
SDR	Software Define Radio
SMA	Sub Miniature version A
SNR	Signal to Noise Ratio
SR	Secondary Receiver
SU	Secondary User
ST	Secondary Transmitter
TDD	Time Division Duplexing
US	Underlay System
USB	Universal Serial Bus
USRP	Universal Serial Radio Peripheral
cdf	cumulative distribution function
cf.	confer (refer to)
e.g.	exempli gratia (for example)
i.e.	id est (that is)
i.i.d.	independent and identically distributed
pdf	probability density function
Rx	Receiver
Tx	Transmitter

Notations and Symbols

Please note that, there exists certain notations that are specific or follow a slightly different definition corresponding to the underlying cognitive radio system (interweave system (IS), underlay system (US) and hybrid system (HS)). Here, these notations have been signified by their underlying systems.

T		Frame duration
f_s		Sampling frequency
f_{LOOffset}		Local oscillator offset frequency
τ_{sen}		Sensing time interval
τ_{est}		Estimation time interval
$\tau_{\text{est}, h_{p,1}}$	HS	Estimation time interval allocated for $h_{p,1}$
$\tau_{\text{est}, h_{p,2}}$	HS	Estimation time interval allocated for $h_{p,2}$
$\tau_{\text{est}, h_{p,3}}$	HS	Estimation time interval allocated for $h_{p,3}$
τ_{est}^*		Estimation time interval for the demonstrator
R_s		Throughput at SR (secondary throughput)
C_0	IS, HS	Date rate at SR without interference from PT, where no power control is employed at ST
C_1	IS, HS	Date rate at SR without interference from PT, where no power control is employed at ST
C_s	US	Date rate at SR, where power control is employed at ST
C_2	IS, HS	Date rate at SR without interference from PT, where power control is employed at ST

Notations and Symbols

C_3	IS, HS	Date rate at SR with interference from PT, where power control is employed at ST
$h_{p,1}$	IS, HS	Channel coefficient for the link PT-ST
$h_{p,1}$	US	Channel coefficient for the link PR-ST
h_s		Channel coefficient for the link ST-SR
$h_{p,2}$		Channel coefficient for the link PT-SR
$h_{p,3}$	HS	Channel coefficient for the link PR-ST
P_d		Detection probability
P_{fa}		False alarm probability
P_c		Confidence probability
\bar{P}_d		Target detection probability
\bar{P}_c		Target confidence probability
μ		Decision threshold
ρ_d		Outage constraint over detection probability at ST
ρ_{cont}		Outage constraint on controlled power at ST
θ_I		Interference temperature at PR
β		Accuracy of the parameter
ϵ		Relative error between the normalized histogram bins and probability density function
$x_{PT}[\cdot]$		Discrete and complex signal transmitted by PT
$x_{PR}[\cdot]$		Discrete and complex signal transmitted by PR
$x_{ST,cont}[\cdot]$	US, HS	Discrete and complex signal transmitted by ST with controlled power
$x_{ST}[\cdot]$	IS, HS	Discrete and complex signal transmitted by ST with no power control
$y_{ST}[\cdot]$		Discrete and complex signal received at ST
$w[\cdot]$		Discrete and complex noise signal
$y_{PR}[\cdot]$		Discrete and complex signal received at PR
$P_{Rx,ST}$	IS	Power received at ST over the PT-ST

$P_{\text{Rx,ST}}$	US	Power received at ST over the PR-ST
$P_{\text{Rx,ST},h_{\text{p},1}}$	HS	Power received at ST over the PT-ST over $h_{\text{p},1}$
$P_{\text{Rx,ST},h_{\text{p},3}}$	HS	Power received at ST over the PR-ST over $h_{\text{p},3}$
$P_{\text{Rx,PR}}$	US, HS	Interference power received at PR over the ST-PR link
$P_{\text{Rx,SR}}$		Interference power received at SR over the PT-SR link
$P_{\text{Tx,ST,cont}}$	US	Transmit power at ST with power control
$P_{\text{Tx,ST}}$	IS, HS	Transmit power at ST with full transmit control
$P_{\text{Tx,PR}}$		Transmit power at PR
σ_w^2		Noise power
σ_s^2		Transmit power at ST and SR, when transmit signal is modeled as OFDM
$\gamma_{\text{p},1}$	IS	Signal to noise power received at ST over PT-ST link
$\gamma_{\text{p},1}$	US	Signal to noise power received at ST over PR-ST link
$\gamma_{\text{p},2}$		Interference (from PT) to noise ratio for PT-SR link
$F(\cdot)$		Cumulative distribution function of random variable (\cdot)
$f(\cdot)$		Probability density function of random variable (\cdot)
$\mathbb{E}(\cdot)$		Expectation with respect to (\cdot)
\mathbb{P}		Probability measure
$T(\cdot)$		Test statistics
$(\tilde{\cdot})$		Suitable value of the parameter (\cdot) that achieves maximum performance
$(\tilde{\cdot})$		Suitable value of the parameter (\cdot) that achieves maximum performance
K		Scaling factor that holds the expected power received at the PR at interference temperature
N_s		Number of pilot symbols used for pilot based estimation at the SR
$N_{\text{p},2}$		Number of samples used for received power based estimation at the SR
\mathcal{N}		Gaussian or normal distribution

Notations and Symbols

χ^2	Central chi-squared distribution
χ_1^2	Non-central chi-squared distribution
$\lambda_{(\cdot)}$ or λ	Non-centrality parameter of a non-central chi-squared distribution
$a_{(\cdot)}, b_{(\cdot)}$ or a, b	Shape and scale parameters of a Gamma distribution
$I_N(\cdot)$	Modified Bessel function of first kind of order N
$Q_N(\cdot, \cdot)$	Marcum Q-function
$\Gamma(\cdot, \cdot)$	Regularized upper-incomplete Gamma function
$\Gamma^{-1}(\cdot, \cdot)$	Inverse function of regularized upper-incomplete Gamma function
\mathcal{H}_1	Hypothesis illustrating the presence of primary user
\mathcal{H}_0	Hypothesis illustrating the absence of primary user (noise only)

Bibliography

- [1] Cisco, “Cisco Visual Networking Index: Global Mobile Data Traffic Forecast Update, 2013–2018,” *White Paper*, February 2014.
- [2] Ericsson, “Ericsson mobility report,” tech. rep., Nov 2015.
- [3] 3GPP. <http://www.3gpp.org/>. [Online; accessed June 1, 2016].
- [4] Qualcomm, “Rising to meet the 1000x mobile challenge,” tech. rep., Sept 2013.
- [5] J. Andrews, S. Buzzi, W. Choi, S. Hanly, A. Lozano, A. Soong, and J. Zhang, “What Will 5G Be?,” *IEEE Journal on Selected Areas in Communications*, vol. 32, pp. 1065–1082, June 2014.
- [6] V. Chandrasekhar, J. Andrews, and A. Gatherer, “Femtocell Networks: A Survey,” *IEEE Communications Magazine*, vol. 46, pp. 59–67, September 2008.
- [7] T. Rappaport, S. Sun, R. Mayzus, H. Zhao, Y. Azar, K. Wang, G. Wong, J. Schulz, M. Samimi, and F. Gutierrez, “Millimeter Wave Mobile Communications for 5G Cellular: It Will Work!,” *IEEE Access*, vol. 1, pp. 335–349, 2013.
- [8] M. McHenry, “NSF Spectrum Occupancy Measurements Project Summary,” *Shared Spectrum Company*, 2005.
- [9] M. McHenry, E. Livosics, T. Nguyen, and N. Majumdar, “XG Dynamic Spectrum Access Field Test Results,” *IEEE Communications Magazine*, vol. 45, pp. 51–57, June 2007.

Bibliography

- [10] P. Pawelczak, K. Nolan, L. Doyle, S. W. Oh, and D. Cabric, “Cognitive radio: Ten Years of Experimentation and Development,” *IEEE Communications Magazine*, vol. 49, pp. 90–100, March 2011.
- [11] A. Goldsmith, S. Jafar, I. Maric, and S. Srinivasa, “Breaking Spectrum Gridlock With Cognitive Radios: An Information Theoretic Perspective,” *Proceedings of the IEEE*, vol. 97, pp. 894–914, May 2009.
- [12] D. Cabric, S. M. Mishra, and R. W. Brodersen, “Implementation issues in spectrum sensing for cognitive radios,” in *Conference Record of the Thirty-Eighth Asilomar Conference on Signals, Systems and Computers*, vol. 1, pp. 772–776 Vol.1, Nov 2004.
- [13] D. Cabric, A. Tkachenko, and R. W. Brodersen, “Experimental Study of Spectrum Sensing Based on Energy Detection and Network Cooperation,” in *Proceedings of the First International Workshop on Technology and Policy for Accessing Spectrum*, ACM, 2006.
- [14] K. Kim, Y. Xin, and S. Rangarajan, “Energy Detection Based Spectrum Sensing for Cognitive Radio: An Experimental Study,” in *IEEE Global Telecommunications Conference (GLOBECOM)*, pp. 1–5, Dec 2010.
- [15] H. ElSawy, E. Hossain, and M. Haenggi, “Stochastic Geometry for Modeling, Analysis, and Design of Multi-Tier and Cognitive Cellular Wireless Networks: A Survey,” *IEEE Communications Surveys Tutorials*, vol. 15, pp. 996–1019, Jun. 2013.
- [16] H. ElSawy, E. Hossain, and D. I. Kim, “Hetnets with cognitive small cells: user offloading and distributed channel access techniques,” *IEEE Communications Magazine*, vol. 51, pp. 28–36, June 2013.
- [17] M. Wildemeersch, T. Q. S. Quek, C. H. Slump, and A. Rabbachin, “Cognitive Small Cell Networks: Energy Efficiency and Trade-Offs,” *IEEE Transactions on Communications*, vol. 61, pp. 4016–4029, September 2013.
- [18] M. Haenggi, *Stochastic Geometry for Wireless Networks*. Cambridge University Press, 2013.
- [19] M. Haenggi and R. K. Ganti, “Interference in Large Wireless Networks,” *Foundations and Trends in Networking*, vol. 3, no. 2, pp. 127–248, 2008. Available at <http://www.nd.edu/~mhaenggi/pubs/now.pdf>.

- [20] ETSI TS 103 113, “Electromagnetic compatibility and Radio spectrum Matters (ERM); System Reference document (SRdoc); Mobile broadband services in the 2300 - 2400 MHz frequency band under Licensed Shared Acces regime,” July 2013.
- [21] F. K. Jondral, “Software-defined radio-basic and evolution to cognitive radio,” *EURASIP Journal on Wireless Communication and Networking*, vol. 2005 Issue 3, pp. 275–283, August 2005.
- [22] M. Paolini, “Meeting the Challenges of High-Capacity Indoor and Outdoor Coverage,” *Senza Fili Consulting*, Dec 2007. Available at http://www.senzafiliconsulting.com/downloads/SenzaFili_IndoorCoverageSurvey.pdf.
- [23] M. Simon and M. Alouini, *Digital Communication over Fading Channels*. Wiley Series in Telecommunications and Signal Processing, Wiley, 2005.
- [24] A. Goldsmith, *Wireless Communications*. New York, NY, USA: Cambridge University Press, 2005.
- [25] D. Tse and P. Viswanath, *Fundamentals of Wireless Communication*. Cambridge University Press, 2005.
- [26] M. A. Maddah-Ali and D. Tse, “Completely stale transmitter channel state information is still very useful,” *IEEE Transactions on Information Theory*, vol. 58, pp. 4418–4431, July 2012.
- [27] A. Ghasemi and E. S. Sousa, “Spectrum sensing in cognitive radio networks: requirements, challenges and design trade-offs,” *IEEE Communications Magazine*, vol. 46, pp. 32–39, April 2008.
- [28] Y.-C. Liang, Y. Zeng, E. Peh, and A. T. Hoang, “Sensing-Throughput Tradeoff for Cognitive Radio Networks,” *IEEE Transactions on Wireless Communications*, vol. 7, pp. 1326–1337, April 2008.
- [29] S. Sharma, S. Chatzinotas, and B. Ottersten, “A hybrid cognitive transceiver architecture: Sensing-throughput tradeoff,” in *9th International Conference on Cognitive Radio Oriented Wireless Networks and Communications (CROWNCOM)*, pp. 143–149, Jun. 2014.
- [30] H. Pradhan, S. Kalamkar, and A. Banerjee, “Sensing-Throughput Trade-off in Cognitive Radio With Random Arrivals and Departures of Multiple Primary Users,” *IEEE Communications Letters*, vol. 19, pp. 415–418, March 2015.

Bibliography

- [31] S. Sharma, T. Bogale, S. Chatzinotas, B. Ottersten, L. Le, and X. Wang, “Cognitive Radio Techniques under Practical Imperfections: A Survey,” *IEEE Communications Surveys Tutorials*, vol. 17, pp. 1858–1884, Fourthquarter 2015.
- [32] E. Axell, G. Leus, E. Larsson, and H. Poor, “Spectrum Sensing for Cognitive Radio : State-of-the-Art and Recent Advances,” *IEEE Signal Processing Magazine*, vol. 29, pp. 101–116, May 2012.
- [33] H. Urkowitz, “Energy detection of unknown deterministic signals,” *Proceedings of the IEEE*, vol. 55, pp. 523 – 531, april 1967.
- [34] V. Kostylev, “Energy detection of a signal with random amplitude,” in *IEEE ICC*, vol. 3, pp. 1606–1610, 2002.
- [35] F. Digham, M.-S. Alouini, and M. K. Simon, “On the energy detection of unknown signals over fading channels,” in *IEEE ICC*, vol. 5, pp. 3575–3579, May 2003.
- [36] S. Herath, N. Rajatheva, and C. Tellambura, “Unified Approach for Energy Detection of Unknown Deterministic Signal in Cognitive Radio Over Fading Channels,” in *IEEE ICC Workshops*, pp. 1–5, June 2009.
- [37] A. Mariani, A. Giorgetti, and M. Chiani, “Energy detector design for cognitive radio applications,” in *International Waveform Diversity and Design Conference (WDD)*, pp. 053–057, Aug 2010.
- [38] E. Peh and Y.-C. Liang, “Optimization for cooperative sensing in cognitive radio networks,” in *IEEE Wireless Communications and Networking Conference (WCNC)*, pp. 27–32, March 2007.
- [39] M. Cardenas-Juarez and M. Ghogho, “Spectrum Sensing and Throughput Trade-off in Cognitive Radio under Outage Constraints over Nakagami Fading,” *IEEE Communications Letters*, vol. 15, pp. 1110–1113, October 2011.
- [40] Y. Sharkasi, M. Ghogho, and D. McLernon, “Sensing-throughput trade-off for OFDM-based cognitive radio under outage constraints,” in *ISWCS*, pp. 66–70, Aug 2012.
- [41] P. Stoica and O. Besson, “Training sequence design for frequency offset and frequency-selective channel estimation,” *IEEE Transactions on Communications*, vol. 51, pp. 1910–1917, Nov 2003.

- [42] W. Gifford, M. Win, and M. Chiani, “Diversity with practical channel estimation,” *IEEE Transactions on Wireless Communications*, vol. 4, pp. 1935–1947, July 2005.
- [43] W. Gifford, M. Win, and M. Chiani, “Antenna subset diversity with non-ideal channel estimation,” *IEEE Transactions on Wireless Communications*, vol. 7, pp. 1527–1539, May 2008.
- [44] V. Chavali and C. da Silva, “Collaborative spectrum sensing based on a new snr estimation and energy combining method,” *IEEE Transactions on Vehicular Technology*, vol. 60, pp. 4024–4029, Oct 2011.
- [45] S. Sharma, S. Chatzinotas, and B. Ottersten, “SNR Estimation for Multi-dimensional Cognitive Receiver under Correlated Channel/Noise,” *IEEE Transactions on Wireless Communications*, vol. 12, pp. 6392–6405, December 2013.
- [46] T. Wang, Y. Chen, E. Hines, and B. Zhao, “Analysis of effect of primary user traffic on spectrum sensing performance,” in *Fourth International Conference on Communications and Networking in China*, pp. 1–5, Aug 2009.
- [47] L. Tang, Y. Chen, E. Hines, and M.-S. Alouini, “Effect of Primary User Traffic on Sensing-Throughput Tradeoff for Cognitive Radios,” *IEEE Transactions on Wireless Communications*, vol. 10, pp. 1063–1068, April 2011.
- [48] B. Zhao, Y. Chen, C. He, and L. Jiang, “Performance analysis of spectrum sensing with multiple primary users,” *IEEE Transactions on Vehicular Technology*, vol. 61, pp. 914–918, Feb 2012.
- [49] S. Kay, *Fundamentals of Statistical Signal Processing: Detection theory*. Prentice Hall Signal Processing Series, Prentice-Hall PTR, 1998.
- [50] R. Tandra and A. Sahai, “SNR Walls for Signal Detection,” *IEEE Journal of Selected Topics in Signal Processing*, vol. 2, pp. 4–17, Feb 2008.
- [51] I. S. Gradshteyn and I. M. Ryzhik, *Table of Integrals, Series, and Products*. San Diego, CA: Academic Press., sixth ed., 2000.
- [52] M. Gans, “The Effect of Gaussian Error in Maximal Ratio Combiners,” *IEEE Transactions on Communication Technology*, vol. 19, pp. 492–500, August 1971.

Bibliography

- [53] R. AnnavaJJala and L. Milstein, "Performance analysis of linear diversity-combining schemes on Rayleigh fading channels with binary signaling and Gaussian weighting errors," *IEEE Transactions on Wireless Communications*, vol. 4, pp. 2267–2278, Sept 2005.
- [54] H. Suraweera, P. Smith, and M. Shafi, "Capacity limits and performance analysis of cognitive radio with imperfect channel knowledge," *IEEE Transactions on Vehicular Technology*, vol. 59, pp. 1811–1822, May 2010.
- [55] H. Kim, H. Wang, S. Lim, and D. Hong, "On the Impact of Outdated Channel Information on the Capacity of Secondary User in Spectrum Sharing Environments," *IEEE Transactions on Wireless Communications*, vol. 11, pp. 284–295, January 2012.
- [56] N. Cao, M. Mao, Y. Chen, and M. Long, "Analysis of collaborative spectrum sensing with binary phase shift keying signal power estimation errors," *IET Science, Measurement and Technology*, vol. 8, no. 6, pp. 350–358, 2014.
- [57] M. Abramowitz and I. A. Stegun, *Handbook of Mathematical Functions with Formulas, Graphs, and Mathematical Tables*. New York: Dover, ninth Dover printing, tenth GPO printing ed., 1964.
- [58] F. W. J. Olver, D. W. Lozier, R. F. Boisvert, and C. W. Clark, eds., *NIST Handbook of Mathematical Functions*. New York, NY: Cambridge University Press, 2010.
- [59] X. Kang, Y.-C. Liang, H. Garg, and L. Zhang, "Sensing-based spectrum sharing in cognitive radio networks," *IEEE Transactions on Vehicular Technology*, vol. 58, pp. 4649–4654, Oct 2009.
- [60] J. Oh and W. Choi, "A hybrid cognitive radio system: A combination of underlay and overlay approaches," in *IEEE 72nd Vehicular Technology Conference Fall (VTC 2010-Fall)*, pp. 1–5, Sept 2010.
- [61] S. Senthuran, A. Anpalagan, and O. Das, "Throughput analysis of opportunistic access strategies in hybrid underlay–overlay cognitive radio networks," *IEEE Transactions on Wireless Communications*, vol. 11, pp. 2024–2035, June 2012.
- [62] H. Song, J. P. Hong, and W. Choi, "On the optimal switching probability for a hybrid cognitive radio system," *IEEE Transactions on Wireless Communications*, vol. 12, pp. 1594–1605, April 2013.

- [63] S. Gmira, A. Kobbane, and E. Sabir, “A new optimal hybrid spectrum access in cognitive radio: Overlay-underlay mode,” in *International Conference on Wireless Networks and Mobile Communications (WINCOM)*, pp. 1–7, Oct 2015.
- [64] X. Jiang, K.-K. Wong, Y. Zhang, and D. Edwards, “On Hybrid Overlay-Underlay Dynamic Spectrum Access: Double-Threshold Energy Detection and Markov Model,” *IEEE Transactions on Vehicular Technology*, vol. 62, pp. 4078–4083, Oct 2013.
- [65] M. C. Filippou, G. A. Ropokis, D. Gesbert, and T. Ratnarajah, “Performance analysis and optimization of hybrid MIMO Cognitive Radio systems,” in *IEEE International Conference on Communication Workshop (ICCW)*, pp. 555–561, June 2015.
- [66] C. Charalambous and N. Menemenlis, “Stochastic models for short-term multipath fading channels: chi-square and Ornstein-Uhlenbeck processes,” in *Proceedings of the 38th IEEE Conference on Decision and Control*, vol. 5, pp. 4959–4964 vol.5, 1999.
- [67] A. Jeffrey and D. Zwillinger, *Table of Integrals, Series, and Products*. Elsevier Science, 2000.
- [68] Ettus Research. <http://www.ettus.com/>. [Online; accessed December 2, 2015].

Related Publications

- [K1] A. Kaushik, M. Mueller, and F. K. Jondral, “Cognitive Relay: Detecting Spectrum Holes in a Dynamic Scenario,” in *Proceedings of the Tenth International Symposium on Wireless Communication Systems (ISWCS 2013)*, pp. 1–2, Apr. 2013.
- [K2] A. Kaushik and F. K. Jondral, “On the estimation of channel state transitions for cognitive radio systems,” in *IEEE Wireless Communications Networking Conference (WCNC)*, pp. 2061–2066, Apr. 2014.
- [K3] A. Kaushik, M. R. Raza, and F. K. Jondral, “On the Deployment of Cognitive Relay as Underlay Systems,” in *9th International Conference on Cognitive Radio Oriented Wireless Networks and Communications (CROWNCOM)*, pp. 329–334, Jun. 2014.
- [K4] A. Kaushik, R. Tanbourgi, and F. Jondral, “Operating characteristics of underlay cognitive relay networks,” in *IEEE 25th Annual International Symposium on Personal, Indoor, and Mobile Radio Communication (PIMRC)*, pp. 1206–1210, Sept 2014.
- [K5] A. Kaushik, S. K. Sharma, S. Chatzinotas, B. Ottersten, and F. K. Jondral, “Sensing-Throughput Tradeoff for Cognitive Radio Systems with Unknown Received Power,” in *10th International Conference on Cognitive Radio Oriented Wireless Networks and Communications (CROWNCOM)*, pp. 308–320, April 2015.
- [K6] A. Kaushik, S. K. Sharma, S. Chatzinotas, B. Ottersten, and F. K. Jondral, “Estimation-Throughput Tradeoff for Underlay Cognitive Radio Systems,” in *IEEE International Conference on Communications (ICC)*, pp. 7701–7706, June 2015.

- [K7] A. Kaushik, F. Wunsch, A. Sagainov, N. Cuervo, J. Demel, S. Koslowski, H. Jäkel, and F. Jondral, “Spectrum sharing for 5G wireless systems (Spectrum sharing challenge),” in *IEEE International Symposium on Dynamic Spectrum Access Networks (DySPAN)*, pp. 1–2, Sept 2015.
- [K8] A. Kaushik, S. K. Sharma, S. Chatzinotas, B. Ottersten, and F. K. Jondral, “Sensing-Throughput Tradeoff for Interweave Cognitive Radio System: A Deployment-Centric Viewpoint,” *IEEE Transactions on Wireless Communications*, vol. 15, pp. 3690–3702, May 2016.
- [K9] A. Kaushik, S. K. Sharma, S. Chatzinotas, B. Ottersten, and F. K. Jondral, “Performance Analysis of Interweave Cognitive Radio Systems with Imperfect Channel Knowledge over Nakagami Fading Channels,” in *IEEE 84th Vehicular Technology Conference (VTC)*, Sept. 2016. (to appear).
- [K10] A. Kaushik, S. K. Sharma, S. Chatzinotas, B. Ottersten, and F. K. Jondral, “On the Performance Analysis of Underlay Cognitive Radio Systems: A Deployment Perspective,” *IEEE Transactions on Cognitive Communications and Networking (TCCN)*. (submitted).
- [K11] A. Kaushik, S. K. Sharma, S. Chatzinotas, B. Ottersten, and F. K. Jondral, “Performance Analysis of Hybrid Cognitive Radio Systems with Imperfect Channel Knowledge,” in *IEEE International Conference on Communications (ICC)*, pp. 5289–5295, May 2016.
- [K12] H. Becker, A. Kaushik, S. K. Sharma, S. Chatzinotas, and F. K. Jondral, “Experimental Study of an Underlay Cognitive Radio System: Model Validation and Demonstration,” in *11th International Conference on Cognitive Radio Oriented Wireless Networks and Communications (CROWNCOM)*, May-June 2016. (to appear).
- [K13] L. Rodes, A. Kaushik, S. K. Sharma, S. Chatzinotas, and F. K. Jondral, “Square-Law Selector and Square-Law Combiner for Cognitive Radio Systems: An Experimental Study,” in *IEEE 84th Vehicular Technology Conference (VTC)*, Sept. 2016. (to appear).